University of Alberta

Characterization of Hypertrophic Scar Formation in Nude and Knockout Mice Deficient in T, B and Natural Killer Cells

by

Moein Momtazi

A thesis submitted to the Faculty of Graduate Studies and Research
in partial fulfillment of the requirements for the degree of

Master of Science
in
Experimental Surgery

Department of Surgery

©Moein Momtazi

Spring 2012
Edmonton, Alberta

Permission is hereby granted to the University of Alberta Libraries to reproduce single copies of this thesis and to lend or sell such copies for private, scholarly or scientific research purposes only. Where the thesis is converted to, or otherwise made available in digital form, the University of Alberta will advise potential users of the thesis of these terms.

The author reserves all other publication and other rights in association with the copyright in the thesis and, except as herein before provided, neither the thesis nor any substantial portion thereof may be printed or otherwise reproduced in any material form whatsoever without the author's prior written permission.

Dedication

I would like to dedicate this thesis to my loving parents:

Keramat and Shohreh Momtazi

Also, with great thanks to my brother for his support during the completion of this work:

Matin Momtazi

Abstract

Introduction: Hypertrophic scar (HSc) is a fibroproliferative disorder lacking a relevant animal model. Our objective is to characterize proliferative scars in human xenografts generated after grafting human skin onto mice deficient in T, B and natural killer cells.

Methods: Nude, T-cell receptor (TCR) $\beta^{-/-}\delta^{-/-}$, RAG(recombination activating gene)-$1^{-/-}$ and RAG-$2^{-/-}\gamma c^{-/-}$ mice were xenografted with split thickness human skin. Controls were autografted with mouse skin. Animals were euthanized at 30, 60, 120 and 180 days postoperatively. Scar biopsies were subjected to hematoxylin and eosin, Masson's trichrome, toluidine blue and picrosirius red staining. Immunohistochemistry included anti-human HLA-ABC, α–smooth muscle actin, decorin and biglycan staining.

Results: Xenografting nude mice with human skin results in scars morphologically, histologically and immunohistochemically similar to human HSc. Knockout animals developed similar scars and demonstrate greater capacity for scar remodeling.

Conclusion: Proliferative xenograft scars in knockout animals better represent the natural history of HSc. The role of activated, profibrotic fibrocytes and macrophages in these animals requires further investigation.

Acknowledgments

I would like to thank Dr. Steven T. Boyce for his expert assistance. I also gratefully acknowledge Yvonne Marcoux and Lisa Budney for their technical support and Heather Shankowsky for assistance with preparing this thesis.

This work was financially supported by:

Clinical Investigator Program (CIP)

Department of Surgery

Fire Fighters Burn Trust Fund

Canadian Institutes of Health Research (CIHR)

Table of Contents

1. Introduction

1.1 Structure and Function of Skin……2

1.2 Hypertrophic Scarring in Humans……...…4

1.2.1 Hypertrophic Scars and Keloids……4

1.2.2 The Burden of Disease……..5

1.2.3 The Clinical Problem…….6

1.3 The Role of the Immune System in Wound Healing……...7

1.3.1 T-cell Responses……8

1.3.2 Fibrocyte Involvement……..9

1.3.3 Role of γδ T-cell Receptor-Bearing Dendritic Epidermal T-cells……11

1.3.4 Role of Natural Killer Cells…….12

1.3.5 Role of Natural Killer T-cells……..14

1.3.6 Role of Mast Cells……...15

1.3.7 Role of Langerhans Cells……16

1.4 Animal Models of Hypertrophic Scar……18

1.4.1 Rabbit Ear Model……18

1.4.2 Porcine Model…….19

1.4.3 Mechanical Load Model……..20

1.5 Nude Mouse Model of Human Hypertrophic Scar……21

1.6 RAG Knockout Mouse Model……...24

1.7 Formulation of Thesis……25

1.8 Tables…….29

1.9 Figures……32

1.10 Bibliography……...……42

2. A Nude Mouse Model of Hypertrophic Scar Demonstrates Morphologic and Histological Characteristics of Human Hypertrophic Scar

2.1 Introduction……63

2.2 Methods……..65

2.3 Results……73

2.4 Discussion……..78

2.5 Conclusions……84

2.6 Tables…….85

2.7 Figures……86

2.8 Bibliography…….101

3. Morphologic and Histological Comparison of Hypertrophic Scar in Nude and Knockout Mice Deficient in T, B and Natural Killer Cells

3.1 Introduction……..112

3.2 Methods……114

3.3 Results……..120

3.4 Discussion……124

3.5 Conclusions……..129

3.6 Figures……..130

3.7 Bibliography…….143

4. Summary

4.1 General Discussion……..149

4.2 Conclusions……..151

4.3 Bibliography…….153

List of Tables

Table 1-1: Distinction between HSc and keloids based on clinical features; page 29

Table 1-2: Cellular differences between fibroblasts derived from HSc and keloids compared to normal skin; page 29

Table 1-3: The International Advisory Panel on Scar Management Scar Classification; page 30

Table 1-4: A comparison of αβ and γδ T-cells; page 31

Table 1-5: Summary of the objectives, methodologies and conclusions of three studies utilizing the athymic mouse model; page 31

Table 2-1: Modified Manchester Scar Scale (MSS); page 86

List of Figures

Figure 1-1: Structure of the skin; page 32

Figure 1-2: HSc affecting the face, chest and trunk following thermal injury; page 33

Figure 1-3: Keloid scar affecting the earlobe, scalp, suprapubic region and shoulder; page 34

Figure 1-4: Subpopulations of T-cells and their respective cytokine profiles; page 34

Figure 1-5: Fibrocytes viewed using light microscopy; page 35

Figure 1-6: Epidermis stained with anti-TCR monoclonal antibody; page 35

Figure 1-7: Natural killer cells viewed using scanning electron and light microscopy; page 36

Figure 1-8: Photomicrograph of mast cells stained with Safranin; page 36

Figure 1-9: Langerhans cells with hallmark Birbeck granules viewed under scanning electron and light microscopy; page 37

Figure 1-10: The role of immune cells in contributing to excess extracellular matrix production; page 38

Figure 1-11: Comparison of histological features of human and pig skin with hematoxylin and eosin staining; page 39

Figure 1-12: Mechanical load model of hypertrophic scar; page 39

Figure 1-13: Heterozygous, normal-haired mouse compared with its hairless homozygous nu/nu littermate at 21 days postnatal life; page 40

Figure 1-14: Homologous recombination with an inactivated gene during embryonic stem cell co-culture and subsequent implantation of blastocyts into a pseudoprenant mother; page 41

Figure 2-1: A nude mouse model of human hypertrophic scar; page 87

Figure 2-2: Morphologic appearance of nude mouse autograft and proliferative xenograft scar at day 30 following grafting; page 88

Figure 2-3: Modified Manchester Scar Scale (MSS) scores for human split thickness xenografts compared to nude mouse autografts over time; page 89

Figure 2-4: Anti-human HLA-ABC antibody staining of human split thickness xenograft sections from nude mice at 30, 60, 120 and 180 days following grafting; page 90

Figure 2-5: Representative images of H & E stained sections of proliferative xenograft scar from a nude mouse, human HSc and normal human skin; page 91

Figure 2-6: Representative images of Masson's trichrome stained sections of a human split thickness xenograft from a nude mouse, human HSc and normal human skin; page 91

Figure 2-7: Proliferative xenograft scar, nude mouse autograft and normal nude mouse skin thickness over time; page 92

Figure 2-8: Percent increase in proliferative xenograft scar, nude mouse autograft and normal nude mouse skin thickness over time; page 93

Figure 2-9: Representative images of α-SMA stained sections of proliferative xenograft scar from a nude mouse, human HSc and normal human skin; page 94

Figure 2-10: Representative immunofluorescent images of decorin stained sections of proliferative xenograft scars in nude mice; page 95

Figure 2-11: Quantification of decorin immunofluorescence in proliferative xenograft scars in nude mice relative to normal human skin over time; page 96

Figure 2-12: Representative immunofluorescent images of biglycan stained sections of proliferative xenograft scars in nude mice; page 97

Figure 2-13: Quantification of biglycan immunofluorescence in proliferative xenograft scars in nude mice relative to normal human skin over time; page 98

Figure 2-14: Representative images of toluidine blue stained sections of a proliferative xenograft scar, human HSc and normal human skin; page 99

Figure 2-15: Quantification of mast cells in proliferative xenograft scars relative to normal skin over time; page 100

Figure 2-16: Representative images of picrosirius red stained sections of proliferative xenograft scar, human HSc and normal human skin; page 101

Figure 3-1: Experimental model for formation of human hypertrophic scar in TCR$\beta^{-/-}\delta^{-/-}$, RAG-$1^{-/-}$ and RAG-$2^{-/-}\gamma c^{-/-}$ animals; page 129

Figure 3-2: Morphologic appearance of TCR$\beta^{-/-}\delta^{-/-}$, RAG-$1^{-/-}$ and RAG-$2^{-/-}\gamma c^{-/-}$ mouse autografts and proliferative xenograft scars at day 30 following grafting; page 130

Figure 3-3: Anti-human HLA-ABC antibody staining of proliferative xenograft scar sections from TCR$\beta^{-/-}\delta^{-/-}$, RAG-$1^{-/-}$ and RAG-$2^{-/-}\gamma c^{-/-}$ mice at 30, 60, 120 and 180 days following grafting; page 131

Figure 3-4: Representative images of H & E stained sections of proliferative xenograft scars from TCRβ$^{-/-}$δ$^{-/-}$, RAG-1$^{-/-}$ and RAG-2$^{-/-}$γc$^{-/-}$ mice, human HSc and normal human skin; page 132

Figure 3-5: Representative images of Masson's trichrome stained sections of proliferative xenograft scars from TCRβ$^{-/-}$δ$^{-/-}$, RAG-1$^{-/-}$ and RAG-2$^{-/-}$γc$^{-/-}$ mice, human HSc and normal human skin; page 133

Figure 3-6: Percent increase in proliferative xenograft scar thickness in nude, TCRβ$^{-/-}$δ$^{-/-}$, RAG-1$^{-/-}$ and RAG-2$^{-/-}$γc$^{-/-}$ mice over time; page 134

Figure 3-7: Representative images of α-SMA stained sections of proliferative xenograft scars from TCRβ$^{-/-}$δ$^{-/-}$, RAG-1$^{-/-}$ and RAG-2$^{-/-}$γc$^{-/-}$ mice, human HSc and normal human skin; page 135

Figure 3-8: Representative immunofluorescent images of decorin stained sections of proliferative xenograft scars in TCRβ$^{-/-}$δ$^{-/-}$, RAG-1$^{-/-}$ and RAG-2$^{-/-}$γc$^{-/-}$ mice; page 136

Figure 3-9: Quantification of decorin immunofluorescence in proliferative xenograft scars in nude, TCRβ$^{-/-}$δ$^{-/-}$, RAG-1$^{-/-}$ and RAG-2$^{-/-}$γc$^{-/-}$ mice relative to normal human skin over time; page 137

Figure 3-10: Representative immunofluorescent images of biglycan stained sections of proliferative xenograft scars in TCRβ$^{-/-}$δ$^{-/-}$, RAG-1$^{-/-}$ and RAG-2$^{-/-}$γc$^{-/-}$ mice; page 138

Figure 3-11: Quantification of biglycan immunofluorescence in proliferative xenograft scars in nude, TCRβ$^{-/-}$δ$^{-/-}$, RAG-1$^{-/-}$ and RAG-2$^{-/-}$γc$^{-/-}$ mice relative to normal human skin over time; page 139

Figure 3-12: Representative images of toluidine blue stained sections of proliferative xenograft scars from TCR$\beta^{-/-}\delta^{-/-}$, RAG-$1^{-/-}$ and RAG-$2^{-/-}\gamma c^{-/}$, human HSc and normal human skin; page 140

Figure 3-13: Quantification of mast cells in proliferative xenograft scars from nude, TCR$\beta^{-/-}\delta^{-/-}$, RAG-$1^{-/-}$ and RAG-$2^{-/-}\gamma c^{-/-}$ mice relative to normal skin over time; page 141

List of Abbreviations

ADCC	Antibody-dependent cell-mediated cytotoxicity
APC	Antigen presenting cell
BALB	Bagg albino laboratory bred
BSA	Bovine serum albumin
CD	Cluster of differentiation
CTGF	Connective tissue growth factor
DAPI	4’6-diamidino-2-phenylindole
DETCs	Dendritic epidermal T-cells
ECM	Extracellular matrix
FcR	Fragment crystallizable receptor
FGF	Fibroblast growth factor
FGFR	Fibroblast growth factor receptor
FITC	Fluorescein isothiocyanate
FOX	Forkhead box
FPD	Fibroproliferative disorder
GM-CSF	Granulocyte/macrophage colony stimulating factor
H & E	Hematoxylin and eosin
HLA	Human leukocyte antigen
HSc	Hypertrophic scar(s)
HSCs	Hematopoietic stem cells
HPCs	Hematopoietic progenitor cells
Ig	Immunoglobulin

IFN	Interferon
IGF	Insulin-like growth factor
IL	Interleukin
KGF	Keratinocyte growth factor
KIRs	Killer inhibitory receptors
MHC	Major histocompatibility complex
MMP	Matrix metalloproteinases
mRNA	Messenger ribonucleic acid
NGF	Nerve growth factor
NK	Natural killer
PBMC	Peripheral blood mononuclear cell
PDGF	Platelet derived growth factor
PMN	Polymorphonuclear neutrophil
RAG	Recombination activating gene
RT-PCR	Reverse transcriptase polymerase chain reaction
SMA	Smooth muscle actin
SLRP	Small leucine-rich proteoglycan
TBS	Tris buffered saline
TBSA	Total body surface area
TCR	T-cell receptor
TGF	Transforming growth factor
T_H	T helper
TLR	Toll-like receptor

TNF	Tumor necrosis factor
Treg	T-regulatory
V(D)J	Variable, diversity, joining
VEGF	Vascular endothelial growth factor

1. Introduction

There are three stages of wound healing: inflammation, proliferation and matrix remodeling [1]. After dermal injury a cascade of events is initiated, which, dictates the later outcome of scar development [2]. Infiltration of neutrophils followed by matrix metalloproteinases (MMP) such as collagenase causes excessive tissue loss in the wound, leaving an area of tissue devoid of matrix, which, is subsequently replaced with scar tissue [3]. Over several months, this matrix accumulates and in a normal scar is seen clinically as tissue that is increased in height, firmness, and redness (vascularity). During the maturation phase, the scar begins to stabilize for a variable length of time, typically 6 to 9 months, before it begins to flatten, soften and decrease in redness [4]. The ultimate outcome of wound repair in children and adults is scar formation [5]. The tensile strength of mature scar, at best reaches 80% that of unwounded skin and will never be composed of the high degree of organization present in normal dermal architecture [6]. When this process is protracted and the deposition and accumulation of repair matrix continues a pathological scar is formed.

Hypertrophic scar (HSc) is one type of pathological scar and is defined as a scar that is red, raised and pruritic, but, has not grown beyond the boundary of the original injury [7]. These scars can be linear, for example, following a surgical incision or widespread as is the case with hypertrophic scarring following burn injury. The adverse affects of HSc on form and function, particularly in these patients, are significantly worse than those of normal scars [8]. The treatment of

HSc to date has been largely empirical and remains an area of unmet clinical need [9]. A key challenge facing research of this condition is that HSc are unique to humans and do not normally occur in animals [10]. As such, the discovery of a relevant, *in vivo*, experimental animal model is crucial to further research into the biology of excessive scarring and the molecular events leading to excessive scar formation [11].

This literature review examines hypertrophic scarring in humans and animals models used to study this complex clinical problem. First, we will discuss the structure and function of normal skin and how patients with thermal injury to this organ with subsequent HSc are affected. Second, we will describe the role of the immune system in the pathogenesis of HSc. Third we will appraise the current animal models used to study HSc, introduce the nude mouse model of HSc and describe the use of recombination activating gene (RAG) knockout animals in wound healing research. Finally, we will formulate an experimental design whereby these models may be validated and used to help elucidate the role of immune cells in the formation of HSc.

1.1 Structure and Function of Skin

The skin is the largest organ of the integumentary system and covers the entire surface of the body [Figure 1-1]. It is divided into three layers: epidermis, dermis and hypodermis [12]. It serves numerous functions including protection, sensation, thermoregulation, metabolic and psychosocial [13-16]. The uninjured

skin is an effective physical barrier, which, guards against infection and protects our bodies from mechanical and chemical insults in the external environment [17-19]. As a sensory organ, it perceives touch, temperature and pain. Its regulatory functions maintain homeostasis of the body through hydration, excretion and lubrication via skin appendages such as hair follicles and sweat glands [20, 21]. Metabolically, it is critical for activation of vitamin D and subsequent calcium absorption [22]. Lastly the psychosocial function of skin based on its appearance, which, can vary depending on culture, race and the individual [23]. A newly appreciated function of the skin is as a neuroimmunoendocrine organ mediated by neuropeptides playing an important role in the maintenance of tissue integrity and the regulation of inflammatory and immune responses in the skin [24]. The role of these immune responses as they pertain to wound healing, to be discussed later, may be one of the keys to understanding HSc formation.

The skin is able to perform all of these functions by way of the integration of the epidermis and dermis, which, transduce energy to provide information to the brain for appropriate responses. The epidermal cells are predominantly keratinocytes (95-97%) and adnexal cells, but, also include melanocytes, Langerhans cells and Merkel cells. The dermal cells include endothelium, smooth muscle, fibroblasts, nerve cells, mast cells, histiocytes and piloerector muscles. However, most of the dermis is made up of extracellular matrix (ECM) (collagens, elastin, reticulin), which, provides the bulk of the skin's mechanical strength as well as support for the various skin appendages. In contrast, the epidermis contains very little ECM,

most of which is carbohydrate polymers and lipids in the stratum corneum, which, provide a barrier to aqueous fluids [25, 26]. The hypodermis is the innermost and thickest layer, however, it is generally not considered a true component of the skin. The adipose tissue in the hypodermis serves a shock absorber, insulation for the body and storage of energy [5].

In patients with deep dermal injury from burns this highly organized and complex structure is destroyed. These deeper wounds, which result in a prolonged immune response, are prone to HSc and contracture, which, lead to an impairment in function [27, 28]. However, before we can begin to consider the different components of the immune system and their role in HSc formation we must first clearly describe HSc as fibroproliferative disorder (FPD) and highlight the burden of disease suffered by burn patients with this clinical problem.

1.2 Hypertrophic Scarring in Humans

1.2.1 Hypertrophic Scars and Keloids

Fibroproliferative disorders are common and serious disorders, which involve a diversity of human tissues including cirrhosis and fibrosis of the liver, idiopathic pulmonary fibrosis, myelofibrosis, atherosclerotic disease of vasculature and multiorgan/tissue systemic diseases including scleroderma and rheumatoid arthritis [29-32]. HSc and keloids are FPD characterized by excessive deposition of collagen in the dermis and subcutaneous tissues [3] [Figures 1-2, 1-3]. The exuberant scarring typically results in disfigurement, pruritus and pain [33].

Despite the similarities between these two disorders there are important clinical and cellular differences [4] [Tables 1-1, 1-2]. Clinically, HSc remain within the confines of the original scar border, whereas keloids will invade the adjacent normal tissue [34]. HSc also generally arise within one month of tissue injury, grow continuously for several months, and then gradually regress, to varying degrees. Keloids on the other hand appear later following injury and will gradually and indefinitely proliferate [35, 36]. Nevertheless, scar classification schemes include HSc and keloids as various degrees of scar within a continuum [38]. To facilitate relevant discussion and treatment of these disorders the International Advisory Panel on Scar Management has put forth standard scar classification terminology [7] [Table 1-3].

As these scars shrink, contractures arise resulting in further disfigurement, reduction in range of motion and impairment of function. A key distinction must be made between wound contraction whereby the edges of an open wound are pulled together and is part of the normal healing process, and scar contracture, a pathological process that occurs in an already healed scar as it matures [10, 37].

1.2.2 The Burden of Disease

HSc can impose great morbidity for patients, particularly following thermal injury [29-31]. In Canada, thermal injuries account for a significant number of hospitalizations annually [38, 39]. In the province of Alberta, hundreds of patients are hospitalized each year, most of which are younger than 45 years of

age [38, 39]. While care for the critically ill has improved the overall mortality rate for those with significant thermal injury, burn patients still experience a prolonged period of hospitalization and rehabilitation [38-41]. This translates into a considerable time off of work for patients with thermal injuries greater than 30% of the total body surface area (TBSA).

1.2.3 The Clinical Problem

During the prolonged inflammation associated with slowly healing dermal wounds following a burn, HSc develops with a very high frequency [41-44]. This is potentially due to a systemically upregulated immune response that may influence both the quantity and phenotype of inflammatory cells and mediators that migrate to the wound area, causing an exaggerated inflammatory phase of wound healing. The rehabilitative phase following a major thermal injury is limited mostly by functional and cosmetic sequelae imposed by HSc [45], including a reduction in range of motion of the extremities and intense pruritus and heat intolerance. These symptoms will continue until remodeling of the HSc has occurred [40, 41, 45].

HSc and keloids are known to respond to current forms of therapy, including pressure garments, topically applied silicone and intralesional steroids; however, this occurs slowly over months or years, and often incompletely [29, 42, 46-49]. While the events that lead to HSc have been extensively studied, the pathogenesis of this condition is still not well understood, making treatment difficult and

largely empirical. Before novel advances in therapy for these disorders can be implemented a broader understanding of the processes leading to their development must be realized. Recent research has shown that immunological reactions are likely to be involved in HSc etiology, however, the exact role of inflammatory response has not been studied in detail and remains to be elucidated.

1.3 The Role of the Immune System in Wound Healing

The immune system is divided into humoral and cellular defenses. While little is known regarding any regulatory role that humoral immunity may play, the cellular immune system (neutrophils, macrophages, lymphocytes) is known to play a major role in the regulation of various phases of wound healing through the secretion of signaling molecules, such as cytokines, lymphokines, and growth factors [50, 51]. Considering the inflammatory response following thermal injury is characteristically increased compared to normal wound healing, it is conceivable that immune cells may play an important contributing factor in post-burn wound healing complications [52].

In normal wound healing, neutrophils are the first immune cells to arrive, approximately 24 hours after injury, and function to débride the wound. Macrophages follow at 48 to 96 hours, as the number of neutrophils begins to decline, and become the predominant wound phagocyte [51]. Macrophages play a critical role in concluding débridement and secreting cytokines and growth factors that activate other macrophages, regulate fibroblast chemotaxis initiating

proliferation and collagen synthesis and activation of lymphocytes [51]. The role of B-lymphocytes has received very little attention; however, given the absence of B-cells in scar biopsies and any activating lymphokines detected in the wound environment, B-cells are unlikely to play a significant role in wound healing based on the current literature [53, 54, 55].

1.3.1 T-cell Responses

T-lymphocytes develop from hematopoietic stem cells (HSCs) in the bone marrow that travel to the thymus where they mature [56]. They can be further divided according to their surface marker proteins into cluster of differentiation (CD)8^+ cytotoxic T-cells and $CD4^+$ helper T-cells [57]. Following tissue injury, they migrate into the wound on the fifth day and peak at day seven [5]. T-cells are not required for initiation of wound healing, which, can in fact progress without their presence, but, are essential for a normal healing outcome [58]. Evidence to support this includes an inhibitory effect on wound healing parameters such as wound breaking strength and reparative collagen synthesized at the wound site in athymic nude mice that lack a normally developed T-cell system compared to thymus bearing mice of the same background [59]. Furthermore, artificial depletion, specifically of $CD4^+$ T-cells in rat wounds, results in the same inhibitory effects on wound healing while depletion of $CD8^+$ T-cells improves collagen content and wound strength providing further clarification that $CD4^+$ T-cells upregulate wound healing while $CD8^+$ T-cells have a downregulatory role [55, 60, 61].

The $CD4^+$ helper T-cells can be further characterized into two subsets based on specific cytokine profiles [51] [Figure 1-4]. Immature $CD4^+$ T-cells have the potential to differentiate into inflammatory T helper (T_H)1 cells or helper T_H2 cells. T_H1 cells are delineated by their expression of interleukin (IL)-2, interferon (IFN)-γ and tumor necrosis factor (TNF)-β. These cytokines are generally involved in cellular and humoral immunity and activate macrophages. T_H2 cells express IL-4, IL-5, IL-6, IL-10 and IL-13 and are involved in humoral immunity and B-cell activation. Both subsets secrete IL-3 and granulocyte/macrophage colony stimulating factor (GM-CSF) [52, 62]. T_H2 cytokines have been shown to regulate stromal cell and fibroblast activation, myofibroblast differentiation and proliferation as well as matrix accumulation and scarring [63]. This is supported by measurement of intracellular cytokine synthesis of circulating T-cells from blood samples taken from burn patients with HSc, which, demonstrates an increase in fibrogenic T_H2 cytokines suggesting that the development of HSc is associated with a polarized T_H2 systemic response to injury [63].

1.3.2 Fibrocyte Involvement

The fibrocyte is a bone marrow-derived cell that co-expresses HSC antigens, markers of monocyte lineage and fibroblast products [64-68]. This cell develops from circulating $CD14^+$ peripheral blood mononuclear cell (PBMC)s [66, 67, 69] and may represent a committed progenitor of hematopoietic lineage originating from the multipotent precursor present in the $CD14^+$ fraction [70] and in the bone

marrow [70, 71, 72] [Figure 1-5]. Evidence from several studies suggests that fibrocytes contribute to the new population of fibroblasts and myofibroblast-like cells that emerge at the wound site during normal or aberrant wound healing [64, 66, 67, 68, 72]. $CD14^+$ PBMCs, from which fibrocytes develop in culture, show phenotypic and functional characteristics of multipotent precursors that have been found to give rise to endothelial cells, epithelial cells, monocytes, dendritic cells, fibroblasts, osteoblasts, adipocytes or neuronal cells under permissive conditions [68, 70, 73]. The signaling pathways involved in development and differentiation of fibrocytes from the $CD14^+$ precursors are incompletely understood, but, several factors have been identified that may promote or inhibit the process. Stimulation of $CD14^+$ PBMCs with transforming growth factor (TGF)-β1, platelet derived growth factor (PDGF) and T_H2 cytokines, IL-4 and IL-13, promote the differentiation into fibrocytes [66, 67, 69, 74]. IFN-α2b has been shown to inhibit TGF-β1 induced differentiation of fibrocytes [75]. Phenotypic changes have been observed both in vitro and in vivo following differentiation of fibrocytes into cells resembling fibroblasts and myofibroblasts [68]. These changes include expression of α-smooth muscle actin (SMA), a contractile protein responsible for ECM contraction and increased production of collagens [66].

In FPD, the major source of ECM is represented by resident fibroblasts and myofibroblasts. However, fibrocytes and fibrocyte-like cells appear to provide an additional, renewable source of fibroblast and myofibroblast-like cells at the site of injury during wound healing [18, 68, 76-78]. Fibrocytes are therefore

important because their accumulation at the site of injury accelerates wound repair and inhibition of their development reduces the efficiency of wound healing [76, 77]. These observations from in vivo animal models have been confirmed in patients with post-burn HSc [68]. Elevated levels of TGF-β1 have been detected in the peripheral blood of patients with post-burn HSc up to twenty days post-burn suggesting a possible factor responsible for the maturation of fibrocytes from their circulating precursors [79]. In these patients, systemic administration of IFN-α2b significantly improved scar quality and coincided with a dramatic decrease in the number of fibrocytes at the wound site suggesting fibrocytes play an important role in the aberrant wound healing that occurs following thermal injury [75].

1.3.3 Role of γδ T-Cell Receptor-Bearing Dendritic Epidermal T-Cells

Following thermal injury, a unique subset of T-cells expressing γδ T-cell receptor (TCR) have been isolated. These cells can be divided into two subtypes, lymphoid, present in only small amounts in the periphery and epithelial, which are relatively abundant in the skin [80, 81]. There are several characteristics that distinguish γδ dendritic epidermal T-cells (DETCs) from αβ T-cells [82] [Table 1-4]. The dendritic morphology of these γδ T-cells puts them in constant contact with many different neighboring epidermal cells, suggesting they interact functionally [81, 83] [Figure 1-6]. As a result, epithelial γδ T-cells are activated and able to recognize self-antigens expressed on neighboring keratinocytes as a result of stress or damage [84]. Following activation, DETCs secrete growth

factors including keratinocyte growth factor (KGF)-1 also known as fibroblast growth factor (FGF)-7, KGF-2 and insulin-like growth factor-1 (IGF-1), which, induce keratinocyte proliferation and maintain keratinocyte viability [84, 86]. This function correlates with the location of DETCs in the epidermal compartment, where they can rapidly respond to damaged keratinocytes during wound healing and suggests a novel role for DETCs in keratinocyte homeostasis and wound healing [83].

DETCs are also thought to play an important role in the body's response to burns because they produce a number of chemokines, which, recruit other immune cells (neutrophils/monocytes) at the time of injury [87, 88]. While the role of DETCs in burn injury continues to be elucidated it is known that γδ T-cell recruitment and activation are suppressed following thermal injury leading to delayed healing at the burn injury site [81, 82].

1.3.4 Role of Natural Killer Cells

Natural killer (NK) cells are large granular lymphocytes of the innate immune system and are derived from $CD34^+$ hematopoietic progenitor cells (HPCs) [56, 89, 90] [Figure 1-7]. The cell surface phenotype defining human NK cells on flow cytometry shows an absence of the pan T-cell marker CD3 and expression of CD56, a neural cell adhesion molecule [91]. According to the intensity of CD56 expression, NK cells are classified into two populations; $CD56^{dim}$ and $CD56^{bright}$ [92, 93]. $CD56^{dim}$ cells make up 90% of circulating NK cells and play a role in

antibody-dependent cell-mediated cytotoxicity (ADCC). $CD56^{bright}$ cells comprise the remaining 10% and predominate in lymph nodes and sites of inflammation, where they are capable of producing abundant cytokines and have an immunoregulatory function [92, 93]. IFN-γ is considered the prototypic NK cell cytokine and its production is known to shape the T_H1 immune response [94]. In vitro differentiation of $CD56^{bright}$ to $CD56^{dim}$ NK cells has been shown to be dependent on cell contact with dermal fibroblasts mediated through fibroblast growth factor receptor (FGFR)-1 and can be inhibited monoclonal antibody to FGFR-1 [95, 96]. Expansion of $CD56^{bright}$ NK cells in peripheral tissue suggests fibroblasts may provide a suitable microenvironment for NK cell maturation at sites of inflammation [96].

NK cells are activated by cytokine signaling the presence of viral pathogens, binding of antibodies to the fragment crystallizable receptor (FcR) in ADCC and activating receptors [56]. The numerous activating and inhibitory receptors are capable of binding major histocompatibility complex (MHC) class 1 molecules, MHC class 1-like molecules and molecules unrelated to MHC [94]. Killer inhibitory receptors (KIRs) transmit an inhibitory signal when MHC class I molecules are recognized on a cell surface preventing NK cell killing. While the function of NK cells in defending the body against early tumor development and virally infected cells is well established their involvement in inflammation and wound healing has received little attention [62, 97].

NK cells are present mostly during the early inflammatory phase of wound healing, appearing by twenty four hours following tissue injury and peaking on the third day afterwhich their numbers decline rapidly to negligible levels between seven and fourteen days after injury [98, 99]. Their presence is thought to be related to their role in defence against microorganisms present at the site of tissue injury [98]. However, a regulatory function of polymorphonuclear neutrophils (PMN)s mediated by PMN-activating factor has been reported and is supported by a rapid decline in NK cell numbers following the period of neutrophil predominance in wounds devoid of contamination [100].

1.3.5 Role of Natural Killer T-cells

NKT cells are a rare subset of lymphocytes, comprising 1-2% of all lymphocytes that participate in both innate and adaptive immune responses [56]. NKT cells express an αβ TCR and CD3 similar to conventional T-cells, however, they differ from conventional T-cells in that their TCRs are sharply limited and they recognize glycolipids and lipids presented by CD1d molecules rather than peptide antigens presented on MHC molecules [101]. NKT cells also express the NK cell marker CD56 on their surface and produce granzyme and IFN-γ similar to NK cells [101]. They differ from NK cells in that they also express IL-4 and IL-13, cytokines associated with T_H2 responses [56].

NKT cells have been shown to participate in burn-induced T-cell immunity in a murine dorsal scald injury model mediated by CD1d signaling, which, contributes

to the production of immunosuppressive cytokines and the suppression of systemic T-cell responses [102, 103]. Burn injury correlated with increased production of IL-4, produced almost exclusively by the NKT cell population and decreased production of IFN-γ [102, 103]. Inhibition of NKT cell activation by anti-CD1d antibody prevented this immune suppression [102, 103]. These findings suggest that defects in T-cell responsiveness following a severe burn are not the consequence of global immunosuppression, but, rather represent an active form of CD1d/NKT cell-dependent immunological tolerance [104].

1.3.6 Role of Mast Cells

Mast cells are derived from HPCs, expressing CD34, but, do not ordinarily circulate in their mature form [56, 105]. Instead, the differentiation and maturation of mast cells occurs locally, after migration of their precursors to the vascularized tissues, usually the dermis, where they will ultimately reside [105, 106] [Figure 1-8]. The role of mast cells as key effector cells in immunoglobulin (Ig)E-associated immune responses and allergic disorders is well documented [107-110], however, they are also a pivotal cell involved in the events of wound healing [106].

Mast cells participate in and influence wound healing at every step, including mediating the early inflammatory response, collagen formation and reepithelialization, vascular permeability and angiogenesis and matrix remodelling [106-108, 111-113]. Mast cells are the source of several growth

factors and mediators such as nerve growth factor (NGF), PDGF, vascular endothelial growth factor (VEGF), FGF-2, histamine, and tryptase, which induce proliferation of epithelial cells and fibroblasts [114-117]. Skin mast cells have also been shown to produce mast cell α-chymase and mast cell-derived IL-4, which, have been shown to be active in tissue matrix remodeling and contribute to the wound cytokine network resulting in stimulation of fibroblast proliferation [118, 119]. Impaired wound healing in mast cell deficient mice further support the role of these cells in the maintenance of tissue homeostasis following injury [120].

1.3.7 Role of Langerhans Cells

Langerhans cells are stellate shaped dendritic cells located in epidermis and comprise 2-4% of the total epidermal cell population [121, 122] [Figure 1-9]. They are derived from blood-borne $CD34^+$ HPCs in the bone marrow and express FcRs, complement receptors and MHC class II molecules [122-125]. In non-inflamed skin, immature Langerhans cells reside in the epidermis, however, upon encountering exogenous antigens they become active participants in the cutaneous immune response [122]. Following recognition and processing of cutaneous antigens, Langerhans cells mature and migrate from the epidermis to the T-cell zone of cutaneous draining lymph nodes, where they present the processed antigens to naïve resting T-cells or by transferring skin-acquired antigens to resident lymph node dendritic cells for presentation [126, 127]. As such they serve as a link between the skin and the secondary lymphoid organs enabling T-

cells to detect antigens from the skin that would not have reached the lymph nodes.

The increased density of Langerhans cells have been found in both the epidermis and dermis of HSc when compared to nomotrophic scar and normal skin [128]. This increase in cell density is associated with an increased expression of epidermal IL-4, which, can stimulate fibroblasts to produce ECM [128]. Release of IL-1α, a stimulator of collagenase release from activated Langerhans cells, has also been found to be significantly reduced in the epidermal area of HSc [129].

Macrophages, T-cells, fibrocytes, NK cells, NKT cells, mast cells, Langerhans cells and keratinocytes are directly and indirectly involved in the activation of (myo)fibroblasts, which, in turn produce excess ECM [130, 131] [Figure 1-10]. The presence and close proximity of activated T-cells and APCs of various phenotypes in the epidermis and dermis of HSc tissues provides evidence of a local immune response involved in the pathogenesis of the disorder. The intricate interactions in scar tissue via cell-cell contact and secreted products are difficult to mimic in in vitro cell systems, thereby largely hampering extrapolation to a human patient. However, animal models in conjunction with observations in patients can help to define which molecular and cellular features are implicated in HSc formation in humans. A reliable animal model is therefore essential to explore the hypotheses pertaining to the role of immune cells in wound healing.

1.4 Animal Models of Hypertrophic Scar

The lack of an animal model in which scars form in vivo has hampered the study of the pathophysiology of hypertrophic scarring [132-134]. The development of an effective animal model for studying HSc is challenging because animals do not normally form these types of scars [135]. However, an animal model of HSc is important both for studying the molecular events leading to HSc, but, also for evaluating the effectiveness of therapeutic modalities [135]. The ideal model would enable the research of pathophysiology, histological changes and molecular events during time as well as allow for testing of prophylactic and therapeutic treatments for humans [136]. The most prevalent animal models currently used in HSc research include the rabbit ear model, porcine models and athymic rodent models. There are deficiencies associated with each, therefore it is worthwhile to appraise these and determine which is most relevant to the study of HSc.

1.4.1 Rabbit Ear Model

It has been noted that surgical scars would last for months following wounding on the ears of rabbits [137]. Following these observations, the adult female New Zealand white rabbit was shown to form reproducible, cutaneous HSc lasting up to 280 days [138]. These scars are similar to human HSc both grossly and histologically [137]. Many researchers have now employed this model to test the efficacy of several wound-modulating agents [137-141]. Decreased scar elevation has been reported following inhibition of prolyl 4-hydroxylase and topical application of corticosteroids, IFN-α2b and Allium cepa, an onion extract with

anti-proliferative and mast cell stabilizing effects [137-141]. The application of the profibrotic growth factors and cytokines PDGF-BB, TGF-β1, and FGF-2 also significantly elevated scars in both epithelial and dermal layers following a single intradermal administration [142] demonstrating that scars created using this model may respond in a similar fashion to human HSc. Decreased hypertrophic scarring incidence in older compared to younger rabbits further reflects similarities in changes seen in humans [143]. However, the rabbit ear model relies on the creation of a wound overlying cartilage that also becomes thickened and shows marked proliferation [137] in conjunction with the overlying HSc that develops. Evidence of irregular, disorganized chrondrocyte proliferation with increased ECM compared to normal cartilage serve as a reminder that while this model is of value for evaluating treatments for HSc it is markedly different from thermal injury causing HSc in humans and as such may not be appropriate in investigating the mechanism of this condition. The use of rabbits is also more expensive, requires more space, food and water than small mammal wound healing models.

1.4.2 Porcine Model

To date, the female red Duroc pig is the animal with skin most similar to humans in terms of its epidermal thickness, dermal-epidermal thickness ratio, hair follicle pattern, blood vessels and dermal collagen and elastic content [144, 145] [Figure 1-11]. Healing of wounds in pigs has been shown to be similar, but, not identical, to healing in humans and as a result deep dermal wounds at specific sites have been used to create HSc that lasts up to five months [145-148]. This model was

further validated when the immunohistochemical pattern of decorin, versican, and IGF-1 as well as equivalent numbers of collagen nodules and myofibroblasts in Duroc pig and human HSc was shown to be similar [149, 150]. Like the rabbit ear model, porcine models have been used to study the potential of treatments for HSc [145, 149], but, given the nature of porcine skin and the depth of wounds that can be created, this model also lends itself to the application of studies investigating wound and burn dressings [145]. One obvious disadvantage to porcine models is the size of the animals used, especially if the duration of the study is longer than a few months. With this added size comes significant cost in terms of obtaining, storing and feeding these animals as well as difficulties in their handling.

1.4.3 Mechanical Load Model

In 2007 Aarabi and colleagues demonstrated a model of HSc in C57/BL6 mice using a biomechanical loading device [150]. A superior and inferior linear incision was first placed on the dorsum of the mouse. These wounds were closed primarily with sutures removed at four days postoperatively. Following this two loading devices were sutured to the dorsum of the animals and serially distracted by 2 mm on postoperative day four and 4 mm every other day thereafter [150] [Figure 1-12]. The inferior wound acted as an internal control in which the loading device was not activated. Scar biopsies harvested over time demonstrated histological features consistent with human HSc including an increase scar thickness, loss of rete pegs, adnexal structures and hair follicles, whorled

arrangement of collagen bundles parallel to the skin surface, increased mast cell density, hypervascularity and hypercellularity [150]. Formation of HSc in this model is thought to be mediated by inhibition of cellular apoptosis though an Akt-dependent mechanism. The mechanical load model is limited in that using force to generate scar does not specifically address the cells involved in HSc formation. The animals used in this study are also immunocompetent, which does not facilitate the use of human skin to generate HSc.

1.5 Nude Mouse Model of Human Hypertrophic Scar

Mice homozygous for the null nu allele, forkhead box (FOX)N1 nu/nu, have a rudimentary thymus not populated by lymphoid progenitors and are unable to produce mature, functional T-cells [151]. The thymic epithelial cells required for T-cell maturation fail to differentiate as a result of the FOXN1 mutation, a gene whose pleiotropic effects also result in macroscopic hairlessness or nudity, giving rise to the nickname nude mice. In actuality, nude mice develop normal hair follicles and produce hair shafts, but, lack a fur coat due to twisting and coiling of hair fibers within the follicle infundibulum [152-155]. The failure of hair shafts to penetrate the epidermis gives the misleading impression that nude mice are completely hairless, however, sparse hair growth can eventually be seen at the head and by postnatal day ten and eventually on other parts of the trunk [152-155] [Figure 1-13]. This phenomenon is particularly prominent in the C57/BL6 background nudes [152].

Nude mice are able to form mature B lymphocytes, as these cells mature in the bone marrow, however, due to their lack of T-cells they are unable to mount most types of immune responses including cell-mediated immune responses (requires $CD4^+$ and/or $CD8^+$ T-cells), delayed type hypersensitivity responses (requires $CD4^+$ T-cells), killing of virus infected or malignant cells (requires $CD8^+$ cytotoxic T-cells) and most importantly graft rejection (requires $CD4^+$ and $CD8^+$ T-cells) [155-160]. As a result, they have become widely used in immunological, dermatological, oncological and transplantation research, but, only under pathogen-free conditions due to their susceptibility to viruses and other microorganisms.

Nude mice and rats have been used extensively in wound healing research and in particular with respect to the pathophysiology of keloids and HSc [162-177] [Table 1-5]. Initial experiments involved these mice as hosts for both subcutaneous and cutaneous transplantation of human keloid and HSc tissues [163-165, 167-171]. The major disadvantages with this methodology include incomplete revascularization of transplanted tissues, lack of an epidermal-dermal interaction with subcutaneous transplants, HSc and keloid regression following transplantation of scars and transplantation of tissue representing the terminal stages of the disorder, precluding study of the molecular processes and initiating factors leading to the condition. Despite improvements in technique and revascularization, these immune deficient animals continue to demonstrate

regression of HSc following xenografting, supporting a systemic immune response theory of pathogenesis [34, 174].

Normal human skin was then grafted onto the backs of nude mice and following revascularization was scalded to form HSc. However, it was noted that even without the application of thermal injury, the mice developed thick, red, raised HSc [177]. This model was superior to those preceding it in that the skin grafts were well vascularized, an anatomic epidermal-dermal interaction was present and the process of HSc formation could be followed clinically and at the cellular level as the wounds healed. HSc persists for an average of 135 days with this model and on histological examination dense collagen fibers and swirl-shaped collagen nodules are seen, typical of changes seen in HSc [177].

One criticism pertaining to this and nearly all murine models of HSc is with regards to the anatomy of their skin relative to humans and the presence of the panniculus carnosus, a layer deep to the dermis that allows these animals to heal by relying primarily on wound contraction, in contrast to reepithelialization of partial thickness wounds as observed in human and pig wounds [143, 177].

There is no ideal animal model for HSc; rather, investigators should choose models that will be the most useful in answering questions regarding the various aspects of this clinical problem. The increasing knowledge base of HSc pathogenesis strongly suggests a systemic immune component as the underlying

cause. An in vivo animal model that shows promise in this regard is the RAG knockout mouse.

1.6 RAG Knockout Mouse Model

As nude mice age, small numbers of $CD4^+$, $CD8^+$ and γδ-DETCs appear to develop and are detectable in their peripheral blood samples [178, 179]. This "leakiness" has made nude mice somewhat less popular, especially with the availability of genetically engineered knockout mice that possess complete defects of the immune system. Gene knockout technology was developed by combining the introduction of mutations into mammalian cells by homologous recombination with techniques of embryonic stem cell culture [180] [Figure 1-14]. By knocking out the RAG genomic locus, which, activates V(D)J (variable, diversity, joining) region recombinase activity, somatic recombination, a process essential to Ig and TCR gene recombination, is inhibited [181]. As a result, functional genes encoding for Ig and TCRs are not formed, leading to arrest of lymphocyte differentiation at a very early stage and non-functional B and T cells [182-184].

In recent years, the *in vivo* function of over one hundred proteins involved in the wound repair process have been delineated through the use of genetically engineered knockout mice [183]. Examples include delayed wound reepithelialization using the FGF-2 knockout mouse, retarded healing in the TGF-β1 knockout mouse and severe deficits in cutaneous repair in the IL-6 knockout mouse [185-187]. RAG-$1^{-/-}$ knockout mice were also used in a study measuring

proinflammatory cytokine response following 25% TBSA scald injury. Compared to B and T-cell depleted wild type mice, the RAG-1$^{-/-}$ mice displayed a far more vigorous inflammatory cytokine response, suggesting that cells of the adaptive immune system play an active role in the innate immune system response to burn injury [188]. Further study identified that naturally occurring $CD4^{+}$ $CD25^{+}$ regulatory T-cells (Treg) are responsible for suppression of proinflammatory reactivity, mediated by control of toll-like receptor (TLR)-2 and TLR4 [188, 189]. However, to date, there have been no studies using RAG knockout mice to study the role of innate and adaptive immunity and the contribution of immune cells in regulating HSc formation.

1.7 Formulation of Thesis

This review of the literature has revealed that HSc are a clinical problem whose pathophysiology remains enigmatic and that a key challenge for studying the events leading to HSc is the lack of a relevant and practical animal model. It is our hypothesis that human FPD such as HSc arise from prolonged and excessive activation of specific, unique fibroblasts in local tissue. These cells stimulate the recruitment of bone marrow derived inflammatory cells that extend the magnitude and duration of inflammation and subsequent fibrosis by excessive and prolonged production of systemic inflammatory growth factors. This milieu of growth factors and activated systemic immune cells leads to a bone marrow-derived cellular immune response, which, contributes substantially to the abnormal excessive fibrotic healing in injured tissues that critically impairs the function of

injured tissues and organs. By understanding the cells resident in tissues, which, are important in initiating the process and determining the mechanism by which they activate local and systemic innate and adaptive components of the immune system, we can demonstrate their role in the development of tissue fibrosis and afford the development of novel approaches to prevention and therapy of FPD in the skin and possibly other tissues.

The first objective of this study is to determine whether transplanting human skin onto nude mice results in scars that are similar grossly and histologically to that seen in humans. In order to further validate this model, 2 x 1.5 cm biopsies of human split thickness abdominal skin were grafted onto the backs of twenty nude mice and compared to both autografts and normal skin controls. Four wild-type Bagg albino laboratory bred/c (BALB/c) mice were also be grafted with split thickness human skin in order to clinically observe the effects of rejection in immune replete animals. Wounds will be digitally photographed weekly to document healing and scar formation. Nude mice autografted with full thickness skin were euthanized at 30 and 60 days postoperatively. Nudes grafted with split thickness human skin were euthanized at 30, 60, 120 and 180 days postoperatively. Wild type BALB/c mice were euthanized at 30 days. Scar evaluation were performed by blinded, independent assessment of scar photographs by five scar evaluators using a modified Manchester Scar Scale. Normal mouse skin, autograft and proliferative xenograft scar thickness measurements were taken at each time point. Engraftment of human skin was

confirmed by direct immunofluorescence for anti-human human leukocyte antigen (HLA)-ABC antigens present on all nucleated human cells. Histological analysis consisted of hematoxylin and eosin, Masson's trichrome, toluidine blue and picrosirius red staining and immunohistochemistry for α-SMA expressing myofibroblasts, decorin and biglycan expression.

The second objective of this study was to replicate the experimental model outlined above using TCR$\beta^{-/-}\delta^{-/-}$, RAG-$1^{-/-}$ and RAG-$2^{-/-}\gamma c^{-/-}$ knockout mice in order to refine our model of HSc formation and to describe morphologic, histologic and cellular changes that occur in scars with the deletion of immune cell subsets. As previously mentioned, RAG knockout mice lack the genes to correctly assemble B and T cell receptors, without which, mature B and T cells do not develop. RAG-$1^{-/-}$ knockout mice are deficient in B and T cells and RAG-$2^{-/-}$ $\gamma c^{-/-}$ double knockout mice additionally lack NK cells [182]. Xenotransplantation studies have shown that NK and Natural Killer T (NKT) cells may contribute substantially to the cell-mediated immune response involved in tissue rejection, however, their role can only be unmasked when the intense T-cell response is withdrawn. Previously, burn injury in these animal models has been used to determine which adaptive immune cell type(s) has the capacity to control the innate inflammatory responses after burn injury. These animals therefore represent useful models for the study of immune cells involved in the pathogenesis of HSc. TCR$\beta^{-/-}\delta^{-/-}$ mice cannot produce any T cells as a result of β and δ TCR gene knockout [190, 191]. These genes are critical for productive T-

cell receptor rearrangement and thymocyte development and differentiation [190, 191]. These animals may represent a more complete T-cell deficient mouse, thereby reducing the potential of an activated T-cell rejection response that may be encountered in aging nude mice that could contribute to scar formation.

1.8 Tables

Table 1-1: Distinction between HSc and keloids based on clinical features [4]

	Hypertrophic Scar	Keloid Scar
Overall incidence	More common	Less common
Association with race	No	Increasing association with increasing racially determined pigmentation
Always preceded by injury	Yes	No
Anatomical association	No	Can occur anywhere but areas particularly prone are earlobes, deltoid region, and presternal region
Extent of growth	Confined to area of original injury	Extends into surrounding tissue
Resolves spontaneously	Most will eventually resolve	No
Recurs after surgery	No	Yes
Associated with contracture	Yes	No

Table 1-2: Cellular differences between fibroblasts derived from HSc and keloids compared to normal skin [4]

	HSc Fibroblasts	KSc Fibroblasts
Proliferation rate	Normal	↑ ↑
MMP-2	↑	↑
MMP-9	↓ ↓	↓ ↓
Collagen synthesis	↑	↑ ↑
Decorin synthesis	↓ ↓	Normal
Versican synthesis	↑	↑
Biglycan synthesis	↑	↑
Elastin synthesis	Normal	↑
TGF-β production	↑ ↑	↑ ↑

HSc, hypertrophic scar; KSc, keloid scar; MMP, matrix metalloproteinase.

Table 1-3: The International Advisory Panel on Scar Management Scar Classification [7]

Mature scar—A light-colored, flat scar.
Immature scar—A red, sometimes itchy or painful, and slightly elevated scar in the process of remodeling. Many of these will mature normally over time and become flat, and assume a pigmentation that is similar to the surrounding skin, although they can be paler or slightly darker.
Linear hypertrophic (e.g., surgical/traumatic) scar—A red, raised, sometimes itchy scar confined to the border of the original surgical incision. This usually occurs within weeks after surgery. These scars may increase in size rapidly for 3–6 months and then, after a static phase, begin to regress. They generally mature to have an elevated, slightly rope-like appearance with increased width, which is variable. The full maturation process may take up to 2 years.
Widespread hypertrophic (e.g., burn) scar—A widespread red, raised, sometimes itchy scar that remains within the borders of the burn injury.
Minor keloid—A focally raised, itchy scar extending over normal tissue. This may develop up to 1 year after injury and does not regress on its own. Simple surgical excision is often followed by recurrence. There may be a genetic abnormality involved in keloid scarring. Typical sites include earlobes.
Major keloid—A large, raised (>0.5 cm) scar, possibly painful or pruritic and extending over normal tissue. This often results from minor trauma and can continue to spread over years.

Table 1-4: A comparison of αβ and γδ T-cells [82]

	αβ T-cells	γδ T-cells
Phenotype	Small agranular	Large granular
Location	Primary and secondary lymphoid tissues, circulation	Mucosal epithelial (skin, gut, reproductive organs)
Thymic selection	Yes	Yes
TCR[a]	Heterodimer, α and β chains 45–50 variable segments. Potential diversity ~10^{16} Broad repertoire	Heterodimer, γ and δ chains two to five variable segments. Potential diversity ~10^{18} via D segment rearrangement. Specific repertoire for bacterial/viral antigens and autoantigens
CD4, CD8 subsets	Yes	No. CD8 only on activated cell
Antigen recognition	MHC[b] restricted. Requires APC[c]	MHC and APC independent Non-peptide ligands (i.e., phospholipids)
Activation kinetics	Hours to days	Rapid (minutes to hours)

[a] TCR: T-cell receptor.
[b] MHC: major histocompatiability class.
[c] APC: antigen presenting cell.

Table 1-5: Summary of the objectives, methodologies and conclusions of three studies utilizing the athymic mouse model [175]

	Gadson et al.[15]	*Bettinger et al.*[16]	*Chau et al.*[17]
Study objective	To examine the differences between glucocorticoid receptors found in keloid and normal dermis fibroblasts using fibroblast cell culture.	To determine the sensitivity of fibroblasts from keloid and normal dermis after addition of exogenous transforming growth factor-*β*.	To determine the response of keloid fibroblasts to the addition of exogenous tamoxifen.
Methodology	The number of fibroblast glucocorticoid receptors and their characteristics from keloid and normal dermis fibroblast culture were determined.	Exogenous TGF-*β* was added to both keloid and normal fibroblast cultures.	Exogenous tamoxifen was added to keloid fibroblast cultures.
Conclusion	No differences in receptor number or characteristics were found between the fibroblasts from keloid tissue or normal dermis.	The keloid fibroblast culture showed an increase in absolute collagen synthesis compared with the normal fibroblast culture.	Tamoxifen was observed to downregulate production of TGF-*β* in the keloid fibroblasts.

1.9 Figures

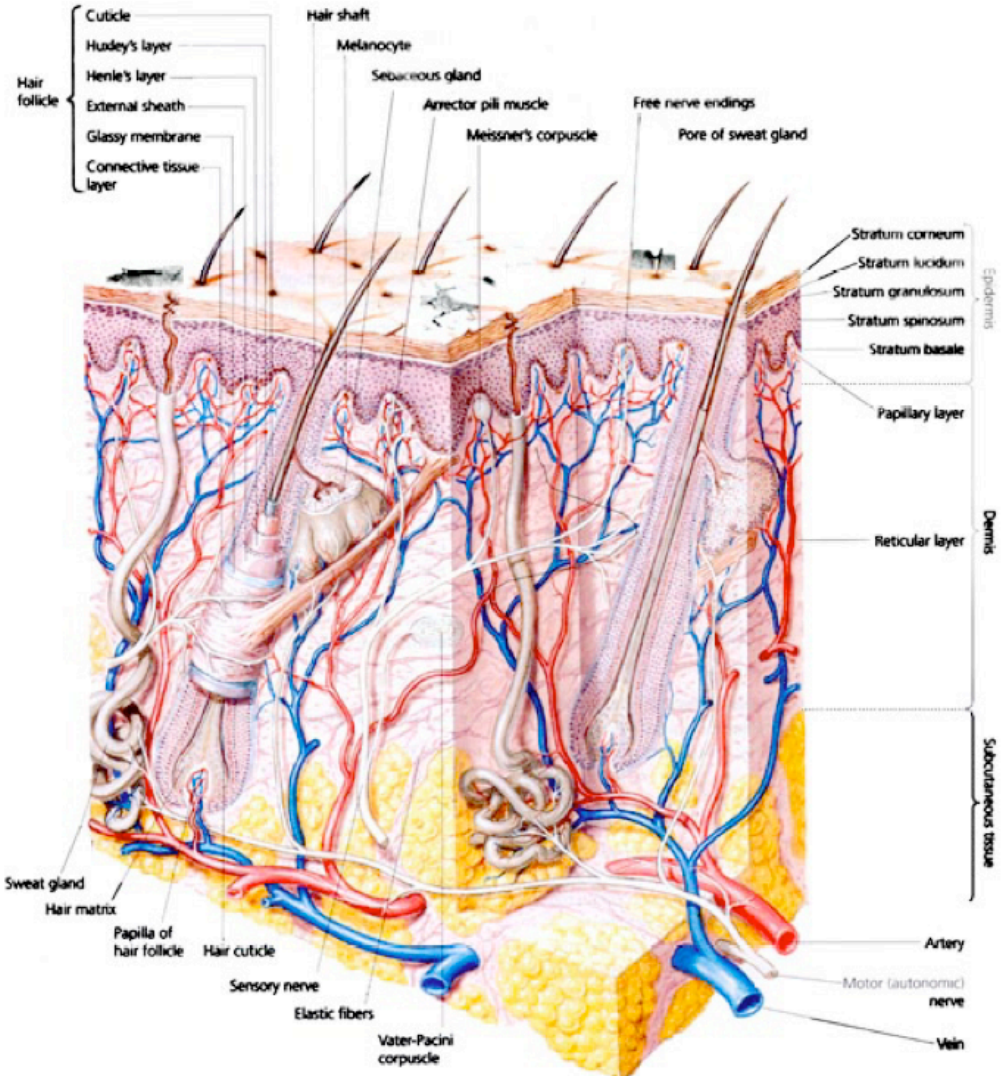

Figure 1-1: Structure of the skin [12].

Figure 1-2: HSc affecting the face, chest and trunk following thermal injury [The Role of Fibrocytes in Wound Repair and Hypertrophic Scarring. [Medina A, Ding J, Momtazi M, Tredget EE. In: Fibrocytes, R. Bucala (ed) World Scientific Press (2011) (In press)].

Figure 1-3: Keloid scar affecting the earlobe, scalp, suprapubic region and shoulder [3].

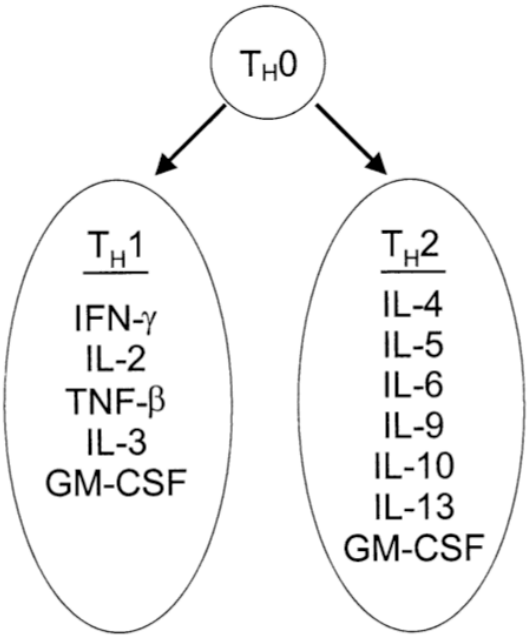

Figure 1-4: Subpopulations of T-cells and their respective cytokine profiles [51].

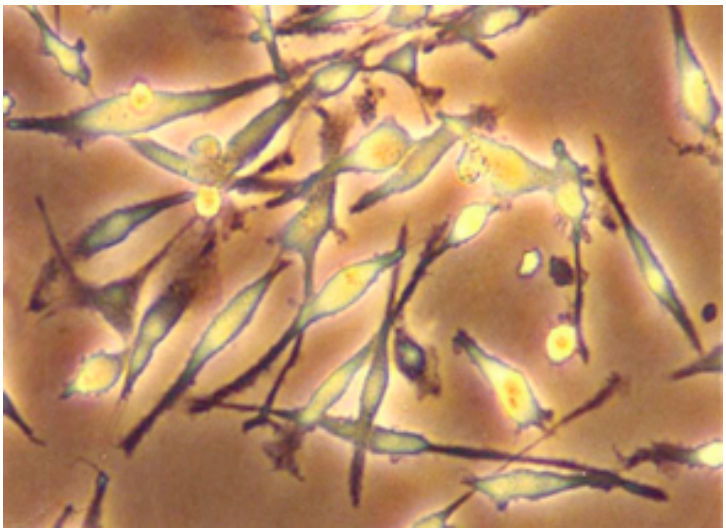

Figure 1-5: Fibrocytes viewed using light microscopy [72].

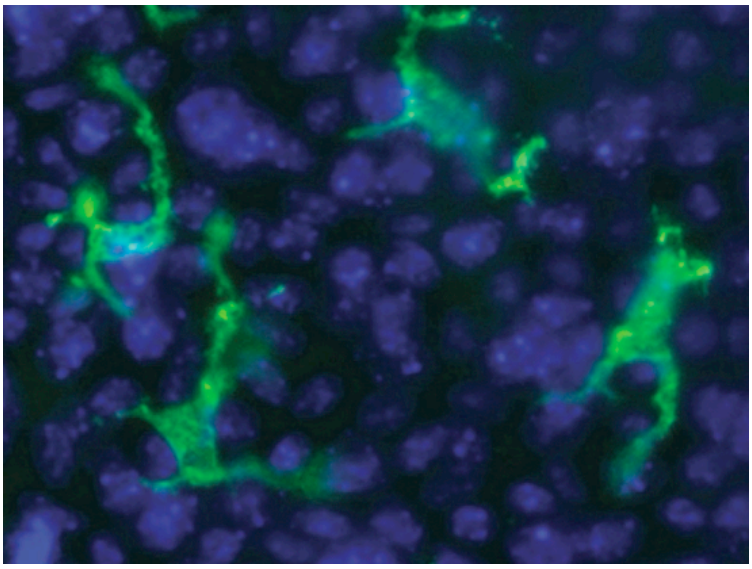

Figure 1-6: Epidermis stained with anti-TCR monoclonal antibody (green fluorescence) to visualize DETCs and 4'-6-Diamidino-2-phenylindole (DAPI) (blue nuclei) to visualize keratinocytes reveals DETCs in contact with multiple keratinocytes through dendritic processes [82].

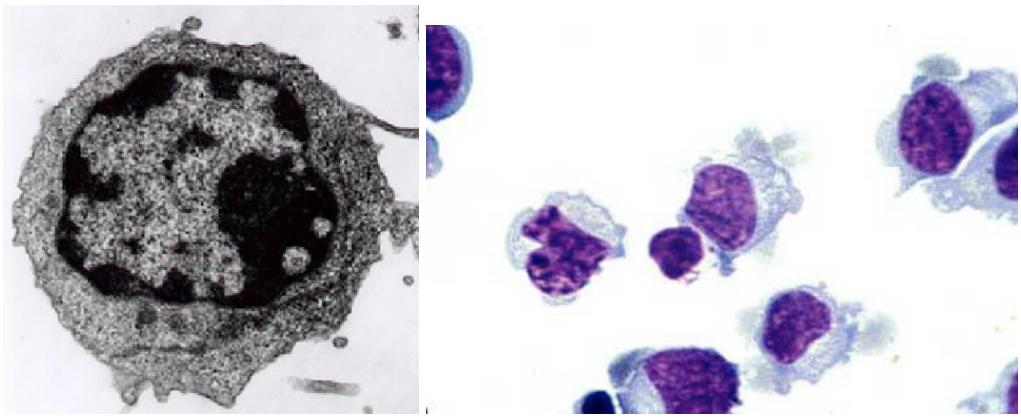

Figure 1-7: Natural killer cells viewed using scanning electron (left) and light microscopy (right) [56].

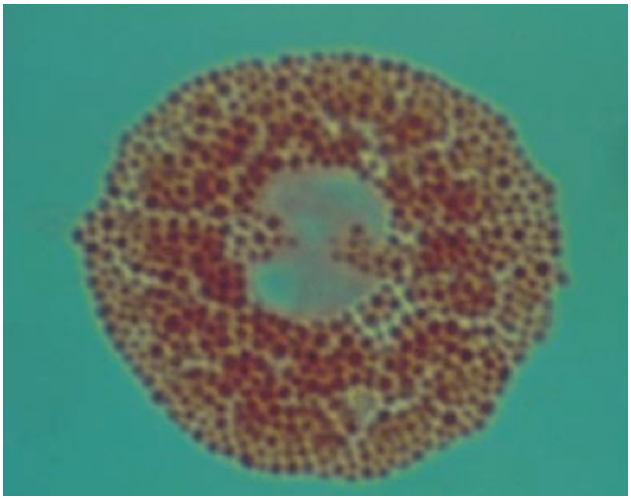

Figure 1-8: Photomicrograph of mast cells stained with Safranin (1000x magnification) [106].

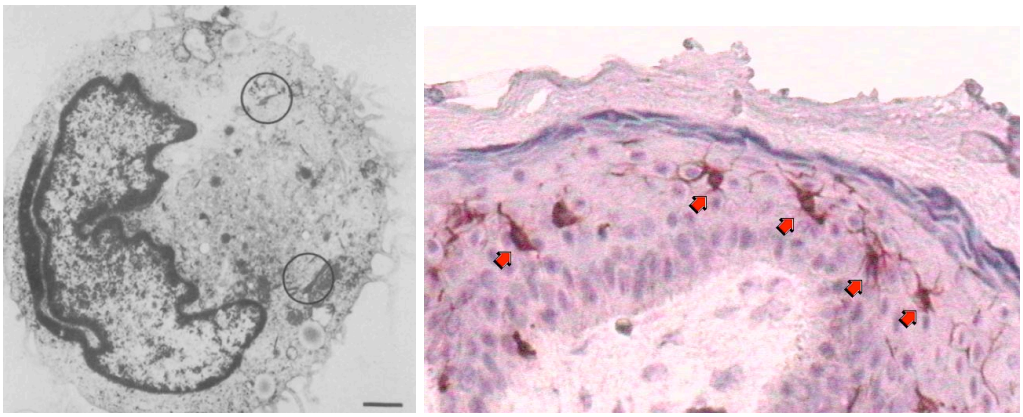

Figure 1-9: Langerhans cells (arrows) with hallmark Birbeck granules (circles) viewed using scanning electron (left) and light microscopy (right) (bar is 0.75 μm) [121].

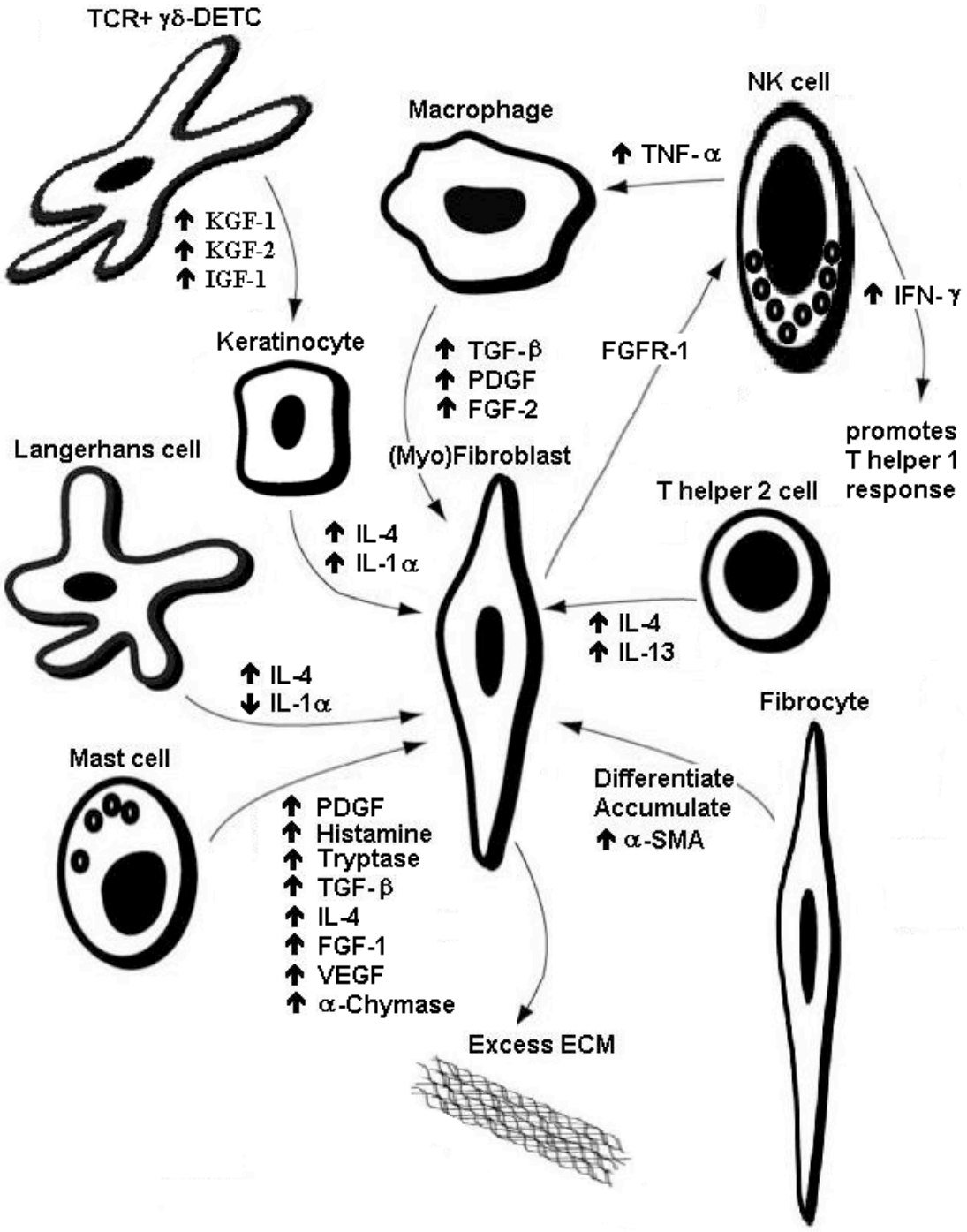

Figure 1-10: The role of immune cells in contributing to excess ECM production (modified) [131].

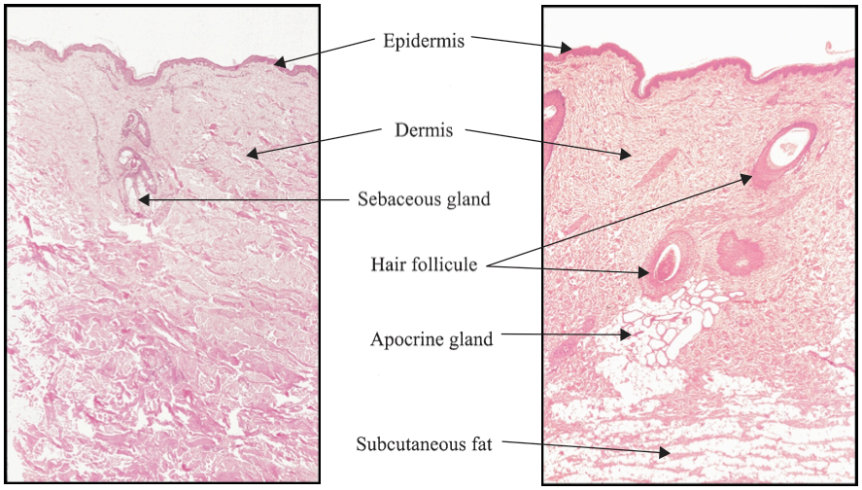

Figure 1-11: Comparison of histological features of human (left) and pig skin (right) taken from the back at similar thicknesses with hematoxylin and eosin (H & E) staining (100x magnification) [145].

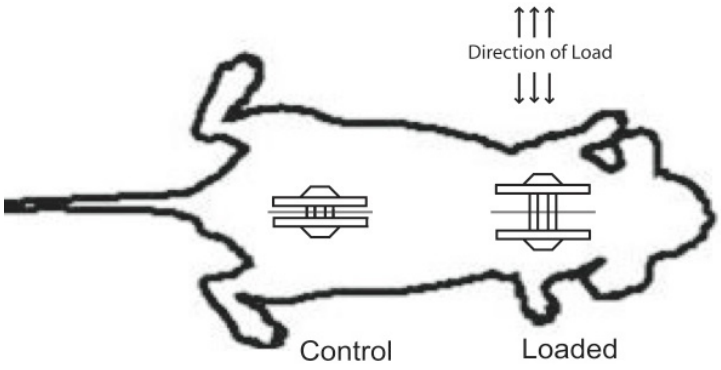

Figure 1-12: Mechanical load model of hypertrophic scar [150].

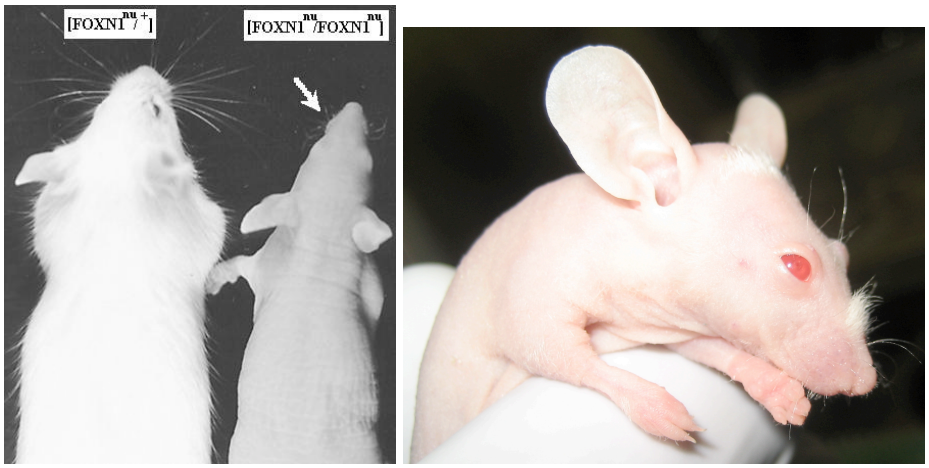

Figure 1-13: Heterozygous, normal-haired mouse (left) compared with its hairless homozygous nu/nu littermate (right) at 21 days postnatal life. The nude mouse is notably smaller in size and demonstrates sparse hair on the face and head [152].

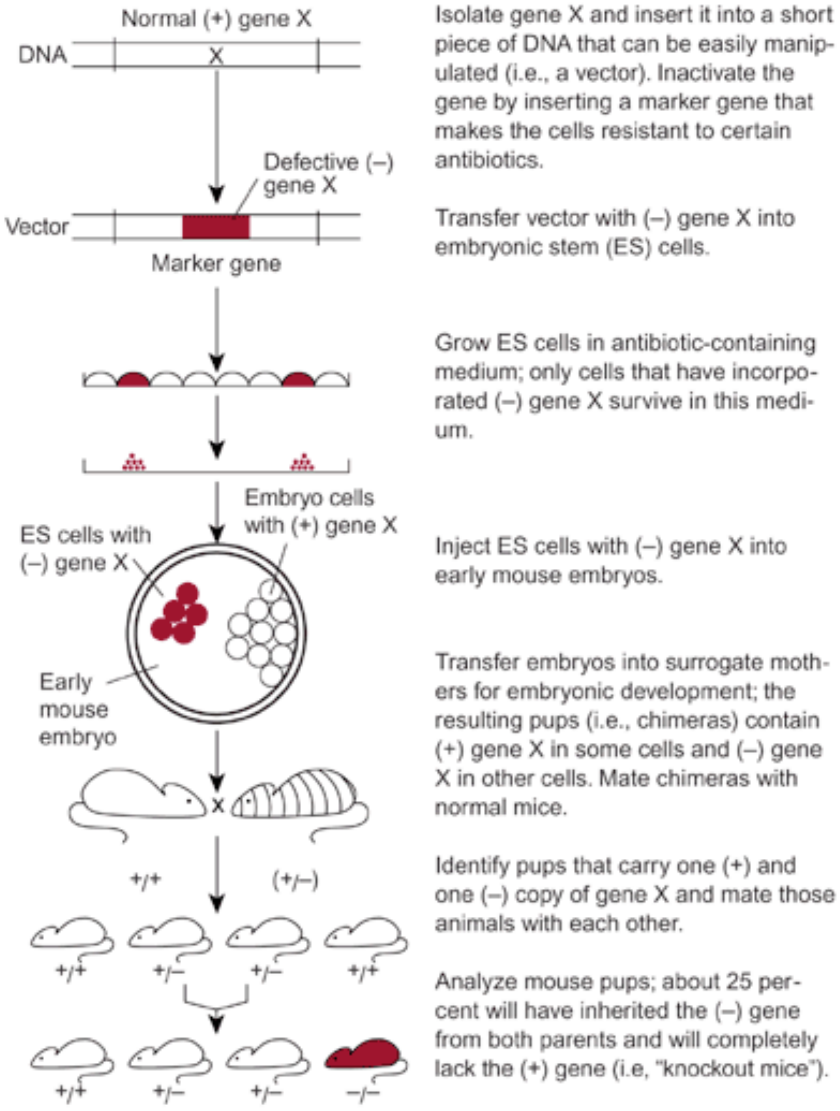

Figure 1-14: Homologous recombination with an inactivated gene during embryonic stem cell co-culture and subsequent implantation of ($^{-/-}$) blastocysts into a pseudopregnant mother. Mating of chimeras with ($^{+/+}$) and heterozygotes in the subsequent generation with each with produce knockout homozygotes ($^{-/-}$) in ~25% of the litter.

1.10 Bibliography

1. Singer AJ, Clark RA. Cutaneous wound healing. *N Engl J Med* 1999;341:738.
2. Reish RG, Eriksson E. Scar treatments: Preclinical and clinical studies. *J Am Coll Surg* 2008;206:719.
3. Reish RG, Eriksson E. Scars: A review of emerging and currently available therapies. *Plast Reconstr Surg* 2008;122:1068-78.
4. Burd A, Huang L. Hypertrophic response and keloid diathesis: Two very different forms of scar. *Plast Reconstr Surg* 2006;116:150e-7.
5. Mathes S. *Plastic Surgery* (Saunders, Philadelphia, 2006).
6. Levenson SM, Greever EF, Crowley LV, *et al.* The healing of rat skin wounds. *Ann Surg* 1965;161:293-308.
7. Mustoe TA, Cooter RD, Gold MH, *et al*. International clinical recommendations on scar management. *Plast Reconstr Surg* 2002;110:560-71.
8. Helm PA. Burn rehabilitation: dimensions of the problem. *Clin Plast Surg* 1992;19:551-9.
9. Mustoe TA. Scars and keloids. *Br Med J* 2004;328:1329-30.
10. Nedelec B, Ghahary A, Scott PG, *et al.* Control of wound contraction. Basic and clinical features. *Hand Clin* 2000;16:289-302.
11. Kwan P, Hori K, Ding J. *et al.* Scar and contracture: Biological principles. *Hand Clin* 2009;25:511-28.
12. Netter FH. *Atlas of Human Anatomy* (Icon Learning Systems, 1997).
13. Boulais N, Misery L. The Epidermis: a sensory tissue. *Eur J Dermatol* 2008;18:119-27.

14. Hunter J, Savin J, Dahl M. in *Clinical Dermatology* 365 (Wiley-Blackwell, 2002).

15. Horch RE, Kopp J, Kneser U, *et al.* Tissue engineering of cultured skin substitutes. *J Cell Mol Med* 2005;9:592-608.

16. Föhn M, Bannasch H. Artificial skin. *Methods Mol Med* 2007;140:167-182.

17. Boyce ST. Epidermis as secretory tissue. *J Invest Dermatol* 1994;102:8-10.

18. Fuchs E. Scratching the surface of skin development. *Nature* 2007;445:834-42.

19. Boyce ST, Warden GD. Principles and practices for treatment of cutaneous wounds with cultured skin substitutes. *Am J Surg* 2002;183:445-46.

20. Elias PM. Epidermal lipids, barrier function, and desquamation. *J Invest Dermatol* 1983;80:44s–9.

21. Elias PM. Stratum corneum architecture, metabolic activity and interactivity with subjacent cell layers. *Exp Dermatol* 1996;5:191-201.

22. Stroud ML. Vitamin D - a review. *Aust Fam Physician* 2008;37:1002-05.

23. Brown BC, McKenna SP, Siddhi K. *et al*. The hidden cost of skin scars: Quality of life after skin scarring. *J Plast Reconstruct Aesthet Surg* 2008;61:1049-58 (2008).

24. Luger TA. Neuromediators - a crucial component of the skin immune system. *J Dermatol Sci* 2002;30:87-93.

25. Sorrell JM, Caterson B, Caplan AI, *et al.* Human keratinocytes contain carbohydrates that are recognized by keratan sulfate-specific monoclonal antibodies. *J Invest Dermatol* 1990;95:347-52.

26. Schurer NY, Elias PM. The biochemistry and role of epidermal lipid synthesis. *Adv Lipid Res* 1991;24:27-56.

27. Cubison TCS, Pape SA, Parkhouse N. Evidence for the link between healing time and the development of hypertrophic scars in pediatric burns due to scald injury. *Burns* 2006;32:992-9.

28. Bayat A, McGrouther DA, Ferguson MWJ. Skin scarring. *BMJ* 2003;326:88-92.

29. Tredget EE, Nedelec B, Scott PG. *et al.* Hypertrophic scars, keloids, and contractures. The cellular and molecular basis for therapy. *Surg Clin North Am* 1997;77:701-30.

30. Tredget EE, Nedelec B, Ghahary A. The molecular biology of wound healing following thermal injury: The role of fibrogenic and antifibrogenic growth factors. in *Critical Care of the Burn Patient* (eds. Lorente JA & Esteban A) (Springer-Verlag, 1998).

31. Scott PG, Ghahary A, Chambers M, *et al*. Biological basis of hypertrophic scarring. in *Advances in Structural Biology*, Vol. 3 197-232 (JAI Press Inc, Greenwich, Connecticut, 1996).

32. Bitterman PB, Henke CA. Fibroproliferative disorders. *Chest* 1991;99:81S-4S.

33. Köse O, Waseem A. Keloids and hypertrophic scars: Are they two different sides of the same coin? *Dermatol Surg* 2008;34:336-46.

34. Al-Attar A, Mess S, Thomassen JM. *et al*. Keloid pathogenesis and treatment. *Plast Reconstr Surg* 2006;117:286-300.

35. Murray JC. Keloids and hypertrophic scars. *Clin Dermatol* 1994;12;27.

36. Seifert O, Mrowietz U. Keloid scarring: bench and bedside. *Arch Dermatol Res* 2009;301: 259-72.

37. Tredget EE. Pathophysiology and treatment of fibroproliferative disorders following thermal injury. *Ann N Y Acad Sci* 1999;888:165-82.

38. Tredget EE, Shankowsky HA, Taerum TV, *et al*. The role of inhalation injury in burn trauma. A Canadian experience. *Ann Surg* 1990;212:720-7.

39. Snelling, C.F. Burn units' share of Canada's total burn care. *J Burn Care Rehabil* 1995;16: 519-24.

40. Brigham PA, McLoughlin E. Burn incidence and medical care use in the United States: estimates, trends, and data sources. *J Burn Care Rehabil* 1996;17:95-107.

41. Ryan CM. Objective estimates of the probability of death from burn injuries. *N Engl J Med* 1998:338:362-6.

42. Deitch EA, Wheelahan TM, Rose MP, *et al*. Hypertrophic burn scars: analysis of variables. *J Trauma* 1983;23:895-8.

43. Dedovic Z, Koupilova I, Brychta P. Time trends in incidence of hypertrophic scarring in children treated for burns. *Acta Chir Plast* 1999;41:87-90.

44. Bombaro KM. What is the prevalence of hypertrophic scarring following burns? *Burns* 2003;29:299-302.

45. Engrav LH. Impairment, time out of school, and time off from work after burns. *Plast Reconstr Surg* 1987;79:927-34.

46. Helm PA. Burn rehabilitation: dimensions of the problem. *Clin Plast Surg* 1992;19:551-9.

47. Fraulin FO, Illmayer SJ, Tredget EE. Assessment of cosmetic and functional results of conservative versus surgical management of facial burns. *J Burn Care Rehabil* 1996;17:19-29.

48. Carr-Collins JA. Pressure techniques for the prevention of hypertrophic scar. *Clin Plast Surg* 1992;19:733-43.

49. Castagnoli C. The HLA-DR beta 16 allogenotype constitutes a risk factor for hypertrophic scarring. *Hum Immunol* 1990;29:229-32.

50. Barbul A. Immune aspects of wound repair. *Clin Plast Surg* 1990;17:433-42.

51. Park JE, Barbul A. Understanding the role of immune regulation in wound healing. *Am J Surg* 2004;187:11s-6s.

52. Schwacha MG, Bjoern MT, Daniel T, *et al*. Impact of thermal injury on wound infiltration and the dermal inflammatory response. *J Surg Res*, 2010;158;112-20.

53. Martin CW, Muir IF. The role of lymphocytes in wound healing. *Br J Plast Surg* 1990;43:655-62.

54. Boyce DE, Harding KG, Moore K. *et al*. Changes in lymphocyte subpopulations during normal human wound healing. *Br J Surg* 1997;84:696.

55. Boyce DE, Ruge WD, Harding KG. *et al*. The role of lymphocytes in human dermal wound healing. *Br J Dermatol* 2000;143:59-65.

56. Kindt TJ, Goldsby RA, Osborne BA. *Kuby Immunology* (W.H. Freeman, New York, 2007).

57. Johnston S, Unsworth J. The immunological system and surgical practice. *Surgery* 2001;19:i-vi.

58. Barbul A, Regan MC. Immune involvement in wound healing. *Otolaryngol Clin North Am* 1995;28:955-68.

59. Davis PA, Corless DJ, Aspinall R, *et al*. Effect of $CD4^+$ and $CD8^+$ cell depletion on wound healing. *Br J Surg* 2001;88:298-304.

60. Barbul A, Breslin RJ, Woodyard JP. *et al*. The effect of *in vivo* T helper and T suppressor lymphocyte depletion on wound healing. *Ann Surg* 1989;209:479-83.

61. Keen D. A review of research examining the regulatory role of lymphocytes in normal wound healing. *J Wound Care* 2008;17:218-21.

62. Wynn TA. Fibrotic disease and the Th1/Th2 paradigm. *Nat Rev Immunol* 2004;4:583-94.

63. Tredget EE, Yang L, Delehanty M, *et al*. Polarized Th2 cytokine production in patients with hypertrophic scar following thermal injury. *J Interferon Cytokine Res* 2006;26:179-89.

64. Bucala R, Spiegel LA, Chesney J, *et al*. Circulating fibrocytes define a new leukocyte subpopulation that mediates tissue repair. *Mol Med* 1994;1:71-81.

65. Chesney J, Metz C, Stavitsky AB, *et al*. Regulated production of type I collagen and inflammatory cytokines by peripheral blood fibrocytes. *J Immunol* 1998 ;160:419-25.

66. Abe R, Donnelly SC, Peng T, *et al*. Peripheral blood fibrocytes: Differentiation pathway and migration to wound sites. *J Immunol* 2001;166: 7556-62.

67. Yang L, Scott PG, Giuffre J, *et al*. Peripheral blood fibrocytes from burn patients: Identification and quantification of fibrocytes in adherent cells cultured from peripheral blood mononuclear cells. *Lab Invest* 2002;82:1183-92.

68. Mori L, Bellini A, Stacey MA, *et al*. Fibrocytes contribute to the myofibroblast population in wounded skin and originate from the bone marrow. *Exp Cell Res* 2005;304:81-90.

69. Shao DD, Suresh R, Vakil V, *et al*. Pivotal advance: Th-1 cytokines inhibit, and Th-2 cytokines promote fibrocyte differentiation. *J Leukoc Biol* 2008;83:1323-33.

70. Romagnani P, Annunziato F, Liotta F, *et al*. $CD14^{+}$ CD34 low cells with stem cell phenotypic and functional features are the major source of circulating endothelial progenitors. *Circ Res* 2005;97:314-22.

71. Badiavas EV, Ford D, Liu P, *et al*. Long-term bone marrow culture and its clinical potential in chronic wound healing. *Wound Rep Reg* 2007;15:856-65.

72. Yang L, Scott PG, Dodd C, *et al*. Identification of fibrocytes in postburn hypertrophic scar. *Wound Rep Reg* 2005;2005:2215-24.

73. Zhao Y, Glesne D, Huberman EA. Human peripheral blood monocyte-derived subset acts as pluripotent stem cells. *Proc Natl Acad Sci USA* 2003;100:2426-31.

74. Varcoe RL, Mikhail M, Guiffre AK, *et al*. The role of the fibrocyte in intimal hyperplasia. *J Thromb Haemost* 2006;4:1125-33.

75. Wang J, Jiao H, Stewart TL, *et al*. Improvement in postburn hypertrophic scar after treatment with IFN-alpha2b is associated with decreased fibrocytes. *J Interferon Cytokine Res* 2007;27:921-30.

76. Wang J, Jiao H, Stewart TL, *et al*. Accelerated wound healing in leukocyte-specific, protein 1-deficient mouse is associated with increased infiltration of leukocytes and fibrocytes. *J Leukoc Biol* 2007;82:554-63.

77. Naik-Mathuria B, Pilling D, Crawford JR, *et al*. Serum amyloid P inhibits dermal wound healing. *Wound Rep Reg* 2008;16:266-73.

78. Ishii G, Sangai T, Sugiyama K, *et al*. *In vivo* characterization of bone marrow-derived fibroblasts recruited into fibrotic lesions. *Stem Cells* 2005;23:699-706.

79. Yang L, Scott PG, Giuffre J, *et al*. Peripheral blood fibrocytes from burn patients: Identification and quantification of fibrocytes in adherent cells cultured from peripheral blood mononuclear cells. *Lab Invest* 2002;82:1183-92.

80. Haas W, Pereira P, Tonegawa S. Gamma/delta cells. *Ann Rev Immunol* 1993;11:637-85.

81. Havran W. A role for epithelial gamma delta T cells in tissue repair. *Immunol Res* 2000;21:63-9.

82. Schwacha MG. γδ T-cells: Potential regulators of the post-burn inflammatory response. *Burns* 2009;35:318-26.

83. Jameson J, Havran W. Skin γδ T-cell functions in homeostasis and wound healing. *Immunol Rev* 2007;215:114-22.

84. Havran WL, Chien Y-H, Allison JP. Recognition of self antigens by skin-derived T cells with invariant gamma/delta antigen receptors. *Science* 1991;252:1430-32.

85. Jameson J, Ugarte K, Chen N. *et al*. A role for skin gamma delta T cells in wound repair. *Science* 2002;296:747-9.

86. Boismenu R, Havran WL. Modulation of epithelial cell growth by intraepithelial gamma delta T cells. *Science* 1994;266:1253-5.

87. Boismenu R, Feng L, Xia YY, *et al*. Chemokine expression by intraepithelial gd T cells. Implications for the recruitment of inflammatory cells to damaged epithelia. *J Immunol* 1996;157:985-92.

88. Toth B, Alexander M, Daniel T, *et al*. The role of γδ T cells in the regulation of neutrophil-mediated tissue damage after thermal injury. *J Leukoc Biol* 2004;76:545-52.

89. Galy A, Travis M, Cen D, *et al*. Human T, B, natural killer, and dendritic cells arise from a common bone marrow progenitor cell subset. *Immunity* 1995;3:459-73.

90. Miller JS, Alley KA, McGlave P. Differentiation of natural killer (NK) cells from human primitive marrow progenitors in a stroma-based long-term culture system: identification of a $CD34^{+}7^{+}$ NK progenitor. *Blood* 1994;83:2594-2601.

91. Ritz J, Schmidt RE, Michon J, *et al*. Characterization of functional surface structures on human natural killer cells. *Adv Immunol* 1988;42:181-211.

92. Farag SS, Caligiuri MA. Human natural killer cell development and biology. *Blood Rev* 2006;20:123-37.

93. Cooper MA, Fehniger TA, Caligiuri MW. The biology of human natural killer-cell subsets. *Trends Immunol* 2001;22:633-40.

94. Caligiuri MA. Human natural killer cells. *Blood* 2008;112:461-9.

95. Root LL, Shipley GD. Normal human fibroblasts produce membrane-bound and soluble isoforms of FGFR-1. *Mol Cell Biol Res Commun* 2000;3:87-97.

96. Chan A, Hong D-L, Atzberger A, *et al*. CD56bright Human NK Cells differentiate into CD56 dim cells: Role of contact with peripheral fibroblasts. *J Immunol* 2007;179:89-94.

97. Trinchieri G. Michiko M-K, Clark SC, *et al*. Response of resting human peripheral blood natural killer cells to interleukin 2. *J Exp Med* 1984;160:1147-69.

98. Bancroft GJ. The role of natural killer cells in innate resistance to infection. *Curr Opin Immunol* 1993;5:503-10.

99. Agaiby AD, Dyson M. Immuno-inflammatory cell dynamics during cutaneous wound healing. *J Anat* 1999;195:531-42.

100. Djeu JY, Blanchard DK. Regulation of human polymorphonuclear neutrophil (PMN) activity against Candida albicans by large granular lymphocytes via release of a PMN-activating factor. *J Immunol* 1987;139:2761-7.

101. Schneider DF, Glenn CH, Faunce DE. Innate lymphocyte subsets and their immunoregulatory roles in burn injury and sepsis. *J Burn Care Res* 2007;28:365-79.

102. Faunce DE, Gamelli RL, Choudhry MA, *et al*. A role for CD1d-restricted NKT cells in injury-associated T cell suppression. *J Leukoc Biol* 2003;73:747-55.

103. Palmer JL, Tulley JM, Kovacs EJ, *et al*. Injury-induced suppression of effector T cell immunity requires CD1d-positive APCs and CD1d-restricted NKT cells. *J Immunol* 2006;177:92-9.

104. Bendelac A, Rivera MN, Park SH, *et al*. Mouse CD1-specific $NK1^+$ T cells: development, specificity, and function. *Annu Rev Immunol* 1997;15:535-62.

105. Kalesnikoff J, Galli SJ. New developments in mast cell biology. *Nature Immunol* 2008;11:1215-23.

106. Noli C, Miolo A. The mast cell in wound healing. *Vet Dermatol* 2001;12:303-13.

107. Mekori YA, Metcalfe DD. Mast cells in innate immunity. *Immunol Rev* 2000;173:131-40.

108. Galli SJ, Grimbaldeston M, Tsai M. Immunomodulatory mast cells: negative, as well as positive, regulators of immunity. *Nat Rev Immunol* 2008;8:445-54.

109. Galli SJ. Mast cells as "tunable" effector and immunoregulatory cells: Recent advances. *Annu Rev Immunol* 2005;23:749-86.

110. Gurish MF, Austen KF. The diverse roles of mast cells. *J Exp Med* 2001;194:F1-5.

111. Rothe MJ, Nowalk M, Kerdel FA. The mast cell in health and disease: A greater role. *J Am Acad Dermatol* 1990;23:615-24.

112. Nishikori Y, Kakizoe E, Kobayashi Y, *et al*. Skin mast cell promotion of matrix remodeling in burn wound healing in mice: relevance of chymase. *Arch Dermatol Res* 1998;290:553-60.

113. Metcalfe DD, Baram D, Mekori YA. Mast cells. *Physiol Rev* 1997;77:1033-79.

114. Abe M, Kurosawa M, Ishikawa O, *et al*. Effect of mast cell-derived mediators and mast cell-related neutral proteases on human dermal fibroblast proliferation and type I collagen production. *J Allergy Clin Immunol* 2000;106:S78-84.

115. Artuc M, Steckelings UM, Henz BM. Mast cell-fibroblast interactions: human mast cells as source and inducers of fibroblast and epithelial growth factors. *J Invest Dermatol* 2002;118:391-5.

116. Garbuzenko E, Nagler A, Pickholtz D, *et al*. Human mast cells stimulate fibroblast proliferation, collagen synthesis and lattice contraction: a direct role for mast cells in skin fibrosis. *Clin Exp Allergy* 2002;32:237-46.

117. Rao KN, Brown MA. Mast cells: Multifaceted immune cells with diverse roles in health and disease. *Ann N Y Acad Sci* 2008;1143:83-104.

118. Nishikori Y, Kakizoe E, Kobayashi Y, *et al*. Skin mast cell promotion of matrix remodeling in burn wound healing in mice: relevance of chymase. *Arch Dermatol Res* 1998;290:553-60.

119. Trautmann A, Toksoy A, Engelhardt E, *et al*. Mast cell involvement in normal human skin wound healing: expression of monocyte chemoattractant protein-1 is correlated with recruitment of mast cells which synthesize interleukin-4 in vivo. *J Pathol* 2000;190:100-6.

120. Weller K, Foitzik K, Paus R, *et al*. Mast cells are required for normal healing of skin wounds in mice. *FASEB J* 2006;20:2366-8.

121. Teunissen MBM. Dynamic nature and function of epidermal Langerhans cells *in vivo* and *in vitro*: a review, with emphasis on human Langerhans cells. *Histochem J* 1992;24:697-716.

122. Loser K, Beissert S. Dendritic cells and T cells in the regulation of cutaneous immunity *Adv Dermatol* 2007;23:307-33.

123. Rowden G, Lewis MG, Sullivan AK. Ia antigen expression on human epidermal Langerhans cells. *Nature* 1977;268:247-8.

124. Klareskog L, Malmnas-Tjernlund U, Forsum U, *et al*. Epidermal Langerhans cells express Ia antigens. *Nature* 1977;268:248-50.

125. Stingl G, Wolff-Schreiner EC, Pichler WJ, *et al*. Epidermal Langerhans cells bear Fc and C3 receptors. *Nature* 1977;268:245-6.

126. Macatonia SE, Knight SC, Edwards AJ, *et al*. Localization of antigen on lymph node dendritic cells after exposure to the contact sensitizer fluorescein

isothiocyanate. Functional and morphological studies. *J Exp Med* 1987;166:1654-67.

127. Borkowski TA, van Dyke BJ, Schwarzenberger K, *et al*. Expression of E-cadherin by murine dendritic cells. E-cadherin as a dendritic cell differentiation antigen characteristic of epidermal Langerhans cells and related cells. *Eur J Immunol* 1994;158:4543-7.

128. Cracco C, Stella M, Teich-Alasia S, *et al*. Comparative study of Langerhans cells in normal and pathological human scars. *Eur J Histochem* 1992;36:53-65.

129. Niessen FB, Schalkwijk J, Vos H, *et al*. Hypertrophic scar formation is associated with an increased number of epidermal Langerhans cells. *J Pathol* 2004;202:121-9.

130. Castagnoli C, Trombotto C, Sabzima O, *et al*. Characterization of T-cell subsets infiltrating post-burn hypertrophic scar tissues. *Burns* 1997;23:565-72.

131. van der Veer WM, Bloeman MCT, Ulrich MMW. Potential cellular and molecular causes of hypertrophic scar formation. *Burns* 2009;35:15-29.

132. Rockwell WB, Cohen IK, Ehrlich HP. Keloids and hypertrophic scars: A comprehensive review. *Plast Reconstr Surg* 1989;84:827-37.

133. Khouri RK, Mustoe TA. Trends in the treatment of hypertrophic scars. in *Advances in Plastic and Reconstructive Surgery,* Vol. 8 (Mosby-Year Book, St. Louis, 1992).

134. Ladin DA, Garner WL, Smith DJ Jr. Excessive scarring as a consequence of healing. *Wound Rep Reg* 1995;3:6-14.

135. Ramos MLC, Gragnani A, Ferreira LM. Is there an ideal animal model to study hypertrophic scarring? *J Burn Care Res* 2008;29:363-8.

136. Morris DE, Wu L, Zhao LL, *et al*. Acute and chronic animal models for excessive dermal scarring: quantitative studies. *Plast Reconstr Surg* 1997;100: 674-81.

137. Reid RR, Mogford JE, Butt R, *et al*. Inhibition of procollagen C-proteinase reduces scar hypertrophy in a rabbit model of cutaneous scarring. *Wound Repair Regen* 2006;14:138-41.

138. Kim I, Mogford JE, Witschi C, *et al*. Inhibition of prolyl 4-hydroxylase reduces scar hypertrophy in a rabbit model of cutaneous scarring. *Wound Rep Reg* 2003;11:368-72.

139. Lee JP, Jalili RB, Tredget EE, *et al*. Anti-fibrogenic effects of liposome-encapsulated IFN-alpha2b cream on skin wounds in a fibrotic rabbit ear model. *J Interferon Cytokine Res* 2005;25:627-31.

140. Saulis AS, Mogford JH, Mustoe TA. Effect of mederma on hypertrophic scarring in the rabbit ear model. *Plast Reconst Surg* 2002;110:177-83.

141. Yagmur C, Guneran E, Kefeli M, *et al*. The effect of surgical denervation on prevention of excessive dermal scarring: A study on rabbit ear hypertrpophic scar model. *J Plast Reconstr Aesthet Surg* 2011;64:1359-65.

142. Marcus JR, Tyrone JW, Bonoma S, *et al*. Celllular mechanisms for diminished scarring with aging. *Plast Reconstr Surg* 2000;105:1591-9.

143. Meyer W, Schwarz R, Neurand K. The skin of domestic mammals as a model for the human skin, with special reference to the domestic pig. *Curr Probl Dermatol* 1978;7:39-52.

144. Sullivan TP, Eaglstein WH, Davis SC, *et al.* The pig as a model for human wound healing. *Wound Repair Regen* 2001;9:66-76.

145. Zhu KQ, Engrav LH, Gibran NS, *et al*. The female, red Duroc pig as an animal model of hypertrophic scarring and the potential role of the cones of skin. 2003;29:649-64.

146. Zhu KQ, Engrav LH, Tamura RN, *et al*. Further similarities between cutaneous scarring in the female, red Duroc pig and human hypertrophic scarring. *Burns* 2004;30:518-30.

147. Gallant-Behm CL, Hart DS. Genetic analysis of skin wound healing and scarring in a porcine model *Wound Rep Reg* 2006;14:46-54.

148. Harunari N, Zhu KQ, Armendariz RT, *et al*. Histology of the thick scar on the female, red Duroc pig: final similarities to human hypertrophic scar. *Burns* 2006;32:669-77.

149. Gallant-Behm CL, Hildebrand KA, Hart DA. The mast cell stabilizer ketotifen prevents development of excessive skin wound contraction and fibrosis in red Duroc pigs. *Wound Rep Reg* 2008;16:226-33.

150. Aarabi S, Bhatt KA, Shi Y, *et al*. Mechanical load initiates hypertrophic scar formation through decreased cellular apoptosis. *FASEB* 2007;21:3250-61.

151. Su D-M, Navarre S, Oh W-J, *et al*. A domain of Foxn1 required for crosstalk-dependent thymic epithelial cell differentiation. *Nature Immunol* 2003;4:1128-35.

152. Mecklenburg L, Tychsen B, Paus R. Learning from nudity: lessons from the nude phenotype. *Exp Dermatol* 2005;14:797-810.

153. Krueger GG, Chambers DA, Shelby J, *et al*. Epidermal proliferation of nude mouse skin, pig skin and pig skin grafts. *J Exp Med* 1980;152:1329-39.

154. Simon GA, Maibach HI. Relevance of hairless mouse as an experimental model of percutaneous penetration in man. *Skin Pharmacol Appl Skin Physiol* 1998;11:80-6.

155. Shultz L. Immunological mutants of the mouse. *Am J Anat* 1991;191:303-11.

156. Nehls M, Pfeifer D, Schorpp M, *et al*. New member of the winged-helix protein family disrupted in mouse and rat nude mutations. *Nature* 1994;372:103-7.

157. Paus R, Muller-Rover S, van der Veen C, *et al*. A comprehensive guide for the recognition and classification of distinct stages of hair follicle morphogenesis. *J Invest Dermatol* 1999;113:523-32.

158. Mecklenburg L, Nakamura M, Sundberg JP, *et al*. The nude mouse skin phenotype: the role of Foxn1 in hair follicle development and cycling. *Exp Mol Pathol* 2001;71:171-8.

159. Godfrey DI, Zlotnik A. Control points in early T-cell development. *Immunol Today* 1993;14:547-53.

160. Fehling HJ, von Boehmer H. Early αβ T cell development in the thymus of normal and genetically altered mice. *Curr Opin Immunol* 1997;9:263-75.

161. Petrie HT. Role of thymic organ structure and stromal composition in steady-state postnatal T-cell production. *Immunol Rev* 2002;189:8-19.

162. Hillmer MP, MacLeod SM. Experimental keloid scar models: A review of methodological issues. *J Cutan Med Surg* 2002;6:354-9.

163. Robb EC, Waymack JP, Warden GD, *et al*. A new model for studying the development of human hypertrophic burn scar formation. *J Burn Care Rehabil* 1987;8:371-5.

164. Kischer CW, Pindur J, Shetlar MR, *et al*. Implants of hypertrophic scars and keloids into the nude (athymic) mouse: viability and morphology. *J Trauma* 1989;29:672-7.

165. Kischer CW, Sheridan D, Pindur J. Use of nude (athymic) mice for the study of hypertrophic scars and keloids: vascular continuity between mouse and implants. *Anat Rec* 1989;225:189-96.

166. Kischer CW, Wagner HN Jr, Pindur J, *et al*. Increased fibronectin production by cell lines from hypertrophic scar and keloid. *Connect Tissue Res* 1989;23:279-88.

167. Shetlar MR, Shetlar CL, Kischer CW, *et al*. Implants of keloid and hypertrophic scars into the athymic nude mouse: changes in the glycosaminoglycans of the implants. *Connect Tissue Res* 1991;26:23-36.

168. Polo M, Kim Y-J, Kucukcelebi A, *et al*. An *in vivo* model of human proliferative scar. *J Surg Res* 1998;74:187-95.

169. Shetlar MR, Shetlar DJ, Bloom RF, *et al*. Involution of keloid implants in athymic mice treated with pirfenidone or with triamcinolone. *J Lab Clin Med* 1998;132:491-6.

170. Wang X, Smith P, Lee L, *et al*. Exogenous transforming growth factor β2 modulates collagen I and collagen III synthesis in proliferative scar xenografts in nude rats. *J Surg Res* 1999;87:194-200.

171. Namrata DB, Supp AP, Kasting GB, *et al*. Improvement of epidermal barrier properties in cultured skin substitutes after grafting onto athymic mice. *Skin Pharmacol Physiol* 2007;20:21-8.

172. Estrem SA, Domayer M, Bardach J, *et al*. Implantation of human keloid into athymic mice. *Laryngoscope* 1987;10:1214-8.

173. Waki EY, Crumley RL, Jakowatz JG. Effects of pharmacologic agents on human keloids implanted in athymic mice: A pilot study. *Arch Otolaryngol Head Neck Surg* 1991;117:1177-81.

174. Greenhalgh DG. Models of wound healing. *J Burn Care Rehabil* 2005;26:293-305.

175. Boyce ST, Supp AP, Harriger MD, *et al*. Topical nutrients promote engraftment and inhibit wound contraction of cultured skin substitutes in athymic mice. *J Invest Dermatol* 1995;104:345-9.

176. Boyce ST, Medrano EE, Abdel-Malek Z, *et al*. Pigmentation and inhibition of wound contraction by skin substitutes with adult melanocytes after transplantation to athymic mice. *J Invest Dermatol* 1993;100:360-5.

177. Yang DY, Li SR, Wu JL, *et al*. Establishment of a hypertrophic scar model by transplanting full-thickness human skin grafts onto the backs of nude mice. *Plast Reconstr Surg* 2007;119:104-9.

178. Hilbert DM, Holmes KL, Anderson AO, *et al*. Long-term thymic reconstitution by peripheral CD4 and CD8 single-positive lymphocytes. *Eur J Immunol* 1993;23:241-8.

179. Ferrick DA, Sambhara SR, Chadwick BS, *et al*. The T-cell receptor repertoire is strikingly similar in older nude mice compared to normal adult mice. *Thymus* 1989;13:103-11.

180. Mak TW, Penninger JM, Ohashi PS, Knockout mice: A paradigm shift in modern immunology. *Nat Rev Immunol* 2001;1:11-9.

181. Schatz DG, Oettinger MA, Baltimore D. The V(D)J recombination activating gene, RAG-1. *Cell* 1998;59:1035-48.

182. Thompson, C.B. RAG knockouts deliver a one/two punch. *Curr Biol* 1992;2:180-2.

183. Swanson PC. The bounty of RAGs: recombination signal consequences and reaction outcomes. *Immunol Rev* 2004;200:90-114.

184. Chen J, Shinkal Y, Young F, *et al*. Probing immune functions in RAG-deficient mice. *Curr Opin Immunol* 1994;6:313-9.

185. Grose R, Werner S. Wound-healing studies in transgenic and knockout mice. *Mol Biotechnol* 2004;28:147-66.

186. Crowe MJ, Doetschman T, Greenhalgh DG. Delayed wound healing in immunodeficient TGF-β1 knockout mice. *J Invest Dermatol* 2000;115:3-11.

187. Gallucci, R.M., Simeonova, P.P., Matheson, J.M., et al. Impaired cutaneous wound healing in interleukin-6-deficient and immunosuppressed mice. *FASEB J* **14,** 2525-31 (2000).

188. Murphy TJ, Ni CN, Zang Y, *et al*. $CD4^{+}CD25^{+}$ regulatory T cells control innate immune reactivity after injury. *J Immunol* 2005;174:2957-63.

189. Maloy KJ, Salaun L, Cahill R, *et al*. $CD4^{+}CD25^{+}$ T(R) cells suppress innate immune pathology through cytokine dependent mechanisms. *J Exp Med* 2003;197:111-9.

190. Mombaerts P, Clarke AR, Rudnicki MA, *et al*. Mutations in T-cell antigen receptor genes alpha and beta block thymocyte development at different stages. *Nature* 1992;360:225-231.

191. Shortman K. Cellular aspects of early T-cell development. *Curr Opin Immunol* 1992;4:140-146.

2. A Nude Mouse Model of Hypertrophic Scar Demonstrates Histological and Morphologic Characteristics of Human Hypertrophic Scar

2.1 Introduction

The ultimate outcome of wound repair in children and adults is scar formation [1]. When this process is protracted and the deposition and accumulation of repair matrix continues unchecked a pathological scar is formed. HSc is one type of pathological scar and can be classified as a fibroproliferative disorder (FPD) affecting the skin [2]. These scars are known to occur following dermal injury at a critical depth [3] and represent a dysregulated wound healing response to injury. Clinically, HSc presents as a red, raised, shiny, inelastic tissue mass limited to the boundaries of the initial injury [4]. Histologically, HSc is characterized by excessive extracellular matrix (ECM) protein deposition, thin, whorled collagen fibers parallel to the skin surface, hypervascularity, hypercellularity and the presence of α-smooth muscle actin (SMA) expressing myofibroblasts [5, 6].

During the prolonged inflammation associated with slowly healing dermal wounds following a burn, HSc develops with increased frequency [7-10]. These patients suffer cosmetic disfigurement and social stigma as well as functional limitations including pain, intense pruritus, heat intolerance, a reduction in extremity range of motion and in some cases lifelong disability secondary to contractures [11-15, 7]. Hypertrophic scars respond slowly and often incompletely to current forms of therapy including pressure garments, topically

applied silicone and intralesional steroids [8, 16-20]. While the events that lead to HSc have been extensively studied, the pathogenesis of this condition is still not well understood, making treatment difficult and largely empirical. Before novel advances in therapy for these disorders can be implemented a broader understanding of the processes leading to their development must be realized.

A key challenge facing research of this condition is that hypertrophic scars are unique to humans and do not normally occur in animals [12]. As such, the discovery of a relevant, *in vivo*, experimental animal model is crucial to further research into the biology of excessive scarring and the molecular events leading to excessive scar formation [21-24]. Several animal models have been previously described in the literature each with their own unique limitations [22, 25-34]. In our experience, nude mice grafted with human skin represent a promising animal model. The nude mouse is homozygous null for the Foxn1 gene resulting in a lack of thymic epithelium and as a consequence lack T-cells [35, 36]. This defect in adaptive immunity facilitates the use of human skin in an animal model capable of generating HSc. Proof of concept has previously been established using full thickness human skin grafted onto nude mice [34, 37]. However, in these models at approximately one month following transplantation of human skin, the graft is described as turning black and shedding the upper portions of the dermis prior to the development of a scar resembling human HSc [34, 37]. These observations question the survival of human skin grafts. The possibility of transplant rejection therefore challenges the reliability of the nude mouse as a model of HSc.

Our objective is to further validate the existing *in vivo* nude mouse models of HSc by testing whether grafting split thickness human skin onto nude mice results in survival of engrafted human tissue that forms scars morphologically and histologically consistent with human HSc. We will improve upon existing information in this model by providing blinded, independent scar assessment data, autografted nude mouse controls and further characterization of immunohistochemical changes in small leucine-rich proteoglycans (SLRPs) in our model consistent with features of human HSc.

2.2 Methods

Preparation of skin grafts

Following informed consent, human skin samples were obtained from female patients undergoing cosmetic abdominoplasty. Human split thickness skin grafts were harvested using a dermatome set at 0.03 cm. Care was taken to avoid harvesting skin containing striae and other skin abnormalities. Using a prefabricated, 2.0 x 1.5 cm plastic template grafts were cut using a scalpal and stored in sterile normal saline until grafting.

Transplantation of skin grafts

All animal studies were performed using protocols approved by the University of Alberta Animal Care and Use Committee and in accordance with the standards of the Canadian Council on Animal Care. Four to six week old male Bagg albino laboratory bred (BALB)/c-nu/nu nude mice (NCI, Frederick, MD) weighing ~25

grams each were purchased and housed in a virus antibody free biocontainment facility for the entire experiment. Animals were conditioned for two weeks prior to grafting. Under isoflurane anesthetic (Halocarbon Laboratories, River Edge, NJ) in the prone position, the fine hairs from dorsal surface of the mouse were removed with commercial hair remover (Nair® hair remover Church & Dwight Co., Inc. Princeton, NJ) and the skin disinfected with iodine. The previously described template was then used to mark a 2.0 x 1.5 section of the dorsal skin, which was then excised using sharp dissection leaving the panniculus carnosus intact. Animals in the experimental group (n=20) were then grafted with split thickness human xenografts. Animals in the control group (n=18) were autografted with excised full thickness nude mouse skin. All grafts were sutured using 4-0 braided, silk suture (Ethicon©, Somerville, NJ) and dressed with a non-adherent petrolatum (Xeroform™, Covidien, Mansfield, MA) and dry gauze tie-over bolus dressing to ensure adherence of the graft to the wound bed. All animals received narcotic analgesia (Hydromorphone HP 10 diluted to 0.05 mg/mL, Sandoz, Boucherville, QC) subcutaneously for pain management immediately following grafting. Wild-type (WT) BALB/c (n=4) (NCI, Frederick, MD) mice were also grafted in the same fashion with split thickness human xenografts in order to clinically observe the effects of tissue rejection in immune replete animals. All sutures and dressings were removed seven days following grafting. Digital photographs were taken weekly to document healing and scar formation. All photographs were taken under standardized conditions in which lighting, exposure time, and distance from the animal were constant. Animals

grafted with split thickness human skin (proliferative xenograft scars) were euthanized at 30, 60, 120 and 180 days postoperatively (n=5 per time point). Animals grafted with full thickness nude mouse skin (autograft controls) were euthanized at 30 and 60 days postoperatively (n=9 per time point). WT BALB/c mice were euthanized at 30 days postoperatively (Fig. 2-1). At each time point normal skin, nude mouse autograft and proliferative xenograft scar biopsies were collected for histological analysis and immunohistochemistry.

Morphological analysis

A previously validated Manchester Scar Scale (MSS) [38, 39] was modified and used to score autograft and proliferative xenograft scar images taken at each time point prior to euthanization (Table 2-1). A panel of five, blinded, independent scar assessors was recruited to score all proliferative xenograft scar (n=160) and nude mouse autograft (n=100) images. In all cases original, unaltered scar images were submitted for assessment. Scar assessors were required to attend an information session where they were briefly shown the range of scars they were being asked to evaluate and given instructions on how to record the two components of their scar assessment for each image. Our panel accessed scar images using a password-protected computer system. Repeat images were included in order to allow us to determine the degree of intrarater consistency within our panel. All data was collected and recorded in a blinded fashion.

Harvesting and processing of skin biopsies

Normal skin, autograft and proliferative xenograft scar biopsies at all time points were harvested and divided in half. One half was fixed in 10% formalin (Zinc Formal Fixx™, Thermo Scientific, Pittsburgh, PA) for at least 24 hours, processed and embedded in paraffin. The remaining half was embedded and frozen in cryomatrix (Shandon Cryomatrix™, Thermo Scientific, Pittsburgh, PA). Paraffin embedded sections were cut to 5 μm, mounted on glass slides and subjected to hematoxylin & esoin (H & E), Masson's trichrome, α-SMA, decorin, biglyan, toluidine blue and picrosirius red staining. Frozen sections were cut to 10 μm and used for anti-human human leukocyte antigen (HLA)-ABC staining. HSc samples were also collected from burn patients with clinical characteristics of HSc including redness, shiny texture, and increased thickness. Informed consent was obtained in all cases.

Skin structure, thickness and collagen morphology

Skin structure, thickness and hypercellularity were assessed in H & E sections. Normal skin, autograft and proliferative xenograft scar thickness were assessed under 100x magnification by measuring the distance from the stratum corneum to the dermal-fat junction in triplicate, in all sections, from each time point. Collagen morphology was assessed in Masson's trichrome and picrosirius red sections under 100x magnification.

Survival of transplanted human split thickness xenografts

Frozen sections were warmed at 37˚C for 10 minutes followed by fixation in cold methanol for 10 minutes and drying in acetone for 2 minutes. Slides were rehydrated in tris-buffered saline (TBS) and 0.2% Triton X-100 (Sigma-Aldrich Inc., St. Louis, MO) and then incubated overnight at 4˚C with FITC-labeled anti-human HLA-ABC antibody (Accurate Chemical & Scientific Corp., Westbury, NY), diluted to 1:50 in 2% bovine serum albumin (BSA) (Sigma-Aldrich Inc., St. Louis, MO) and 2% goat serum (Jackson ImmunoReseach Laboratories Inc., West Grove, PA). Samples were washed with TBS and distilled water and slides were coverslipped using Fluoromount-G mounting media (Southern Biotechnology Associates, Birmingham, AL). In controls for anti-human HLA-ABC staining, primary antibodies were omitted resulting in negative staining.

Immunohistochemical analysis of α-SMA

Immunohistochemistry for α-SMA was performed on paraffin embedded sections. Sections were deparaffinized and rehydrated through five changes of decreasing gradient ethanol and permeabilized with 0.01% Triton X-100. Sections were treated with 3% hydrogen peroxide to quench endogenous peroxidase activity and blocked with 10% goat serum and 10% BSA for 1 hour at room temperature. Endogenous biotin and avidin were blocked using a kit (Vector Laboratories Inc., Burlingame, CA) followed by Fc receptor block (Innovex Biosciences, Richmond, CA). Slides were then incubated with rabbit monoclonal anti-α-SMA antibody (Millipore, Temecula, CA), 1:200 dilution, overnight at 4˚C followed by

a goat anti-rabbit biotinylated secondary antibody (Vector Laboratories Inc., Burlingame, CA), 1:200 dilution, for 1 hour at room temperature. Sections were then washed with avidin-biotin complex (Vectastain ABC kit, Vector Laboratories Inc., Burlingame, CA) and developed using diaminobenzidine (Sigma-Aldrich Inc., St. Louis, MO). In negative controls for all anti-α-SMA staining, primary antibodies were replaced with rabbit IgG (Vector Laboratories Inc., Burlingame, CA) resulting in negative staining (data not shown).

Immunohistochemical analysis of decorin and biglycan

Immunohistochemistry for decorin and biglycan was performed on paraffin embedded sections. As previously reported, [40] sections were deparaffinized and rehydrated through five changes of decreasing gradient ethanol and permeabilized with 0.05% saponin (Sigma-Aldrich Inc., St. Louis, MO) at room temperature for 30 minutes. Sections were washed with phosphate buffered saline and blocked with BSA and 0.01% Triton X-100 for 1 hour at room temperature. Slides were then incubated with either mouse monoclonal anti-human decorin or rabbit polyclonal anti-human biglycan antibody (Santa Cruz Biotechnology, Santa Cruz, CA), 1:100 dilution, overnight at 4˚C. Sections were then washed and incubated with the appropriate secondary antibody (Alexa Fluor 546 Alexa® goat anti-mouse IgG, Alexa Fluor 546® goat anti-rabbit IgG, Invitrogen, Burlington, ON) for 1 hour at room temperature prior to mounting (ProLong® Gold Antifade Reagent with DAPI, Invitrogen, Burlington, ON). In controls for decorin and

biglycan staining, primary antibodies were omitted resulting in negative staining (data not shown).

Toluidine blue staining for mast cell detection

Mast cells were detected using toluidine blue staining as previously described [Wang 2011]. Briefly, paraffin sections were deparaffinized and rehydrated through five changes of decreasing gradient ethanol. Sections were then stained in toluidine blue (Toluidine Blue O, Fisher Scientific Company, Fair Lawn, NJ) solution for 3 minutes followed by washing in distilled water and dehydration through five changes of increasing gradient ethanol. Sections were cleared in two changes of xylene and mounted with glass coverslips. Mast cells were quantified by counting the number of reddish-purple cells in 5 random, high-power fields under 200x magnification in all sections and from each time point.

Picrosirius red staining of collagen fibers

Picrosirius red staining on paraffin embedded sections was performed as previously described [41] in order to exploit differences in the birefringence of collagen fibers enhanced by Sirius red. Briefly, sections were first deparaffinized and rehydrated through five changes of decreasing gradient ethanol and incubated in a solution containing Sirius red (Sigma-Aldrich Inc., St. Louis, MO) and picric acid (Sigma-Aldrich Inc., St. Louis, MO) for 1 hour at room temperature. Sections were then washed in two changes of acidified water, dehydrated in 100%

ethanol, cleared in xylene and mounted with Permount (Fisher Scientific Company, Fair Lawn, NJ).

Microscopy and image analysis

H & E, Masson's trichrome, α-SMA and toluidine blue stained sections were examined using a Zeiss Axioplan 2 microscope and photographed using an AxioCam MRc digital camera. Anti-human HLA-ABC, decorin and biglycan stained sections were examined using a Colibri microscope and photographed using an AxioCam HRm digital camera. Picrosirius red stained sections were examined using a polarizing microscope (AxioImager.A1, Carl Ziess MicroImaging Inc., Thornwood, NY) and photographed using a Canon PowerShot A640 (Canon Canada Inc., Mississauga, ON). Scar thickness measurements, image processing and scale bars were added using Zeiss AxioVision 4.6.3 (Carl Ziess MicroImaging Inc., Thornwood, NY) and Adobe Photoshop® CS5 Extended Version 12.0 x64 for Macintosh (Adobe Systems Inc., San Jose, CA). Decorin and biglycan immunofluorescence was quantified using ImageJ for Macintosh version 1.43r (NIH, USA).

Statistical analysis

Animal studies involved 5 mice per treatment group and experiments were carried out in at least triplicate. Statistical analysis was performed using STATA for Macintosh version 10.0 (College Station, TX). Statistical tests used include a 2-tailed, unpaired Student's t-test or in cases of paired data a paired t-test and an

analysis of variance (ANOVA). Intraclass correlation coefficient was used to estimate interrater agreement. Results are presented as means ± SE. Probability values of p-value < 0.05 were considered significant.

2.3 Results

Morphologic observations

Transplanted human skin grafts remained clinically viable throughout the entire course of the experiment. In one animal, the graft was lost due to mechanical shearing in the early postoperative period. This wound healed by contraction and without complication. The remaining 19 animals grafted with human split thickness xenografts developed red, thickened scars, with a shiny skin texture consistent with human HSc (Fig. 2-2). These scars were firm on palpation and inelastic compared to the surrounding normal skin. In contrast, full thickness nude mouse autografts were completely healed two weeks after grafting and at one month appeared slightly hyperpigmented, with flush contour, matte skin texture and minimal to no contraction (Fig. 2-2). At seven days postoperatively, human xenografts on WT BALB/c mice had not taken to the wound bed. By fourteen days grafts were hard and black and by 1 month they had been completely rejected and the wound healed by contraction.

Objective scar assessment

Blinded, independent evaluation by 5 scar assessors of n=160 proliferative xenograft scar images and n=100 autograft images shows an average MSS score

of 15.9 ±0.2 for proliferative xenograft scars compared to 8.2 ±0.1 for autografted controls ($p < 0.01$) (Fig. 2-3). The intraclass correlation coefficient amongst all scar assessors was 0.91. This demonstrates strong interrater agreement. In order to determine the level of intrarater consistency repeat scar images were included in the scar assessment. The vast majority of differences (>95%) were either 0 or ±1. The mean difference between repeat images was 0.6 ±0.08. Blinded, independent, morphologic scar assessment therefore supports the contention that split thickness human skin grafts transplanted onto nude mice consistently and reliably resemble human HSc.

Survival of engrafted human skin

One of the strengths of this model is that human skin is used to generate HSc. To confirm survival of engrafted human split thickness skin transplants, immunofluorescent staining for HLA-ABC antigens, present on all nucleated human cells, was performed. Direct immunofluorescence for human HLA-ABC antigens in proliferative xenograft scars confirms revascularization and survival of transplanted human skin at all postoperative time points up to 180 days following grafting (Fig. 2-4). The green, net-like, immunofluorescent staining pattern seen in animals grafted with split thickness human skin is identical to the staining pattern observed in normal human skin positive controls (Fig. 2-4). This staining is absent in normal mouse skin negative controls (data not shown).

Histological characteristics

Histopathological features of human HSc scar were also demonstrated in our proliferative xenograft scars and noticeably absent in both nude mouse normal skin and autografts. Consistent with human HSc our proliferative xenograft scars showed evidence of loss of hair follicles, rete pegs and adnexal structures and hypercellularity on H & E staining (Fig. 2-5). There was also a change in collagen fiber morphology. The normal basket-weave organization of collagen fibers seen in normal skin and nude mouse autografts using Masson's trichrome staining was replaced by fine, whorled bundles of collagen seen in HSc (Fig. 2-6). Skin measurements showed an average proliferative xenograft scar thickness of 540.9 ±15.7 μm, compared to 217.8 ±5.1 μm for autograft controls and 157.0 ±3.3 μm for normal unwounded mouse skin ($p < 0.01$) (Fig. 2-7). This represents an average increase in thickness of 154.0 ±7.4% compared to the original split thickness human skin graft (Fig. 2-8). Therefore, the increase observed in proliferative xenograft scar thickness is not attributable to simply placing a thicker graft onto the mouse. Moreover, a modest 33.8 ±3.4% increase in thickness seen in nude mouse autografts indicates that increased proliferative xenograft scar thickness cannot be accounted for by changes that occur in normal wound healing. The increased thickness in proliferative xenograft scars peaks at 60 days postoperatively and remains elevated up to 180 days. The increase in thickness was noted in both the epidermal and dermal layers as seen in human HSc.

Elevated expression of α-SMA in proliferative xenograft scars

α-SMA, a protein expressed in vascular smooth muscle and also by α-SMA expressing myofibroblasts, is a pathognomonic feature of human HSc [6]. Proliferative xenograft scar sections stained for α-SMA demonstrate a positive, brown staining pattern throughout the dermis consistent with α-SMA expression in human HSc (Fig. 2-9). In contrast, normal human dermis negative controls only stain positive for SMA surrounding blood vessels (Fig. 2-9).

Decreased decorin and increased biglycan expression in proliferative xenograft scars

Decorin is one of two class 1 small leucine-rich proteoglycans (SLRPs) with cysteine-rich clusters at both ends and a single dermatan sulfate side chain [42, 43]. It is the most abundant proteoglycan in the skin [42]. While the role of decorin in wound healing continues to be elucidated what is known is that it is an important molecule in collagen fibrillogenesis [44]. Decorin interacts with type I collagen *in vivo* and modulates fibril structure [44-47]. In HSc decorin has been shown to be significantly downregulated [48-50]. Decorin is also known to downregulate transforming growth factor (TGF)-β, a potent profibrotic cytokine involved in HSc [51-53]. The other class 1 SLRP is biglycan. The structure of biglycan is similar to decorin in that it also has a leucine-rich repeat core flanked by cysteine-rich regions, however it differs in that it carries two dermatan sulfate chains [45, 54]. Recently, biglycan has been shown to be upregulated in HSc

while decorin expression is downregulated compared to normal skin and mature scar [40].

Indirect immunofluorescent staining for decorin in our model qualitatively demonstrates decreased expression of decorin in proliferative xenograft scars at 30 and 60 days postoperatively with increased expression at 120 and 180 days compared to normal human skin (Fig. 2-10). Quantification of decorin immunofluorescence relative to normal human skin confirms decreased expression in proliferative xenograft scars for as long as two months following grafting ($p < 0.01$) (Fig. 2-11). In contrast, staining for biglycan in proliferative xenograft scars shows increased expression at 30 and 60 days postoperatively with decreased expression at 180 days compared to normal human skin (Fig. 2-12). Quantification of biglycan expression in proliferative xenograft scars relative to normal human skin reveals a greater than 2-fold increase at 30 and 60 days with normalization at 120 days and decreased expression at 180 days postoperatively ($p < 0.01$) (Fig. 2-13).

Increased mast cell density in proliferative xenograft scars

Increased mast cell density has been previously demonstrated in both human HSc [55] as well as animal models of HSc [56, 34]. Toluidine blue staining of proliferative xenograft scars reveals infiltration of dark, reddish-purple mast cells (Fig. 2-14). Qualitatively there are increased numbers of mast cells in proliferative xenograft scar sections compared to normal skin (Fig. 2-14). This

observation is verified by quantification of mast cells in five random, high-power fields under 200x magnification. In proliferative xenograft scars there are 20.3 ±1.9, 22.4 ±2.2, 18.8 ±3.1 and 27.0 ±4.4 mast cells per high power field at 30, 60, 120 and 180 days respectively. In contrast, there are 9.8 ±0.9 mast cells per high power field in normal mouse skin ($p < 0.05$) (Fig. 2-15).

Collagen fibers arranged parallel to skin surface

Collagen fiber organization and morphology was examined by viewing picrosirius red stained sections of normal skin, human HSc and proliferative xenograft scars with polarized light. Fibrillar collagen in proliferative xenograft scars and human HSc appears thin, orange-yellow in color and was oriented parallel to the skin surface (Fig. 2-16). In contrast (Fig. 2-16) normal skin fibers appear thicker and organized in a random, basket-weave pattern.

2.4 Discussion

In the last two decades several reports have described animal models of HSc [22, 25, 32-34, 37, 56-58]. These models attempt to improve our understanding of HSc and guide treatment, however, because of limitations inherent in each the precise pathophysiology of HSc remains unknown. The rabbit ear model involves full-thickness wounds overlying ear cartilage [22]. In this model the underlying cartilage undergoes inflammation and also hypertrophies. This wound environment is different from deeper burns affecting humans, which do not usually overlie cartilage, but rather deep dermis or subcutaneous tissues. The

female, red Duroc pig model uses deep to full thickness wounds on the back of the animal to create scar [32, 33, 59]. Although normal pig skin is the most similar to human skin, the resulting scars generated on these animals were depressed and therefore morphologically dissimilar to human HSc. This large animal model is also expensive. Numerous models have transplanted heterologous HSc and keloid tissue into immune deficient mice [26-28, 30]. Initially the concern with these models was poor revascularization of transplanted tissue. More importantly, isolation of scar in its terminal stage of formation from its offending environment limits the study of local and systemic factors responsible for its development. Recently, a mechanical load model [56] showed morphologic and histologic similarities to human HSc. This model is limited in that it does not address the cells involved in HSc pathophysiology or use human tissue.

In 2007 Yang *et al.* established proof of concept for HSc formation in nude mice after transplantation of full thickness human skin grafts [37]. In this model, shedding of the epidermis and part of the dermis at one month prior to the formation of HSc suggests poor revascularization and possible transplant rejection [37]. Subsequently, the molecular and cellular biology of this model was further characterized [34], but survival of human tissue remains controversial.

In our model, human tissue transplanted to WT BALB/c mice was rejected at approximately ten days and healed by contraction without scar formation. In contrast, proliferative xenograft scars remained viable throughout the experiment

and showed objective signs of morphologic resemblance to human HSc 30 days after transplantation. One advantage of this model is the use of autografts as controls for morphologic scar comparison. Autografts healed favorably with minimal signs of pathologic scarring. Blinded review of scar images shows a significant difference in morphology of proliferative xenograft scars compared to autografts.

Clinical evidence of human skin transplant survival was verified histologically by positive staining for HLA-ABC antigens in all proliferative xenograft scars at all time points. Positive HLA-ABC staining was observed throughout the epidermis, the most distal and therefore the most difficult area of the graft to revascularize. As a result, potential prophylactic or therapeutic scar treatments could be tested on human tissue, without the need for human subjects.

The presence of other well established histologic criteria for HSc including loss of hair follicles, adnexal structures and rete pegs, hypercellularity and increase in thickness are represented in this model. Myofibroblasts pathognomonic for HSc are also present in increased numbers in proliferative xenograft scar sections compared to normal skin. In terms of changes in absolute and percent increase in thickness, use of nude mouse autografts provides the most appropriate comparison as it takes into account increases in thickness associated with normal wound healing.

Derangement of collagen architecture is illustrated with Masson's trichrome staining showing thin, whorled collagen fibers. These changes are further characterized by picrosirius red staining. Analysis of collagen fibers stained with picrosirius red under crossed polars shows thin fibers oriented parallel to the skin surface identical to human HSc. Alteration in expression patterns of proteoglycans in the ECM of proliferative xenograft scars may be responsible for the deposition of disorganized, small diameter collagen fibers in this model.

A novel feature observed in this model is the inverse expression of class 1 SLRPs, decorin and biglycan in proliferative xenograft scars. Decorin is known to be significantly lower in HSc tissue compared to normal skin [49, 52]. Decorin's ability to bind type I collagen and delay fibrillogenesis taken together with downregulation of decorin expression at 30 and 60 days may explain the resulting accumulation of thin, loosely packed collagen fibrils seen in proliferative xenograft scars. The role of decorin in proper ECM assembly has been demonstrated in decorin knockout mouse models of incisional wounds, myocardial infarction and tendon healing [47, 61, 62]. These data provide evidence to support disorganization of HSc collagen related to decorin levels and suggest a potential role for exogenous decorin replacement in the early phases of wound healing to lessen HSc formation [62-64]. Decorin binding and inactivation of TGF-β is also reduced in decorin-deficient wound environments. This relative increase in TGF-β acts via the Smad pathway to regulate fibrosis and can be suppressed by exogenous decorin administration [65].

Concordant increase in biglycan expression at 30 and 60 days reflects compensatory changes that occur with SLRPs of the same class. Subsequent overexpression of decorin and downregulation of biglycan at 120 and 180 days following grafting likely represents remodeling of proliferative xenograft scars and stabilization of wound healing [66]. Immunohistochemical localization of other proteoglycans in scars including fibromodulin and versican requires further study.

Clinical observation of increased frequency of HSc following thermal injury suggests prolonged inflammation associated with slowly healing dermal wounds as a potential etiology. Several inflammatory cells may play a role in HSc formation. An increased density of histamine-releasing mast cells observed in proliferative xenograft scars results clinically in vasodilation and redness of scars and symptoms of pruritus. During normal wound healing mast cell numbers peak by day two to three then return to normal. Increased mast cell density in our model persists up to six months and indefinitely in human HSc [67]. Histamine release is also linked to increased collagen synthesis [68], fibroblast and endothelial cell proliferation [69, 70]. However, normal wound healing is also supported by activation of cutaneous mast cells, which degranulate, release histamine and promote extravasation and recruitment of neutrophils. H1 receptor blockade impairs normal wound healing [71] highlighting a precise balance and role of mast cells in wound repair and HSc that is not completely understood.

Chymase, a neutral protease, released from mast cell secretory granules has been shown to degrade ECM [72] and free matrix-bound TGF-β [73] *in vitro*. *In vivo*, increased mast cells and chymase activity suggest a possible role for mast cell chymase in HSc formation [74].

Wang et al. have shown an increased infiltration of macrophages and fibrocytes in the nude mouse model [34]. Fibrocytes are bone marrow-derived cells that differentiate from CD14+ precursors and migrate into regions of tissue injury [75]. Fibrocytes normally represent <1% of peripheral blood mononuclear cells; however, following burn injury they can constitute up to 10% of inflammatory cells [76]. Fibrocytes play a role in fibrogenic cytokine production, chemokine production, secretion of angiogenic factors and ECM deposition in numerous FPDs including pulmonary fibrosis [77], atherosclerosis [78, 79], scleroderma [80], nephrogenic systemic fibrosis [81], liver cirrhosis [82] and HSc [83]. Fibrocytes are increased in the blood of burn patients with HSc [76] and have been identified in post-burn HSc tissue [84].

We speculate that the interaction between an activated tissue injury response in prepared human split thickness skin grafts and local and systemic upregulation of profibrotic growth factors and proinflammatory cytokines in response to foreign antigens is sufficient to create a wound milieu conducive to transformation of circulating fibrocytes into activated, profibrotic fibrocytes.

2.5 Conclusions

In conclusion, we observed that grafting split thickness human skin onto the backs of nude mice results in proliferative xenograft scars that are morphologically, histologically and immunohistochemically consistent with human HSc. However, it is unclear if this process of scar formation is fully consistent with human HSc formation. To our knowledge this is the first animal model of HSc to demonstrate reciprocal changes in SLRP expression known to be consistent with patterns observed in human HSc. Lastly, the survival of human skin up to 180 days after transplantation would facilitate the trial of therapeutic and prophylactic scar treatments on human tissues. Therefore, this model provides a promising technique to examine both the cause of HSc and treatments for patients.

2.6 Tables

Table 2-1: Modified Manchester Scar Scale (MSS).

Color Match	
Perfect	1
Slight mismatch	2
Obvious mismatch	3
Gross mismatch	4

Contour	
Flush with surrounding skin	1
Slight Change in Elevation	2
Moderate Change in Elevation	3
Severe Change in Elevation	4

Contraction/Distortion	
No Contraction/Distortion	1
Mild Contraction/Distortion	2
Moderate Contraction/Distortion	3
Severe Contraction/Distortion	4

Quality of Surface	
Matte (Dull)	1
Shiny	2

Score Range: 4-14

Visual Analogue Scale

Excellent ———————————————————— **Poor**

Score Range: 1-10

2.7 Figures

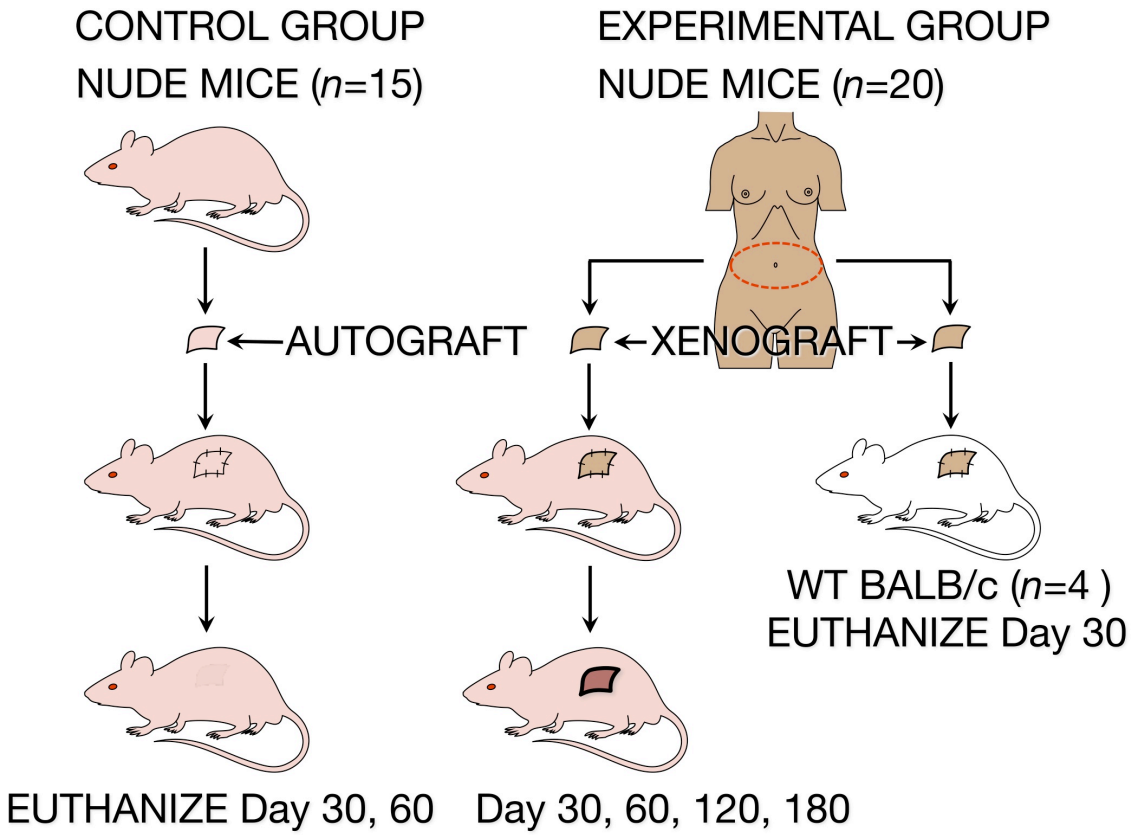

Figure 2-1: A nude mouse model to test the development of human hypertrophic scar. Controls (*n*=18) consisted of nude mice autografted with full thickness nude mouse skin. Experimental group (*n*=20) included nude mice xenografted with split thickness human skin. Wild-type BALB/c (*n*=4) mice were also xenografted with split thickness human skin in order to observe tissue rejection.

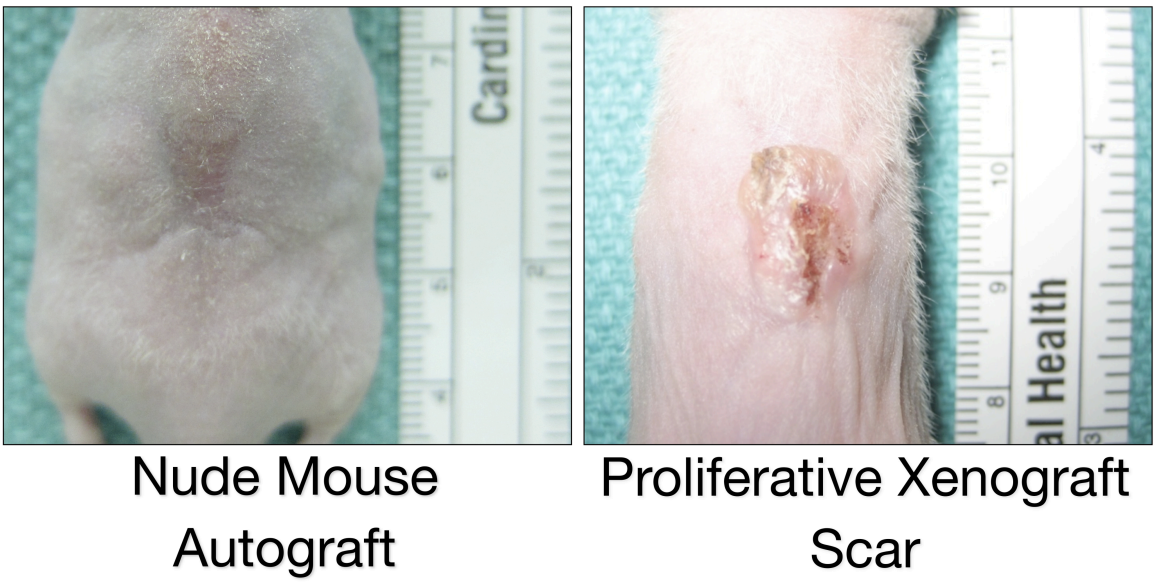

Figure 2-2: *(Left)* Nude mouse autograft and *(Right)* proliferative xenograft scar morphologic appearance at 30 days following grafting. *(Left)* The nude mouse autograft control demonstrates a favorable healing result with minimal hyperemia, relatively flush contour and a dull appearance to the skin. *(Right)* In contrast, our proliferative xenograft scar demonstrates an obvious color mismatch and hyperemia, an increase in thickness and shiny surface texture consistent with human hypertrophic scar.

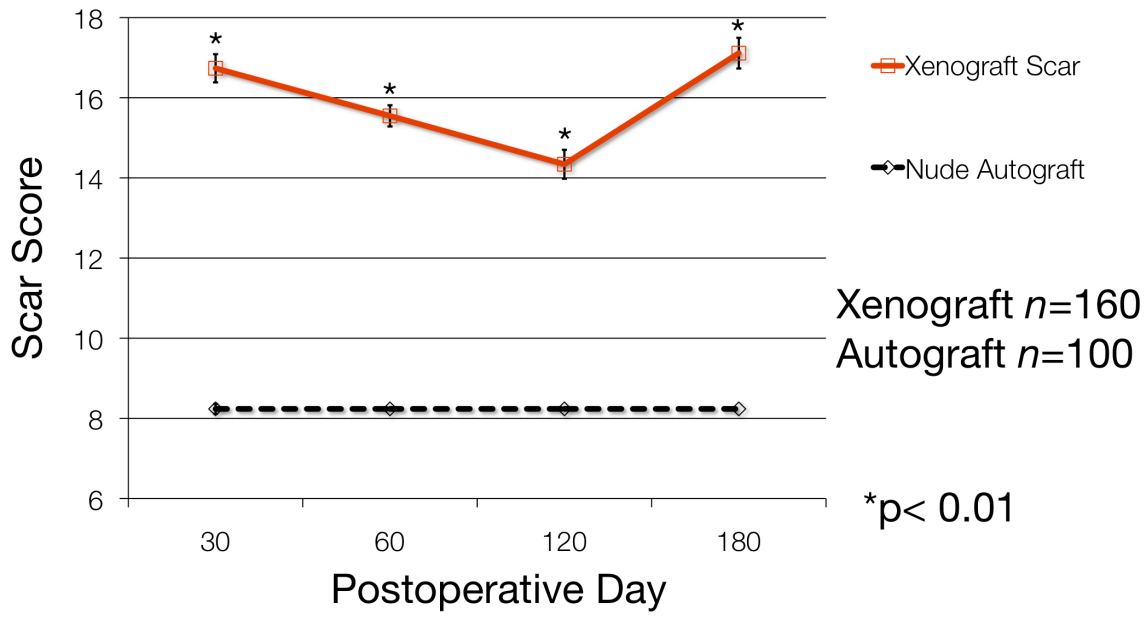

Figure 2-3: Modified Manchester Scar Scale (MSS) scores for proliferative xenograft scars compared to nude mouse autografts over time. Average MSS score of 15.9 ±0.2 for proliferative xenograft scars compared to 8.2 ±0.1 for autografted controls ($p < 0.01$) with an intraclass correlation coefficient of 0.91 demonstrating strong rater reliability.

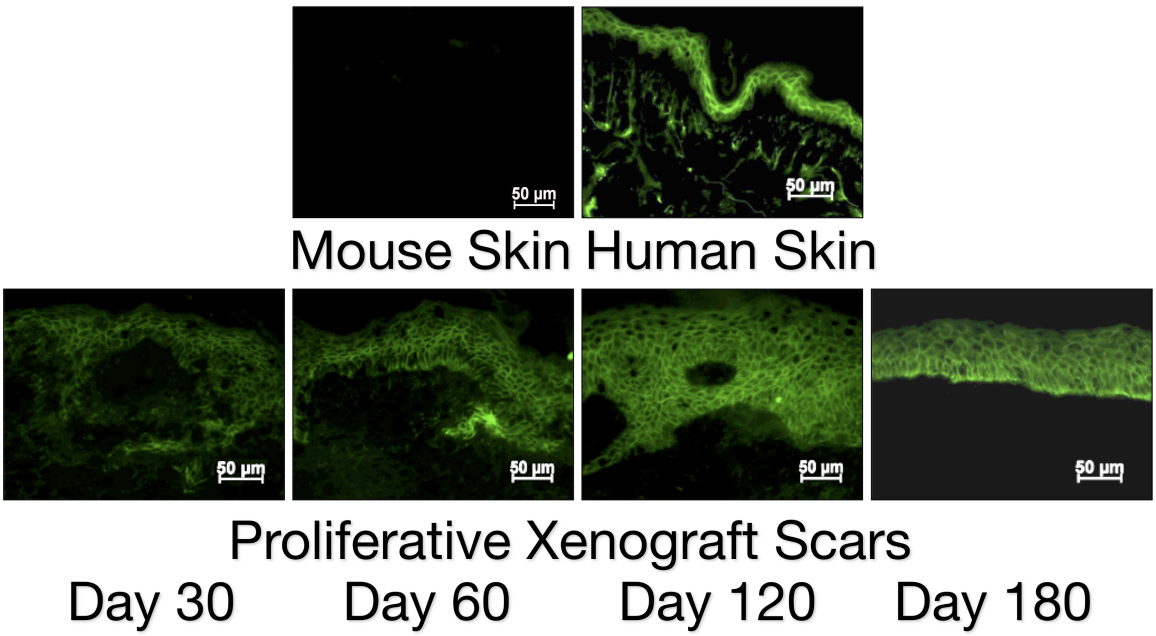

Figure 2-4: *(Second row, right)* Representative images of anti-human FITC HLA-ABC antibody stained sections confirm engraftment and survival of transplanted human skin at 30, 60, 120 and persisting up to 180 days following grafting. *(First row)* This green, net-like, immunofluorescent staining pattern is consistent with positive staining seen in normal human skin. (Second row, left) There is no visible green staining present in the mouse skin negative control.

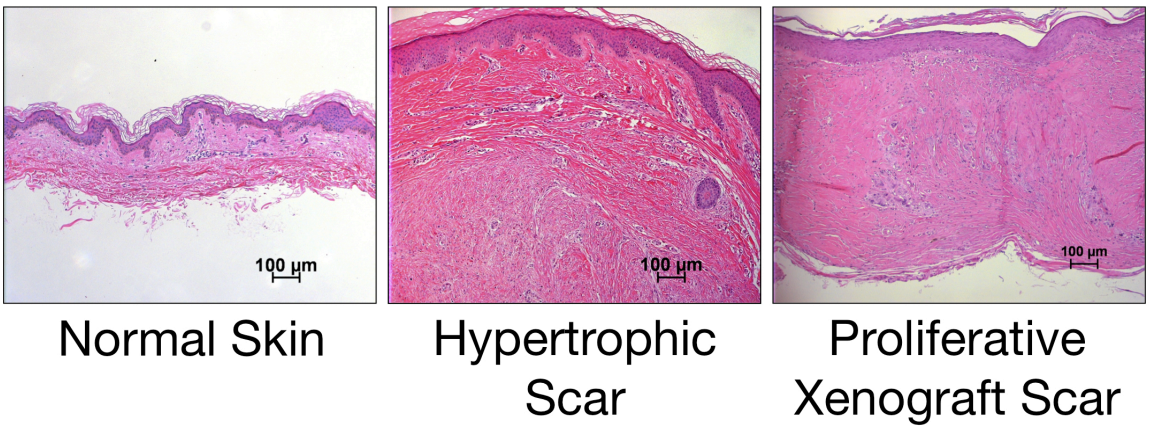

Figure 2-5: *(Right)* Representative image of a hematoxylin and eosin stained section of proliferative xenograft scar demonstrates loss of hair follicles, adnexal structures, and rete pegs and hypercellularity consistent with *(Center),* human hypertrophic scar and in contrast to *(Left)* normal human skin.

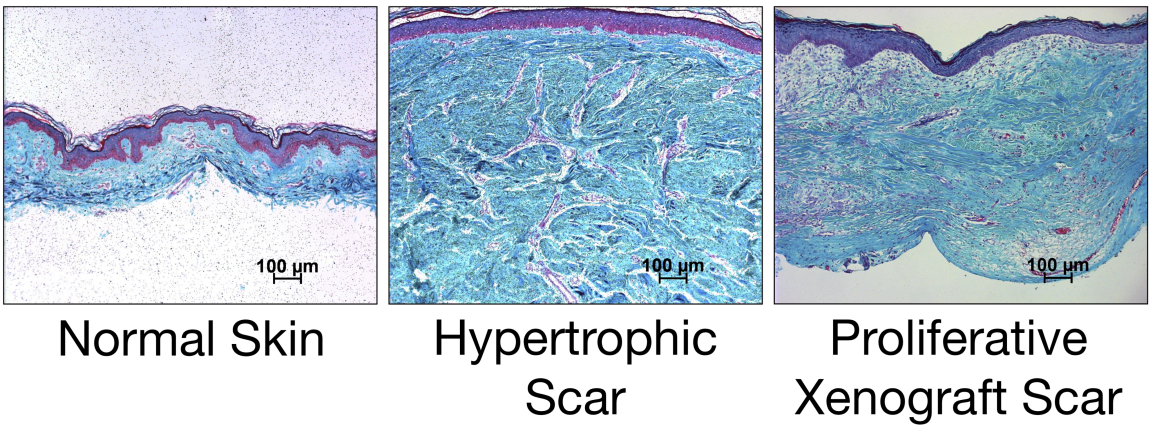

Figure 2-6: *(Right)* Representative image of a Masson's trichrome stained section of proliferative xenograft scar demonstrates abnormal, whorled collagen bundle morphology consistent with *(Center)* human hypertrophic scar and in contrast to the basket-weave collagen bundle pattern seen in *(Left)* normal skin.

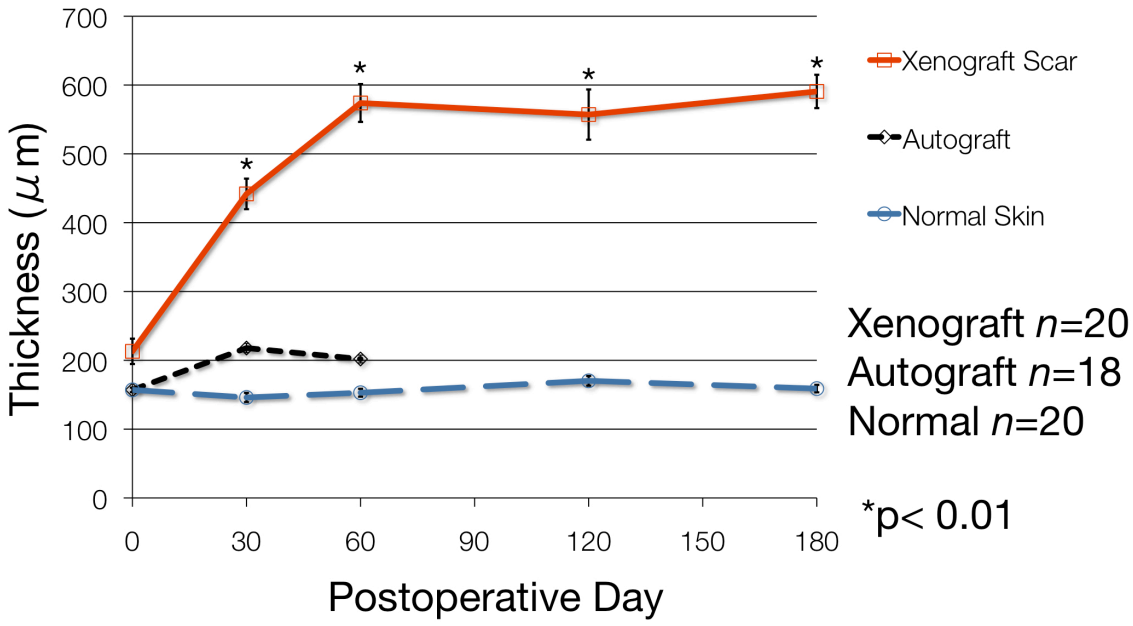

Figure 2-7: Normal nude mouse skin, nude mouse autograft and proliferative xenograft scar thickness over time. Average proliferative xenograft scar thickness of 540.9 ±15.7 μm, compared to 217.8 ±5.1 μm for autograft controls and 157.0 ±3.3 μm for normal, unwounded mouse skin ($p < 0.01$).

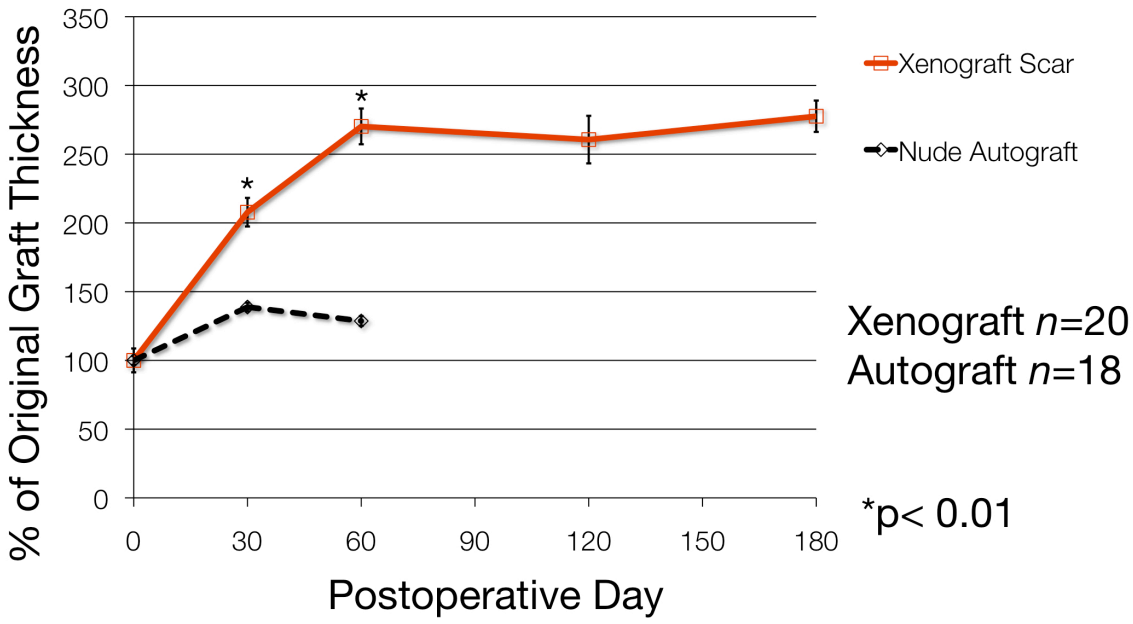

Figure 2-8: Percent increase in nude mouse autograft and proliferative xenograft scar thickness compared to original graft thickness over time. Proliferative xenograft scars increased in thickness by 154.0 ±7.4% compared to 33.8 ± 3.4% for nude mouse autografts ($p < 0.01$).

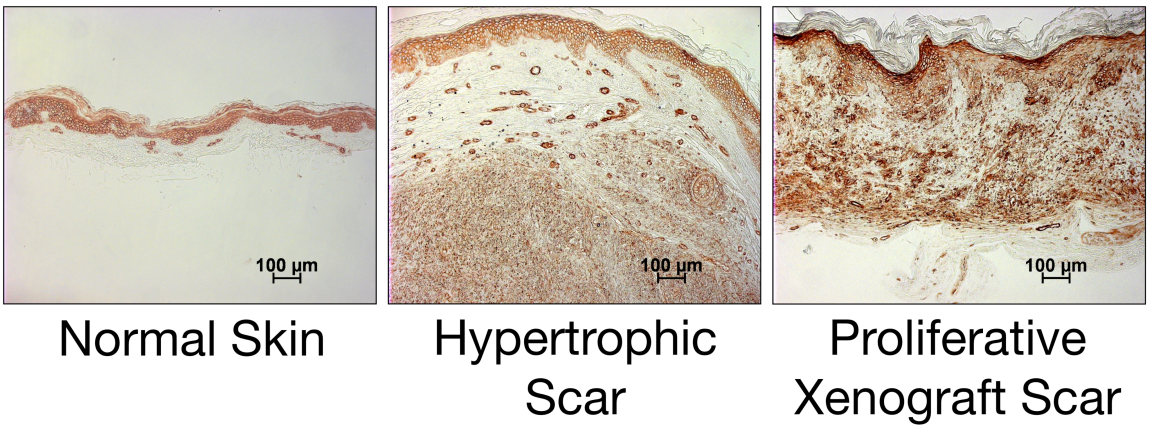

Figure 2-9: *(Right)* Representative image of an α-SMA stained section of proliferative xenograft scar demonstrates a positive brown staining pattern indicating the presence of myofibroblasts throughout the dermis similar to that seen in *(Center)* human hypertrophic scar. In contrast, *(Left)* normal human dermis does not stain positive for α-SMA except surrounding blood vessels.

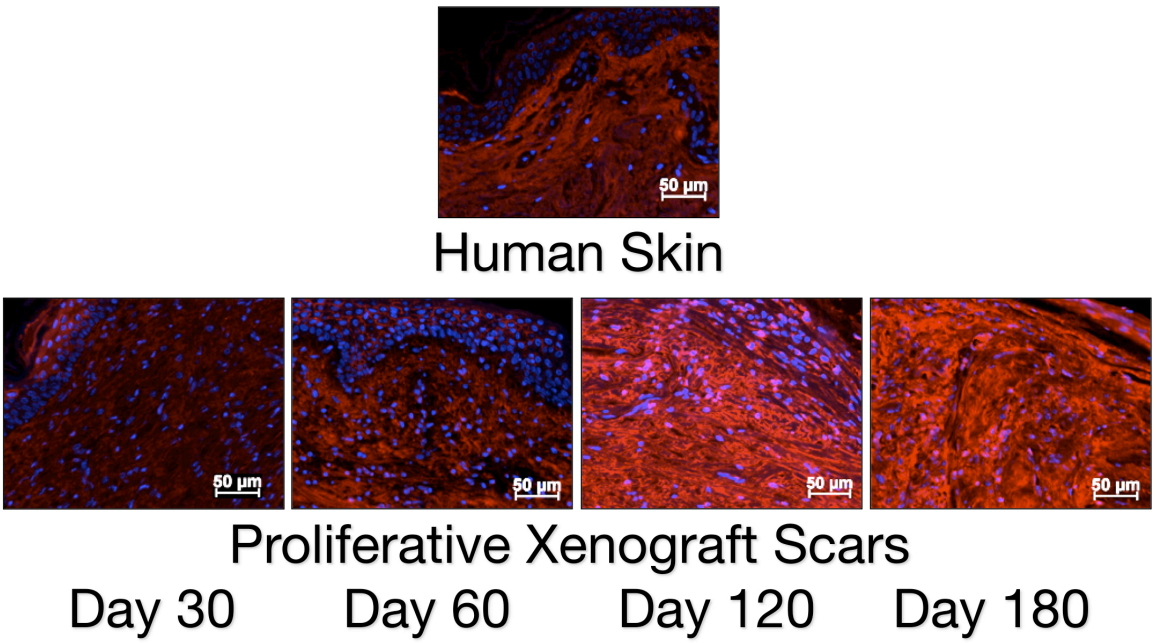

Figure 2-10: *(Second row, first and second)* Representative immunofluorescent images of decorin stained sections of proliferative xenograft scars demonstrate decreased expression at 30 and 60 days postoperatively. *(Second row, third and fourth)* Increased decorin expression is observed at 120 and 180 days postoperatively compared to *(First row)* the normal human skin control.

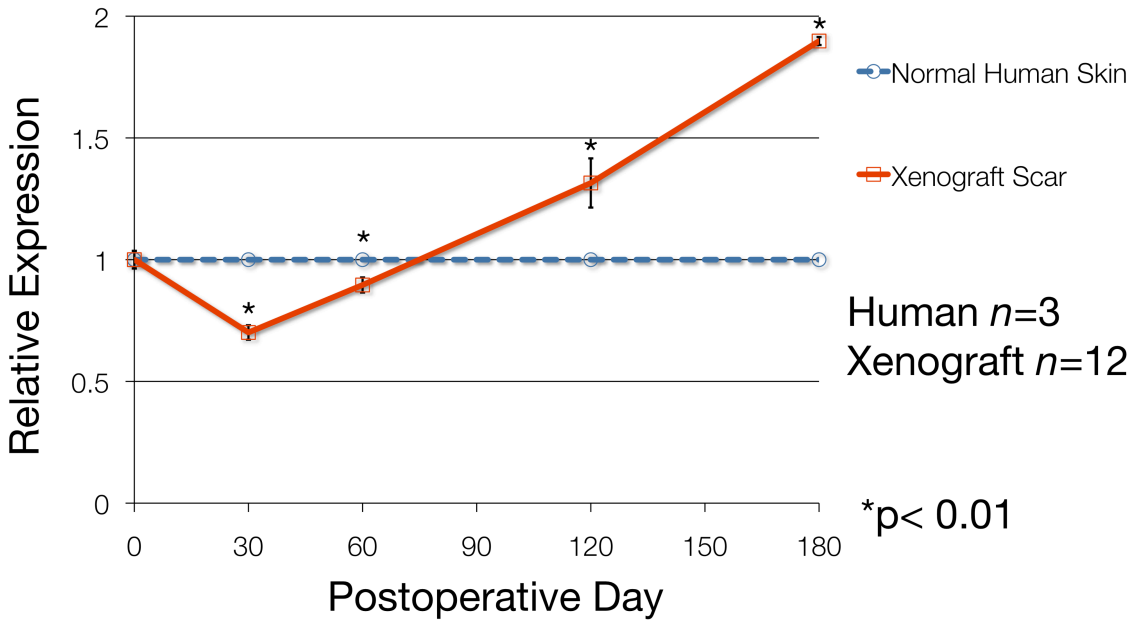

Figure 2-11: Quantification of decorin immunofluorescence in proliferative xenograft scars (*n*=12) relative to normal human skin (*n*=3) demonstrates less decorin expression at 30 and 60 days postoperatively ($p < 0.01$). However this expression pattern changes at 120 and 180 days following transplantation where there is increased expression of decorin in proliferative xenograft scars compared to normal human skin.

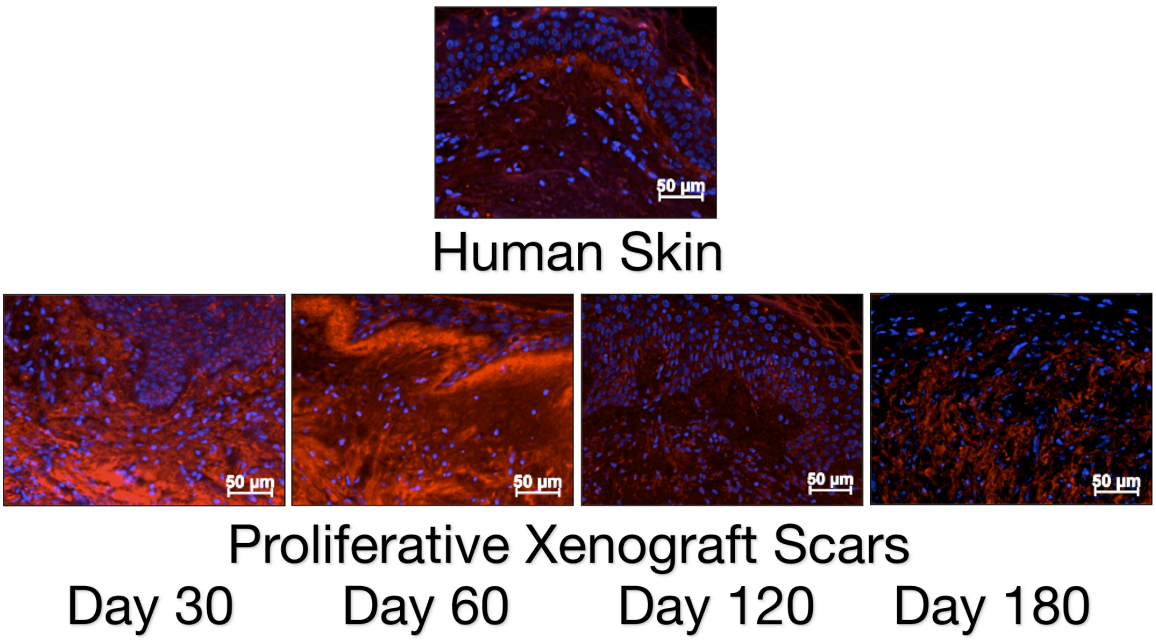

Figure 2-12: *(Second row, first and second)* Representative immunofluorescent images of biglycan stained sections of proliferative xenograft scars demonstrate increased expression at 30 and 60 days postoperatively. *(Second row, third)* Decreased biglycan expression is observed at 120 and 180 days postoperatively compared to *(First row)* the normal human skin control.

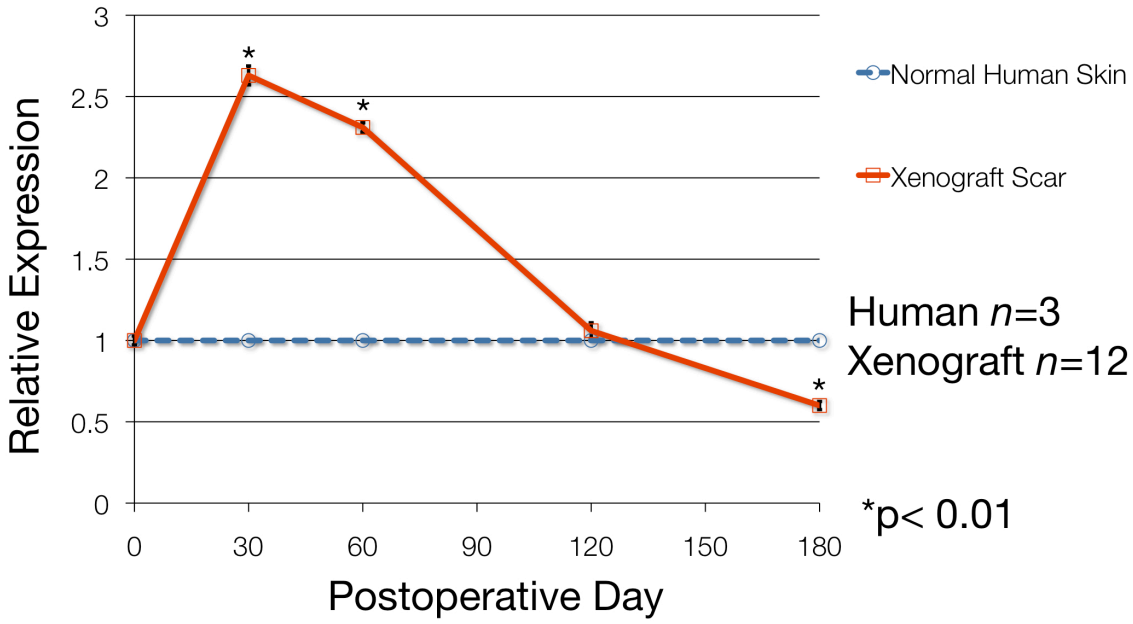

Figure 2-13: Quantification of biglycan immunofluorescence in proliferative xenograft scars (*n*=12) relative to normal human skin (*n*=3) demonstrates increased biglycan expression at 30 and 60 days postoperatively ($p < 0.01$). At 120 days there is normalization of biglycan expression in proliferative xenograft scars followed by decreased expression at 180 days compared to normal human skin.

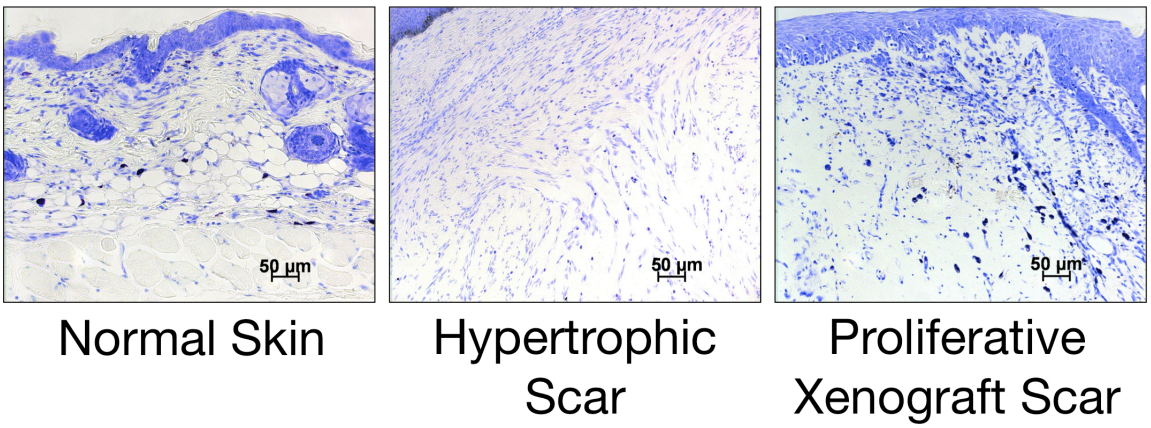

Figure 2-14: *(Right)* Representative image of a toluidine blue stained section of a proliferative xenograft scar at postoperative day 180 demonstrates an increased density of dark, red-purple staining mast cells similar to that seen in *(Center)* human hypertrophic scar. In contrast, *(Left)* there are fewer mast cells seen in normal skin.

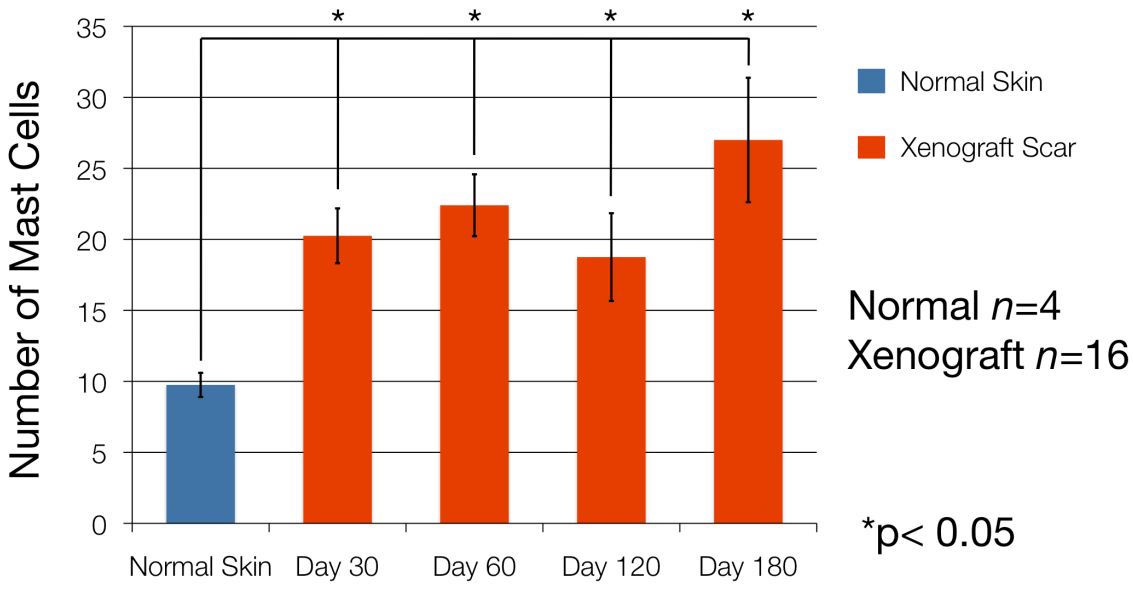

Figure 2-15: Quantification of mast cells in 5 random, high-power fields under 200x magnification demonstrates 20.3 ±1.9, 22.4 ±2.2, 18.8 ±3.1 and 27.0 ±4.4 mast cells at 30, 60, 120 and 180 days respectively compared to 9.8 ±0.9 mast cells in normal mouse skin ($p < 0.05$).

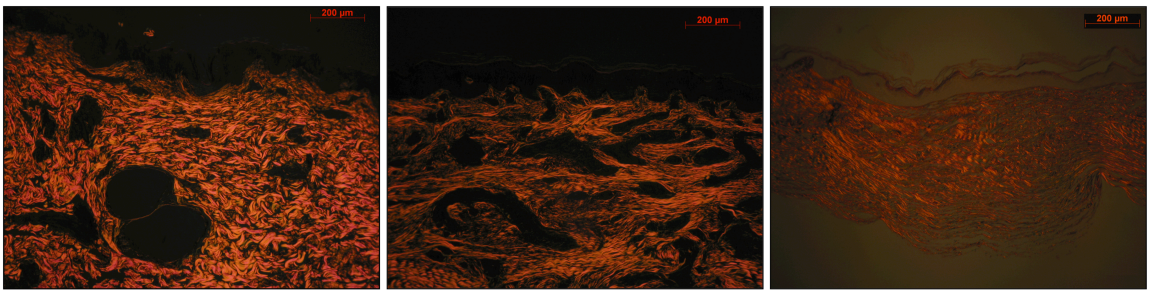

Figure 2-16: *(Right)* Representative image of a picrosirius red stained section of proliferative xenograft scar demonstrates thin, orange-yellow collagen fibers oriented parallel to the skin surface and consistent with *(Center)* collagen fiber orientation in human hypertrophic scar. In contrast *(Left)* thicker, random, basket-weave pattern collagen fiber organization is seen in normal human skin.

2.8 Bibliography

1. Lorenz HP, Longaker MT. Wound healing: Repair biology and wound and scar treatment. In: Mathes SJ, eds. *Plastic Surgery.* Vol. 1, 2nd ed. Philadelphia: Saunders; 2006:209-234.
2. Murray JC Keloids and hypertrophic scars. *Clin Dermatol* 1994;12:27-37.
3. Dunkin CSJ, Pleat JM, Gillespie PH, et al. *Plast Reconstr Surg* 2007;119:1722-1732.
4. Mustoe TA, Cooter RD, Gold MH, et al. International clinical recommendations on scar management. *Plast Reconstr Surg* 2002;110:560-571.
5. Mustoe TA. Scars and keloids. *Br Med J* 2004;328:1329-1330.
6. Ehrlich HP, Desmoulière A, Diegelmann RF, et al. Morphological and immunochemical differences between keloid and hypertrophic scar. *Am J Pathol* 1994;145:105-113.
7. Ryan CM Objective estimates of the probability of death from burn injuries. *N Engl J Med* 1998;338:362-366.
8. Deitch EA, Wheelahan TM, Rose MP, et al. Hypertrophic burn scars: analysis of variables. *J Trauma* 1983;23:895-898.
9. Dedovic Z, Koupilova I, Brychta, P. Time trends in incidence of hypertrophic scarring in children treated for burns. *Acta Chir Plast* 1999;41:87-90.
10. Bombaro KM. What is the prevalence of hypertrophic scarring following burns? *Burns* 2003;29:299-302.

11. Köse O, Waseem A. Keloids and hypertrophic scars: Are they two different sides of the same coin? *Dermatol Surg* 2008;34:336-346.
12. Nedelec B, Ghahary A, Scott, PG, et al. Control of wound contraction. Basic and clinical features. *Hand Clin* 2000;16:289-302.
13. Tredget EE. Pathophysiology and treatment of fibroproliferative disorders following thermal injury. *Ann N Y Acad Sci* 1999;888:165-182.
14. Brigham PA, McLoughlin E. Burn incidence and medical care use in the United States: estimates, trends, and data sources. *J Burn Care Rehabil* 1996;17:95-107.
15. Engrav LH. Impairment, time out of school, and time off from work after burns. *Plast Reconstr Surg* 1987;79:927-934.
16. Tredget EE, Nedelec B, Scott PG. et al. Hypertrophic scars, keloids, and contractures. The cellular and molecular basis for therapy. *Surg Clin North Am* 1997;77:701-730.
17. Helm PA. Burn rehabilitation: dimensions of the problem. *Clin Plast Surg* 1992;19:551-559.
18. Fraulin FO, Illmayer SJ, Tredget EE. Assessment of cosmetic and functional results of conservative versus surgical management of facial burns. *J Burn Care Rehabil* 1996;17:19-29.
19. Carr-Collins JA. Pressure techniques for the prevention of hypertrophic scar. *Clin Plast Surg* 1992;19:733-743.
20. Castagnoli, C. The HLA-DR beta 16 allogenotype constitutes a risk factor for hypertrophic scarring. *Hum Immunol* 1990;29:229-232.

21. Greenhalgh DG. Models of wound healing. *J Burn Care Rehabil* 2005;26:293-305.

22. Morris DE, Wu L, Zhao LL, et al. Acute and chronic animal models for excessive dermal scarring: quantitative studies. *Plast Reconstr Surg* 1997;100:674-681.

23. Ramos, MLC, Gragnani A, Ferreira LM. Is there an ideal animal model to study hypertrophic scarring? *J Burn Care Res* 2008;29:363-368.

24. Kwan P, Hori K, Ding J. et al. Scar and contracture: Biological principles. *Hand Clin* 2009;25:511-528.

25. Lee JP, Jalili RB, Tredget EE, Demare JR, Ghahary A. Antifibrogenic effects of liposome-encapsulated INF-alpha1b cream on skin wounds in a fibrotic rabbit ear model. *J Interferon Cytokine Res* 2005;25:627-631.

26. Kischer CW, Sheridan D, Pindur J. Use of nude (athymic) mice for the study of hypertrophic scars and keloids: vascular continuity between mouse and implants. *Anat Rec* 1989;225:189-196.

27. Kischer CW, Wagner HN Jr., Pindur J, et al. Increased fibronectin production by cell lines from hypertrophic scar and keloid. *Connect Tissue Res* 1989;23:279-288.

28. Kischer CW, Pindur J, Shetlar MR, et al. Implants of hypertrophic scars and keloids into the nude (athymic) mouse: viability and morphology. *J Trauma* 1989;29:672-677.

29. Shetlar MR, Shetlar CL, Kischer CW, et al. Implants of keloid and hypertrophic scars into the athymic nude mouse: changes in the glycosaminoglycans of the implants. *Connect Tissue Res* 1991;26:23-36.
30. Polo M, Kim Y-J, Kucukcelebi A, et al. An *in vivo* model of human proliferative scar. *J Surg Res* 1998;74:187-195.
31. Silverstein P, Helmkamp GM Jr., Walker HL, McKeel DW Jr., Pruit BA Jr. Laboratory evaluation of enzymatic burn wound debridement *in vitro* and *in vivo*. *Surg Forum* 1972;23:31-33.
32. Zhu, K.Q., Engrav, L.H., Gibran, N.S., et al. The female, red Duroc pig as an animal model of hypertrophic scarring and the potential role of the cones of skin. *Burns* 2003;29:649-664.
33. Harunari N, Zhu KQ, Armendari RT, et al. Histology of the thick scar on the female, red Duroc pig: final similarities to human hypertrophic scar. *Burns* 2006;32:669-677.
34. Wang JF, Ding J, Jiao H, et al. Human hypertrophic scar-like nude mouse model: Characterization of the molecular and cellular biology of the scar process. *Wound Repair Regen* 2011;19:274-285.
35. Su D-M, Navarre S, Oh W-J, et al. A domain of Foxn1 required for crosstalk-dependent thymic epithelial cell differentiation. *Nature Immunol* 2003;4:1128-1135.
36. Mecklenburg L, Tychsen B, Paus, R. Learning from nudity: lessons from the nude phenotype. *Exp Dermatol* 2005;14:797-810.

37. Yang DY, Li SR, Wu JL, et al. Establishment of a hypertrophic scar model by transplanting full-thickness human skin grafts onto the backs of nude mice. *Plast Reconstr Surg* 2007;119:104-119.

38. Beausang E, Floyd H, Dunn KW, Orton CI, Ferguson MW. A New Quantitative Scale for Clinical Scar Assessment. *Plast Reconstr Surg* 1998;102:1954-1961.

39. Duncan JAL, Bond JS, Mason, T, et al. Visual Analogue Scale Scoring and Ranking: A Suitable and Sensitive Method for Assessing Scar Quality? *Plast Reconst Surg* 2006;118:909-918.

40. Honardoust D, Varkey M, Hori K, et al. Small leucine-rich proteoglycans, decorin and fibromodulin, are reduced in postburn hypertrophic scar. *Wound Repair Regen* 2011;19:368-378.

41. Junqueira LCU, Cossermelli W, Brentani R. Differential staining of collagens type I, II and III by Sirius red and polarization microscopy. *Arch Histol Jap* 1978;41:267-274.

42. Krusius T, Ruoslahti E. Primary structure of an extracellular matrix proteoglycan core protein deduced from cloned cDNA. *Proc Natl Acad Sci USA* 1986;83:7683-7687.

43. Chopra RK, Pearson CH, Pringle GA, Fackre DS, Scott PG. Dermatan sulphate is located on ser-4 of bovine skin proteodermatan sulphate. *Biochem J* 1985;231:277-279.

44. Rühland C, Schönherr E, Robenek H, Hansen U, et al. The glycosaminoglycan chain of decorin plays an important role in collagen

fibril formation at the early stages of fibrillogenesis. *FEBS J* 2007;274:4246-4255.

45. Iozzo R. The biology of the small leucine-rich proteoglycans. *J Biol Chem* 1999;274:18843-18846.
46. Zhang G, Ezura Y, Chervoneva I, Robinson PS, et al. Decorin regulates assembly of collagen fibrils and acquisition of biomechanical properties during tendon development. *J Cell Biochem* 2006;98:1436-1449.
47. Neame PJ, Kay CJ, McQuillan DJ, Beales MP, Hassell JR. Independent modulation of collagen fibrillogenesis by decorin and lumican. *Cell Mol Life Sci* 2000;57:859-863.
48. Wang J, Dodd C, Shankowsky HA, Scott PG, et al. Deep dermal fibroblasts contribute to hypertrophic scarring. *Lab Invest* 2008;88:1278-1290.
49. Scott PG, Dodd CM, Ghahary A, Shen YJ, Tredget EE. Fibroblasts from post-burn hypertrophic scar tissue synthesize less decorin than normal dermal fibroblasts. *Clin Sci (Lond)* 1998;94:541-547.
50. Zhang Z, Li XJ, Liu Y, Zhang X, Recombinant human decorin inhibits cell proliferation and downregulates TGF-beta1 production in hypertrophic scar fibroblasts. *Burns* 2007;33:634-641.
51. Yamaguchi Y, Mann DM, Ruoslahti E. Negative regulation of transforming growth factor-beta by the proteoglycan decorin. *Nature* 1990;346:281-284.

52. Scott PG, Dodd CM, Tredget EE, Ghahary A, Rahemtulla F. Immunohistochemical localization of the proteoglycans decorin, biglycan and versican and transforming growth factor-β in human post-burn hypertrophic and mature scars. *Histopathology* 1995;26:423-431.

53. Wang R, Ghahary A, Shen Q, Scott PG, et al. Hypertrophic scar tissues and fibroblasts produce more transforming growth factor-beta1 mRNA and protein than normal skin and cells. *Wound Repair Regen* 2000;8:128-137.

54. Neame PJ, Choi Hu, Rosenberg LC. The primary structure of the core protein of the small leucine-rich proteoglycan (PG 1) from bovine articular cartilage. *J Biol Chem* 1989;264:8653-8661.

55. Tredget EE, Shankowsky HA, Pannu R, et al. Transforming growth factor-beta in thermally injured patients with hypertrophic scars: effects of interferon alpha-2b. *Plast Reconstr Surg* 1998;102:1317-1328.

56. Aarabi S, Bhatt KA, Shi Y, et al. Mechanical load initiates hypertrophic scar formation through decreased cellular apoptosis. *FASEB J* 2007;21:3250-3261.

57. Saulis, AS, Mogford JH, Mustoe TA. Effect of Mederma on hypertrophic scarring in the rabbit ear model. *Plast Reconstr Surg* 2002;110:177-186.

58. Kim I, Mogford JE, Witschi C, Nafissi M, Mustoe TA. Inhibition of prolyl 4-hydroxylase reduces scar hypertrophy in a rabbit model of cutaneous scarring. *Wound Rep Reg* 2003;11:368-372.

59. Gallant CL, Olson ME, Hart DA. Molecular, histologic, and gross phenotype of skin wound healing in red Duroc pigs reveals an abnormal healing phenotype of hypercontracted, hyperpigmented scarring. *Wound Rep Reg* 2004;12:305-319.

60. Järveläinen H, Puolakkainen P, Pakkanen S, et al. A role for decorin in cutaneous wound healing and angiogenesis. *Wound Repair Regen* 2006;14:443-452.

61. Weis SM, Zimmerman SD, Shah M, et al. A role for decorin in the remodeling of myocardial infarction. *Matrix Biol* 2005;24:313-324.

62. Raspanti M, Viola M, Sonaggere M, Tira ME, Tenni R. Collagen fibril structure is affected by collagen concentration and decorin. *Biomacromolecules* 2007;8:2087-2091.

63. Border WA, Noble NA, Yamamoto T, et al. Natural inhibitor of transforming growth factor-beta protects against scarring in experimental kidney disease. *Nature* 1992;360:361-364.

64. Kolb M, Margetts PJ, Sime PJ, Gauldie J. Proteoglycans decorin and biglycan differentially modulate TGF-beta-mediated fibrotic responses in the lung. *Am J Physiol Lung Cell Mol Physiol* 2001;280:L1327-L1334.

65. Zheng F, Lu W, Wu F, Li H, Hu X, Zhang F. Recombinant decorin ameliorates the pulmonary structure alterations by down-regulating transforming growth factor-beta1/SMADS signaling in diabetic rats. *Endocr Res* 2010;35:35-49.

66. Sayani K, Dodd CM, Nedelec B, et al. Delayed appearance of decorin in healing burn scars. *Histopathology* 2000;36:262-272.

67. Kischer CW, Bunce H 3rd, Shetlah MR. Mast cell analyses in hypertrophic scars, hypertrophic scars treated with pressure and mature scars. *J Invest Dermatol* 1978;70:355-357.

68. Rothe M, Nowalk M, Kerdel FA. The mast cell in health and disease: A greater role. *J Am Acad Dermatol* 1990;23:615-624.

69. Russell JD, Russel SB, Trupin KM. The effect of histamine on the growth of cultured fibroblasts isolated from normal and keloid tissue. *J Cell Physiol* 1977;93:389-393.

70. Marks RM, Roche WR, Czerniecki M, Penny R, Nelson DS. Mast cell granules cause proliferation of human microvascular endothelial cells. *Lab Invest* 1986;55:289-294.

71. Weller K, Foitzik K, Paus R, Syska W, Maurer M. Mast cells are required for normal healing of skin wounds in mice. *FASEB J* 2006;20:E1628-E1635.

72. Taipale J, Lohi J, Saarinen J, Kovanen PT, Keski-Oja J. Human mast cell chymase and leukocyte elastase release latent transforming growth factor beta from the extracellular matrix of culture human epithelial and endothelial cells. *J Biol Chem* 1995;270:4689-4696.

73. Vario T, Seepä H, Vaheri A. Susceptibility of soluble and matrix fibronectins to degradation by tissue proteinases, mast cell chymase and cathepsin G. *J Bio Chem* 1981;256:471-477.

74. Nishikori Y, Kakizoe E, Kobayashi Y, Shimoura K, Okunishi H, Dekio S. Skin mast cell promotion of matrix remodeling in burn wound healing in mice: Relevance of chymase. *Arch Dermatol Res* 1998;290:553-560.

75. Bucala R, Spiegel LA, Chesney J, Hogan M, Cerami A. Circulating fibrocytes define a new leukocyte subpopulation that mediates tissue repair. *Mol Med* 1994;1:71-81.

76. Yang L, Scott PG, Giuffre J et al. Peripheral blood fibrocytes from patients: Identification and quantification of fibrocytes in adherent cells cultured from peripheral blood mononuclear cells. *Lab Invest* 2002;82:1183-1192.

77. Hashimoto N, Jin H, Liu T, Chensue SW, Phan SH. Bone marrow-derived progenitor cells in pulmonary fibrosis. *J Clin Invest* 2004;113:243-252.

78. Han CI, Campbell GR, Campbell JH. Circulating bone marrow cells can contribute to neointimal formation. *J Vasc Res* 2001;38:113-119.

79. Varcoe RL, Mikhail M, Guiffre AK, Pennings G, Vicaretti M, Hawthorne WJ, Fetcher JP, Medbury HJ. The role of the fibrocytes in intimal hyperplasia. *J Thromb Haemost* 2006;4:1125-33.

80. Chesney J, Bucala R. Peripheral blood fibrocytes: mesenchymal precursor cells and the pathogenesis of fibrosis. *Curr Rheumatol Rep* 2000;2:501-505.

81. Cowper SE, Su LD, Bhawan J, Robin HS, LeBoit PE. Nephrogenic fibrosing dermatopathy. *Am J Dermatopathol* 2001;23:383-393.

82. Kisseleva T, Uchinami H, Feirt N, Quintana-Bustamante O, Segovia JC, Schwabe RF, Brenner DA. Bone marrow-derived fibrocytes participate in pathogenesis of liver fibrosis. *J Hepatol* 2006;45:429-438.

83. Bellini A, Mattoli S. The role of the fibrocyte, a bone marrow-derived mesenchymal progenitor, in reactive and reparative fibroses. *Lab Invest* 2007;87:858-870.

84. Yang L, Scott PG, Dodd C, et al. Identification of fibrocytes in postburn hypertrophic scar. *Wound Repair Regen* 2005;13:398-404.

3. Morphologic and Histological Comparison of Hypertrophic Scar in Nude and Knockout Mice Deficient in T, B and Natural Killer Cells

3.1 Introduction

Hypertrophic scar (HSc) is a fibroproliferative disorder (FPD) affecting the skin [1]. It has been shown that hypertrophic scarring occurs at a critical depth of dermal injury [2] and with increased frequency following burns [3-6]. In general, these pathological scars are limited to the area of original injury [7]. Macroscopically they appear hyperemic, shiny and elevated in relation to the surrounding skin. Histological features characterizing this disorder include thin, whorled collagen fibers oriented parallel to the skin, increased epidermal and dermal thickness, loss of rete ridges, hair follicles and adnexal structures, hypercellularity and hypervascularity [8]. Decreased expression of extracellular matrix (ECM) proteins such as small leucine-rich proteoglycans (SLRPs) decorin and fibromodulin and increased biglycan has also been shown [9]. Cellular changes include the presence of myofibroblasts [10, 11] and an increase in fibroblast, mast cell and macrophage density compared to normal skin [8, 12].

Patients with post-burn HSc suffer cosmetic disfigurement and significant morbidity secondary to functional limitations requiring prolonged rehabilitation [13]. Given our limited understanding of HSc pathophysiology, treatment for this disorder has been proven largely based on experience over decades. One of the barriers towards understanding pathophysiology as well testing of novel treatments is the lack of an appropriate animal model [14-16]. The benefits and

limits of the most extensively used animal models have been described previously in detail [8, 12, 14-16]. Our studies using nude mice to generate HSc have demonstrated encouraging results [12, 17]. We have shown that xenografting nude mice with human skin results in proliferative xenograft scars that have morphologic, histologic and cellular changes consistent with human HSc [12, 17]. Nude mice cannot produce mature, functional T-cells secondary to a lack of thymic epithelium [18, 19]. This defect in adaptive immunity facilitates the use of human skin in this model. However, nude mice have immature thymocytes and have been shown to accumulate lymphocytes expressing CD3, CD4 and CD8 surface markers with increasing age, through extrathymic T-cell maturation [20-23]. These observations directed us to consider more modern strains of genetically engineered immune deficient mice in order to refine our model and investigate the role of specific immune cells on HSc formation.

TCR (T-cell receptor) knockout mice lack the genes for productive T-cell receptor rearrangement, which is critical for thymocyte development to the $CD4^+$, $CD8^+$ double-positive stage and necessary for T-cell differentiation to continue [24, 25]. As a result, these animals are unable to produce functional T-cells and may represent a more complete T-cell deficient mouse, thereby reducing the potential of an activated T-cell rejection response contributing to scar formation in our experiments. $TCR\beta^{-/-}\delta^{-/-}$ mice specifically cannot produce functional T-cells or γδ T-cells. Knock out of the recombination activating gene (RAG) genomic locus, which, activates V(D)J (variable, diversity, joining) region recombinase activity, inhibits somatic recombination, a process essential for immunoglobulin and TCR

gene recombination. As a result, genes encoding for immunoglobulin and TCRs are not formed, leading to early arrest of T and B lymphocyte differentiation [26-28]. RAG-1$^{-/-}$ mice are deficient in B and T cells and RAG-2$^{-/-}$γc$^{-/-}$ mice additionally lack NK cells.

Our first objective is to determine if grafting human skin onto TCRβ$^{-/-}$δ$^{-/-}$, RAG-1$^{-/-}$ and RAG-2$^{-/-}$γc$^{-/-}$ mice will result in proliferative xenograft scars that are morphologically and histologically similar to human HSc as observed in the nude mouse model [12, 17]. Our second objective is to investigate the changes that occur in scars with the deletion of immune cells. Analysis consisted of hematoxylin and eosin (H & E), Masson's trichrome and toluidine blue staining as well immunohistochemistry for anti-human human leukocyte antigen (HLA)-ABC, α–smooth muscle actin (SMA), decorin and biglycan. Results obtained from TCRβ$^{-/-}$δ$^{-/-}$, RAG-1$^{-/-}$ and RAG-2$^{-/-}$γc$^{-/-}$ experiments will be compared to nude mouse data from a previous study [17].

3.2 Methods

Preparation of skin grafts

Following informed consent, human skin samples were obtained from female, cosmetic abdominoplasty patients. Using a dermatome set at 0.03 cm split thickness human skin grafts were harvested. Skin abnormalities such as striae were avoided. A 2.0 x 1.5 cm plastic template was used to trace and cut human

skin grafts to a desired size. Grafts were stored in sterile normal saline until grafting.

Transplantation of skin grafts

All animal studies were performed using protocols approved by the University of Alberta Animal Care and Use Committee and in accordance with the standards of the Canadian Council on Animal Care. TCRβ$^{-/-}$δ$^{-/-}$ (B6.129P2-Tcrb^{tm1Mom} Tcrd^{tm1Mom}/J), RAG-1$^{-/-}$ (B6.129S7-Rag1^{tm1Mom}/J) (Jackson Laboratories, Bar Harbor, ME) and RAG-2$^{-/-}$γc$^{-/-}$ (C57BL/6J x C57BL/10SgSnA1)-[KO]γc-[KO]Rag2 (Taconic Farms Inc. Hudson, NY), mice weighing ~25 grams each were purchased and housed in a virus antibody free biocontainment facility during the experiment. Animals were individually housed for two weeks prior to grafting. In the prone position, using isoflurane anesthetic (Halocarbon Laboratories, River Edge, NJ) mice were shaved using clippers. Remaining finer hairs were removed with a commercial hair remover (Nair® hair remover, Church & Dwight Co., Inc. Princeton, NJ) and the skin disinfected with iodine. A plastic template, pre-cut to 2.0 x 1.5 cm was used to mark the dorsal skin. A scalpal was used to create a full thickness skin defect with intact panniculus carnosus. TCRβ$^{-/-}$δ$^{-/-}$, RAG-1$^{-/-}$ and RAG-2$^{-/-}$γc$^{-/-}$ animals (*n*=20 per strain) received split thickness human skin transplants. Control mice (*n*=5 per strain) received full thickness autografts. Grafts were sutured using 4-0 braided, silk suture (Ethicon©, Somerville, NJ) and dressed with a non-adherent petrolatum (Xeroform™, Covidien, Mansfield, MA) and dry gauze tie-over bolus dressing. Narcotic

analgesia (Hydromorphone HP 10 diluted to 0.05 mg/mL, Sandoz, Boucherville, QC) was administered subcutaneously postoperatively. Dressings and sutures were removed seven days after transplantation. Grafts were photographed weekly to document scar formation. Photographs were standardized for light, exposure time and distance from the subject. Mice were euthanized at 30, 60, 120 and 180 days at which point scar biopsies were harvested for analysis (Fig. 3-1).

Harvesting and processing of skin biopsies

Scar biopsies were either fixed in 10% formalin (Zinc Formal Fixx™, Thermo Scientific, Pittsburgh, PA) for at least 24 hours and embedded in paraffin or frozen in cryomatrix (Shandon Cryomatrix™, Thermo Scientific, Pittsburgh, PA). Frozen sections cut to 10 μm were used for anti-human HLA-ABC staining. Paraffin sections cut to 5 μm were used for H & E, Masson's trichrome, α-SMA, decorin, biglyan and toluidine blue staining. Following informed consent, HSc samples were collected from burn patients with HSc.

Skin structure, thickness and collagen morphology

Skin structure, thickness, hypercellularity and thickness were assessed using H & E sections under 100x magnification. Skin thickness was defined as the distance from the stratum corneum to the dermal-fat junction. Collagen morphology was assessed in Masson's trichrome sections under 100x magnification.

Survival of transplanted human split thickness xenografts

Survival of engrafted human skin was confirmed using frozen sections as previously described [17]. Briefly, frozen sections were first warmed, fixed in cold methanol, dried in acetone for 2 minutes and rehydrated in tris-buffered saline (TBS) and 0.2% Triton X-100 (Sigma-Aldrich Inc., St. Louis, MO). Sections were then incubated overnight at 4˚C with a 1:50 dilution of fluorescein isothiocyanate (FITC)-labeled anti-human HLA-ABC antibody (Accurate Chemical & Scientific Corp., Westbury, NY), washed with TBS and distilled water, coverslipped and mounted with ProLong® Gold Antifade Reagent with 4'6-diamidino-2-phenylindole (DAPI) (Invitrogen, Burlington, ON). Primary antibodies were omitted in controls resulting in negative staining.

Immunohistochemical analysis of α-SMA

Myofibroblasts were detected on paraffin sections as previously described [17]. Briefly, sections were deparaffinized and rehydrated through gradient ethanol and permeabilized with 0.01% Triton X-100. Sections were treated with 3% hydrogen peroxide to quench endogenous peroxidase activity and blocked with 10% goat serum (Jackson ImmunoReseach Laboratories Inc., West Grove, PA) and 10% bovine serum albumin (BSA) (Sigma-Aldrich Inc., St. Louis, MO) for 1 hour at room temperature. Endogenous biotin and avidin were blocked using a kit (Vector Laboratories Inc., Burlingame, CA) followed by Fc receptor block (Innovex Biosciences, Richmond, CA). Slides were incubated with overnight at 4˚C with a 1:200 dilution of rabbit monoclonal anti-α-SMA antibody (Millipore,

Temecula, CA) followed by incubation with goat anti-rabbit biotinylated secondary antibody (Vector Laboratories Inc., Burlingame, CA). Sections were then washed with avidin-biotin complex (Vectastain ABC kit, Vector Laboratories Inc., Burlingame, CA) and developed using diaminobenzidine (Sigma-Aldrich Inc., St. Louis, MO). Primary antibody was replaced with rabbit IgG (Vector Laboratories Inc., Burlingame, CA) in controls resulting in negative staining (data not shown).

Immunohistochemical analysis of decorin and biglycan

Decorin and biglycan staining was performed on paraffin sections as previously described [17]. Briefly, sections were first deparaffinized and rehydrated through gradient ethanol, permeabilized with 0.05% saponin (Sigma-Aldrich Inc., St. Louis, MO) washed with phosphate buffered saline and blocked with BSA and 0.01% Triton X-100. Sections were then incubated overnight at 4˚C at 1:100 dilution with either mouse monoclonal anti-human decorin or rabbit polyclonal anti-human biglycan antibody (Santa Cruz Biotechnology, Santa Cruz, CA) followed by incubation with the appropriate secondary antibody. Primary antibodies were omitted in controls resulting in negative staining (data not shown).

Toluidine blue staining for mast cell detection

Mast cells were detected on paraffin sections as previously described [17]. Briefly, paraffin sections were deparaffinized and rehydrated through gradient

ethanol and stained for 3 minutes in toluidine blue (Toluidine Blue O, Fisher Scientific Company, Fair Lawn, NJ) followed by washing in distilled water, dehydration in ethanol and clearing in xylene. Mast cells were quantified by counting the number of reddish-purple cells in 5 random, high-power fields under 200x magnification.

Microscopy and image analysis

H & E, Masson's trichrome, α-SMA and toluidine blue stained sections were examined using a Zeiss Axioplan 2 microscope and photographed using an AxioCam MRc digital camera. Anti-human HLA-ABC, decorin and biglycan stained sections were examined using a Colibri microscope and photographed using an AxioCam HRm digital camera. Scar thickness measurements, image processing and scale bars were added using Zeiss AxioVision 4.6.3 (Carl Ziess MicroImaging Inc., Thornwood, NY) and Adobe Photoshop® CS5 Extended Version 12.0 x64 for Macintosh (Adobe Systems Inc., San Jose, CA). Decorin and biglycan immunofluorescence was quantified using ImageJ for Macintosh version 1.43r (NIH, USA).

Statistical analysis

Animal studies involved five mice per treatment group. All staining was completed in triplicate. Statistical analysis was performed using STATA for Macintosh version 10.0 (College Station, TX). Statistical tests used include a 2-tailed, unpaired Student's t-test or in cases of paired data a paired t-test and an

analysis of variance (ANOVA). Results are presented as means ± SE. Probability values of p-value < 0.05 were considered significant.

3.3 Results

Morphologic observations

Transplanted xenografts remained clinically viable in all strains throughout the experiment. At 30 days postoperatively xenografted mice had developed hyperemic, firm, thickened scars, with a shiny skin texture and moderate to severe distortion of surrounding skin consistent with human HSc (Fig. 3-2). Full thickness autografts healed completely two weeks. At 30 days following grafting autografts from all strains demonstrated an excellent healing result with natural skin color, flush contour with surrounding skin, a dull skin surface and absence of contraction or distortion (Fig. 3-2). In comparison to autograft controls, scars developed in TCR$\beta^{-/-}\delta^{-/-}$, RAG-$1^{-/-}$ and RAG-$2^{-/-}\gamma c^{-/-}$ show significant hyperemia and distortion of the surrounding skin. Inelasticity of proliferative xenograft scars was observed on palpation in contrast to the supple quality of normal skin and autograft controls.

Survival of engrafted human skin

As previously shown [17], survival of engrafted human split thickness skin could be confirmed using direct immunofluorescence for HLA-ABC antigens. Staining of TCR$\beta^{-/-}\delta^{-/-}$, RAG-$1^{-/-}$ and RAG-$2^{-/-}\gamma c^{-/-}$ sections from all time points shows a

positive green, net-like, staining pattern in proliferative xenograft scars (Fig. 3-3). Stained sections contain both grafted human skin and adjacent normal mouse skin. Mouse skin shows no positive green staining. Counterstaining with DAPI highlights the lack of any positive green staining at transition zones where proliferative xenograft scars join normal mouse skin.

Histological characteristics

Known histological features of HSc [8], previously demonstrated in the nude mouse model [17] are also present in proliferative xenograft scars generated by grafting split thickness human skin onto TCR$\beta^{-/-}\delta^{-/-}$, RAG-$1^{-/-}$ and RAG-$2^{-/-}\gamma c^{-/-}$ mice. Sections from all strains of knockout mice showed loss of hair follicles, rete pegs and adnexal structures and hypercellularity on H & E staining (Fig. 3-4). Abnormalities in collagen fiber morphology include thinning of fibrils and whorled collagen bundles normally seen in human HSc (Fig. 3-5). An increase in dermal and epidermal thickness occurred in all strains. Average proliferative xenograft scar thickness for TCR$\beta^{-/-}\delta^{-/-}$, RAG-$1^{-/-}$ and RAG-$2^{-/-}\gamma c^{-/-}$ mice over time was 612.7 ±18.2 μm, 563.8 ±21.7 μm and 660.1 ±26.6 μm respectively compared to 246.6 ±4.8 μm for normal, unwounded mouse skin ($p< 0.01$). Average autograft thickness in these strains over time was 254.6 ±3.8 μm, 258.7 ±7.2 μm and 257.6 ±7.8 μm respectively. Proliferative xenograft scars in all strains were therefore also significantly thicker than autograft controls ($p< 0.01$). Conversion of absolute scar thickness to percent increase in thickness compared to the original skin graft allows scar thickness comparison of knockout strains to nude

mice. Average percent increase in thickness for nude mouse proliferative xenograft scars was 154.0 ±7.4% compared to 265.3 ±10.8% for TCRβ$^{-/-}$δ$^{-/-}$, 164.7 ±10.2% for RAG-1$^{-/-}$ and 208.0 ±12.8% for RAG-2$^{-/-}$γc$^{-/-}$ mice ($p< 0.01$) (Fig. 3-6). The percent increase observed in TCRβ$^{-/-}$δ$^{-/-}$, RAG-1$^{-/-}$ and RAG-2$^{-/-}$γc$^{-/-}$ autografts was 3.7 ±1.6%, 5.2 ±2.9% and 4.7 ±3.2% respectively compared to 33.8 ±3.4% in nude mouse autografts ($p< 0.01$). The trend in proliferative xenograft scar thickness in knockout strains is a dramatic initial increase at 30 days followed by reduction in scar thickness at each subsequent time point. In comparison, nude mouse scar thickness increases at 30 days and peaks to a maximum at 60 days and remains elevated up to 180 days after grafting.

Elevated expression of α-SMA in proliferative xenograft scars

TCRβ$^{-/-}$δ$^{-/-}$, RAG-1$^{-/-}$ and RAG-2$^{-/-}$γc$^{-/-}$ sections stained positive for α-SMA-expressing myofibroblasts at all time points consistent with human HSc [11] (Fig. 3-7). Normal human skin and controls stained negatively for myofibroblasts. In all knockout strains α-SMA staining intensity appeared to be greatest at 30 days after grafting and decreased over time. In nude mice α-SMA expression remained consistent over time.

Decreased decorin and increased biglycan expression in proliferative xenograft scars

Qualitatively there is decreased decorin immunofluorescence in proliferative xenograft scars from nude, TCRβ$^{-/-}$δ$^{-/-}$, RAG-1$^{-/-}$ and RAG-2$^{-/-}$γc$^{-/-}$ mice at 30 days

following grafting compared to normal human skin (Fig. 3-8). At 120 days all strains show increased immunofluorescence for decorin. Quantification of decorin immunofluorescence relative to normal human skin confirms these significant qualitative observations ($p < 0.01$) (Fig. 3-9). Knockout strains and nude mice differ in their decorin expression patterns at day 60 where nude mice express marginally less decorin than normal human skin, while knockout animals express more decorin (Fig. 3-9). Biglycan immunofluorescence in all strains is increased at 30, 60 and 120 days after grafting compared to normal human skin and appears to return to baseline at 180 days (Fig. 3-10). Quantification of biglycan immunofluorescence in proliferative xenograft scars relative to normal human skin reveals a greater than 2-fold increase at 30 days in all strains ($p < 0.01$) (Fig. 3-11). Over time there is normalization of biglycan expression by 120 days in nude, RAG-$1^{-/-}$ and RAG-$2^{-/-}\gamma c^{-/-}$ mice.

Increased mast cell density in proliferative xenograft scars

Toluidine blue staining in TCR$\beta^{-/-}\delta^{-/-}$, RAG-$1^{-/-}$ and RAG-$2^{-/-}\gamma c^{-/-}$ sections shows an increase in mast cell density compared to normal skin (Fig. 3-12). Quantification of mast cells at all time points reveals in increase in mast cell density in all strains compared to normal human skin ($p < 0.05$) (Fig. 3-13). The average mast cell density by strain is 22.4 ±1.6, 14.8 ±1.5, 14.8 ±0.8 and 16.5 ±1.1 mast cells per high power field for nude, TCR$\beta^{-/-}\delta^{-/-}$, RAG-$1^{-/-}$ and RAG-$2^{-/-}\gamma c^{-/-}$ mice respectively. Mast cell density appears to remain elevated in nude mice,

whereas in RAG-1$^{-/-}$ and RAG-2$^{-/-}\gamma c^{-/-}$ mice mast cell density peaks at 60 days and declines thereafter.

3.4 Discussion

In these experiments we have shown that grafting split thickness human skin onto TCR$\beta^{-/-}\delta^{-/-}$, RAG-1$^{-/-}$ and RAG-2$^{-/-}\gamma c^{-/-}$ mice is sufficient to generate proliferative xenograft scars that are morphologically and histologically similar to human HSc. At 30 days postoperatively, these scars are grossly comparable to those seen in nude mice (Fig. 3-2) [17]. However, proliferative xenograft scars in knockout animals became flatter, paler and softer over time. As previously demonstrated in the nude mouse model [12, 17] xenografted knockout strains also possess key histological features of human HSc. These include thin, whorled bundles of collagen (Fig. 3-5), myofibroblasts (Fig. 3-7) loss of hair follicles, adnexal structures and rete ridges, hypercellularity (Fig. 3-4) and an increase in epidermal and dermal thickness (Fig. 3-6). Decreased expression of decorin (Fig. 3-8), increased expression of biglycan (Fig. 3-9) and increased mast cell density (Fig. 3-12) are also present in proliferative xenograft scars generated in knockout mice. Within these observations, temporal and pattern differences exist between nude and knockout mice that warrant further investigation.

In proliferative xenograft scars from knockout animals the presence of myofibroblasts was most dramatic at days 30 following grafting. At 60, 120 and 180 days positive staining for α-SMA was still present in these sections, but

decreasing incrementally in staining intensity. This observation is in keeping with a reduction in fibroblasts and myofibroblasts seen in burn patients undergoing serial biopsies of post-burn HSc [29]. Similarly, the magnitude of mast cell density was highest in RAG-1$^{-/-}$ and RAG-2$^{-/-}\gamma c^{-/-}$ knockout animals at 60 days after grafting (Fig. 3-13). At 120 and 180 days mast cell density in proliferative xenograft scars from these mice is still significantly elevated above that of normal skin, however, demonstrates an overall trend of decreasing density. Release of histamine from mast cells causes vasodilation giving tissues a hyperemic appearance. Over time, with the decrease in mast cell density, proliferative xenograft scars in RAG-1$^{-/-}$ and RAG-2$^{-/-}\gamma c^{-/-}$ mice became paler in appearance. This is analogous to the partial resolution of redness seen in HSc as it matures. Nude mouse proliferative xenograft scars on the other hand do not demonstrate a decrease in mast cell density over time and also remain reddened clinically up to 180 days after grafting. In summary, a decrease in myofibroblast and mast cell density in proliferative xenograft scars in knockout strains over time reflects remodelling of hypercellular, immature HSc to mature HSc seen in humans.

All strains of mice show an increase in percent thickness at 30 days after grafting. This increase in thickness is greatest in knockout strains; specifically the TCR$\beta^{-/-}\delta^{-/-}$ and RAG-2$^{-/-}\gamma c^{-/-}$ animals whose increase in percent thickness at day 30 is nearly double that of nude mice (Fig. 3-6). Interestingly, while the knockout strains demonstrate a rapid, early increase in thickness this in fact represents the peak in scar thickness. Knockout animals decrease in percent thickness at 60 days

and fall below nude mice by 120 days after grafting. Nude mice reach a peak in percent thickness at ~60 day after grafting. In contrast to knockout strains, scars in nude mice do not decrease in percent thickness following this peak; rather they continue to remain elevated at 180 days. This pattern of persistent elevation is not in keeping with human HSc. Conversely, the pattern of change in percent thickness of scars in knockout strains reflects the remodeling kinetics of human hypertrophic scars, which become flatter to some extent as they mature.

Within knockout strains, a significant difference in percent thickness exists between RAG-$1^{-/-}$ and RAG-$2^{-/-}\gamma c^{-/-}$ mice. These strains are similar in that they both lack B and T cells. RAG-$2^{-/-}\gamma c^{-/-}$ mice additionally lack NK cells, which are functional and known to be elevated in RAG-$1^{-/-}$ mice [30]. NK cells are large granular lymphocytes and play an important role in innate immune responses [31]. Interferon (IFN)-γ, is the prototypic NK cell cytokine and is involved in the pathogenesis of several fibrotic conditions including liver fibrosis, idiopathic pulmonary fibrosis and HSc [32-36]. In humans following tissue injury there is migration of T-cells into the wound. Immature, $CD4^+$ T-cells have the potential to differentiate into inflammatory T helper (T_H)1 or fibrogenic T_H2 cells [37]. In FPDs, profibrotic T_H2 responses predominate [38]. This is mediated in part by promotion of IL-13 stimulated macrophage production of transforming growth factor (TGF)-β1, which stimulates collagen synthesis by fibroblasts [39, 40]. In burn patients with HSc a systemic, polarized T_H2 cytokine response has been demonstrated with absence of IFN-γ noted in the serum of these patients [41].

This is further supported by increased production of TGF-β1, accelerated deposition of collagen and rapid wound closure in IFN-knockout mice [42]. T_H1 cytokines such as IFN-γ have recognized antifibrotic activity able to suppress collagen deposition [38]. *In vitro* IFN-γ treatment of HSc fibroblasts antagonizes TGF-β1 messenger ribonucleic acid (RNA) and protein levels and tissue inhibitor of metalloproteinase (TIMP)-1 mRNA [35, 36]. The net result is decreased TGF-β stimulated collagen metabolism. T_H1 cells are also able to abrogate fibrosis by downregulating profibrotic cytokines in T_H2 cells [38]. Given this evidence, it is conceivable that RAG-$1^{-/-}$ mice, with elevated numbers of NK cells, may also have increased levels of IFN-γ capable of reducing collagen deposition in proliferative xenograft scars. We therefore speculate that the relative reduction in percent increase in scar thickness observed in RAG-$1^{-/-}$ mice compared to RAG-$2^{-/-}\gamma c^{-/-}$ mice may be secondary to elevated IFN-γ producing NK cells. Identification of NK cells within proliferative xenograft scars and quantification of NK cell density would be an important first step in investigating this hypothesis.

Variation in the initial magnitude and pattern of percent increase in proliferative xenograft scar thickness observed in nude and TCR$\beta^{-/-}\delta^{-/-}$ mice can potentially be explained on the basis of two differences. The first is the mechanism by which each strain is T-cell deficient. Due to a lack of thymic epithelium thymocytes in nude mice do not encounter self-antigens in the thymus and therefore remain in the double negative stage of development. In contrast, TCR$\beta^{-/-}\delta^{-/-}$ mice are

exposed to these antigens during development, but lack β and δ genes necessary for functional TCR rearrangement [24, 25]. In nudes, extrathymic T-cell maturation has been shown to occur with increasing age [20-23]. Presumably, some immature thymocytes in the nude mouse migrate to the spleen or lymph nodes where they can interact with antigen presenting cells and receive the necessary maturation stimulus to differentiate into mature T-cells. Alternatively, ~30% of spleen cells are committed precursors of T-cells, which could also be induced to mature [43]. Therefore, nudes may have increased numbers of mature T-cells compared to TCR$\beta^{-/-}\delta^{-/-}$ mice. However, the biological significance of these cells in performing immunologic functions is not known.

The second is the discrepancy is background strain. Nudes in our experiments are a Bagg albino laboratory bred (BALB)/c background while TCR$\beta^{-/-}\delta^{-/-}$ mice are C57BL/6. Given that increasing numbers of mature T-cells were observed in both aging BALB/c and B6 nude mice the effect of discordant background strains is less likely to be important, but cannot be ruled out as a source for observed differences in proliferative xenograft scars in nude and TCR$\beta^{-/-}\delta^{-/-}$ mice.

In spite of T, B and NK cell deficiency nude, TCR$\beta^{-/-}\delta^{-/-}$, RAG-$1^{-/-}$ and RAG-$2^{-/-}$ $\gamma c^{-/-}$ are still able to develop scars resembling human HSc. A common cell type present in all strains capable of orchestrating a fibrotic response is the macrophage. Macrophages, through their interactions with fibroblasts and $CD4^{+}$ T-cells are ideally situated to play an important role in the initiation of fibrotic

disorders. Following tissue injury, local macrophages and circulating monocytes home to the site of injury and produce TGF-β causing fibroblasts to produce collagen [44]. Macrophages also produce matrix metalloproteinases and tissue inhibitor of metalloproteinases, which serve to degrade the preserve ECM produced by fibroblasts [44]. The antigen-presenting function of macrophages allows them to interact with T-cells. In FPDs this interaction induces a polarized T_H2 response whereby IL-13 stimulated macrophages produce TGF-β1 that propagates fibrosis [41, 44, 45]. Advancing our understanding of the interactions between macrophages, fibroblasts and T-cells is pivotal to discerning important features in the pathogensis of fibrotic conditions such as HSc and in turn treatment for patients.

3.5 Conclusions

In conclusion, we observed that similar to nude mice, grafting split thickness human skin onto the backs of TCRβ$^{-/-}$δ$^{-/-}$, RAG-1$^{-/-}$ and RAG-2$^{-/-}$γc$^{-/-}$ also generates scars with morphologic, histologic and cellular features similar to human HSc. In contrast, proliferative xenograft scars in knockout strains exhibit the capacity to remodel over time secondary to cellular changes known to occur in human HSc. Therefore these animal models may be better suited for the study of HSc. Lastly, RAG-1$^{-/-}$ mice demonstrate a reduction in the overall magnitude scar thickness compared to RAG-2$^{-/-}$γc$^{-/-}$ mice suggesting an important role for IFN-γ releasing NK cells in HSc pathogenesis and treatment.

3.6 Figures

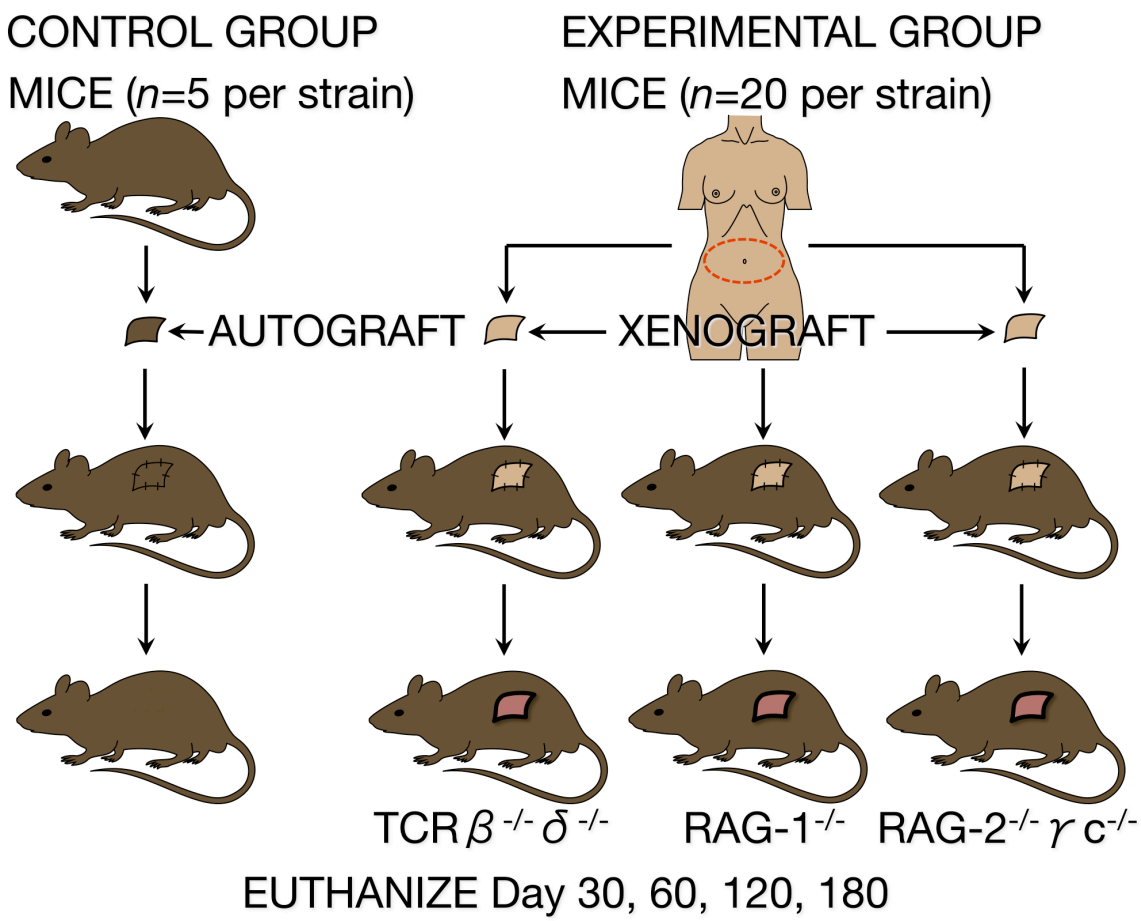

Figure 3-1: Experimental model to test the development of human hypertrophic scar in TCRβ$^{-/-}$δ$^{-/-}$, RAG-1$^{-/-}$ and RAG-2$^{-/-}$γc$^{-/-}$ animals. Controls (*n*=5 per strain) consisted of full thickness autografts. Experimental group (*n*=20 per strain) included TCRβ$^{-/-}$δ$^{-/-}$, RAG-1$^{-/-}$ and RAG-2$^{-/-}$γc$^{-/-}$ mice xenografted with split thickness human skin.

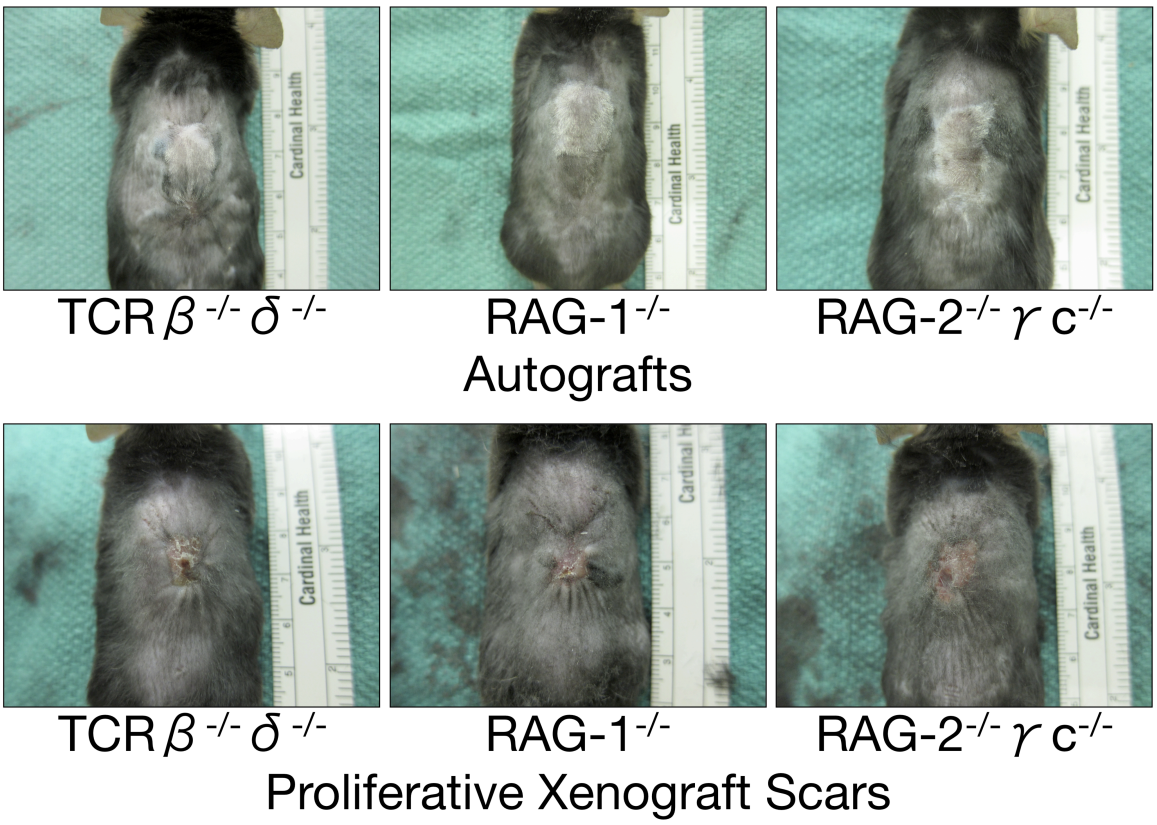

Figure 3-2: *(First row)* TCRβ$^{-/-}$δ$^{-/-}$, RAG-1$^{-/-}$ and RAG-2$^{-/-}$γc$^{-/-}$ mouse autografts compared to *(Second row)* proliferative xenograft scars showing gross morphologic appearance at 30 days following grafting. *(First row)* Autograft controls demonstrate excellent healing result with natural skin color, flush contour with surrounding skin, a dull skin surface and absence of contraction or distortion. *(Second row)* In contrast, proliferative xenograft scars are hyperemic, thickened, shiny and markedly distort the surrounding skin.

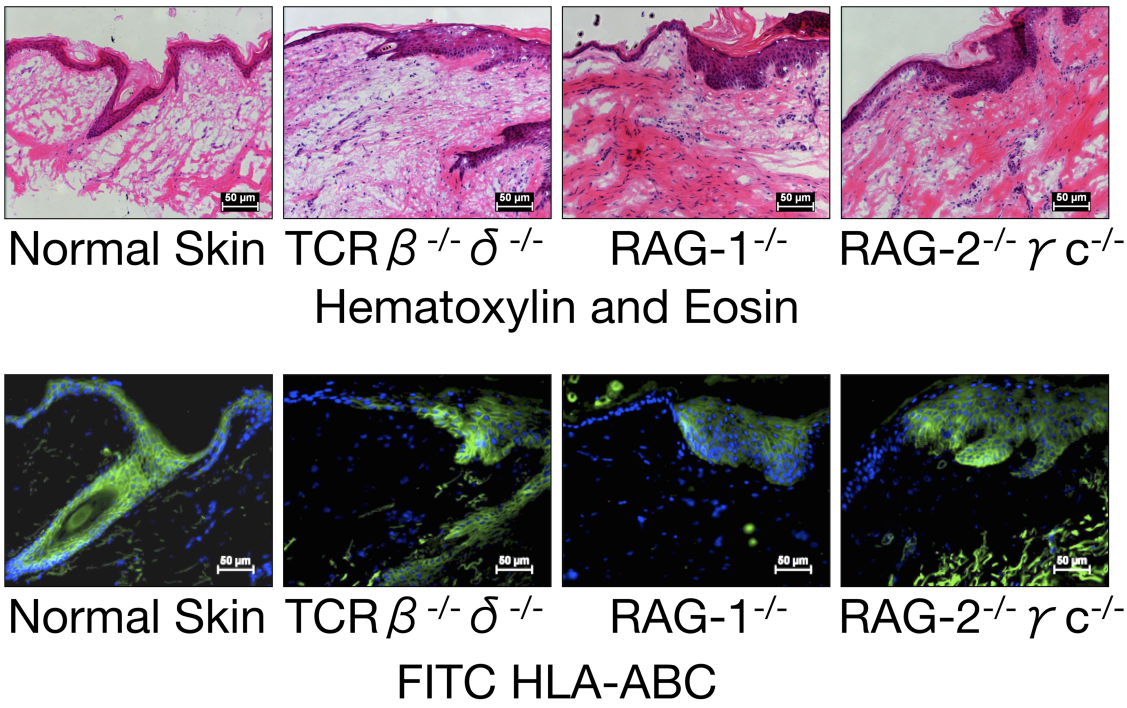

Figure 3-3: Representative images of *(First row)* H & E and *(Second row)* anti-human FITC HLA-ABC antibody stained sections. *(First row, second, third and fourth)* H & E sections show normal mouse epidermis on the left, which is thin and lacks rete ridges compared to the thicker engrafted human skin on the right. *(Second row, first)* Direct immunofluorescence for HLA-ABC antigens shows a positive green, net-like, staining pattern throughout the normal human skin positive control. *(Second row, second, third and fourth)*. TCRβ$^{-/-}$δ$^{-/-}$, RAG-1$^{-/-}$ and RAG-2$^{-/-}$γc$^{-/-}$ stained sections demonstrate positive staining in engrafted human skin on the right. Adjacent mouse epidermis stains negatively for HLA-ABC antigens. Nuclei have been counterstained blue with DAPI.

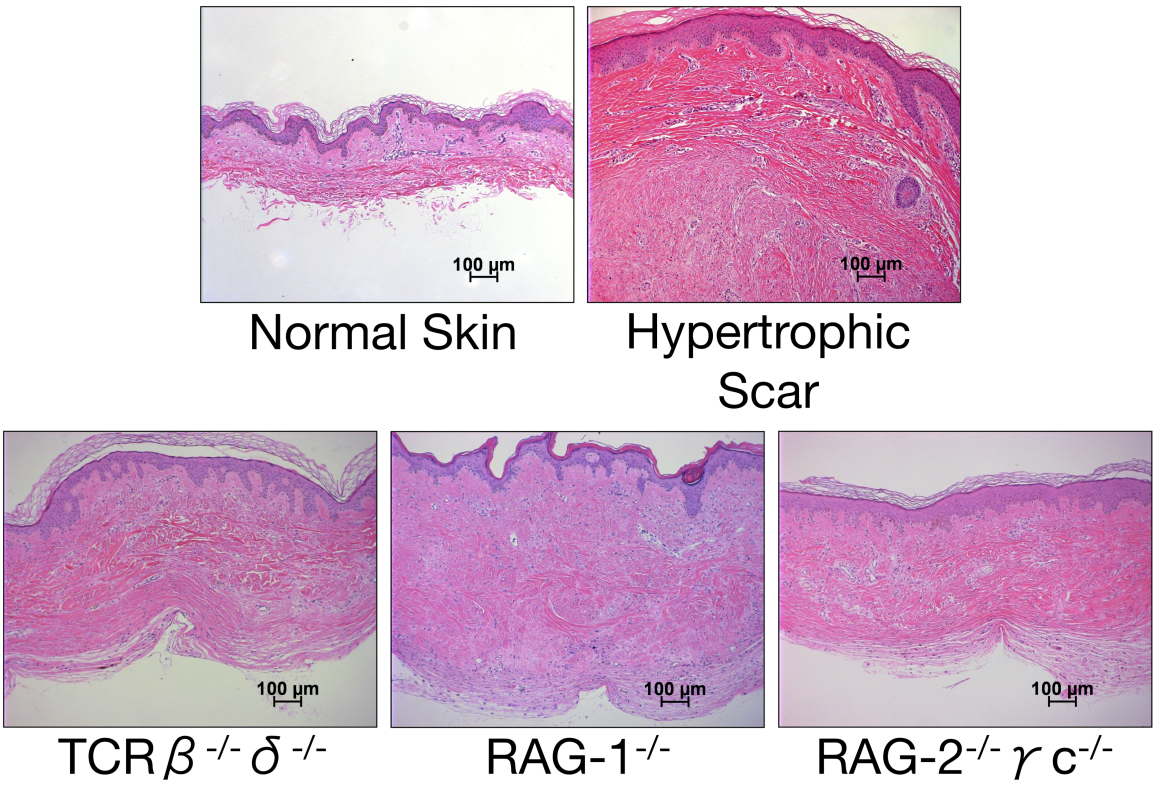

Figure 3-4: Representative images of H & E stained sections of proliferative xenograft scars from *(Second row, left)* TCRβ$^{-/-}$δ$^{-/-}$, *(Second row, center)* RAG-1$^{-/-}$ and *(Second row, right)* RAG-2$^{-/-}$γc$^{-/-}$ mice demonstrate loss of hair follicles, adnexal structures, and rete pegs and hypercellularity consistent with *(First row, right),* human HSc and in contrast to *(First row, left)* normal human skin.

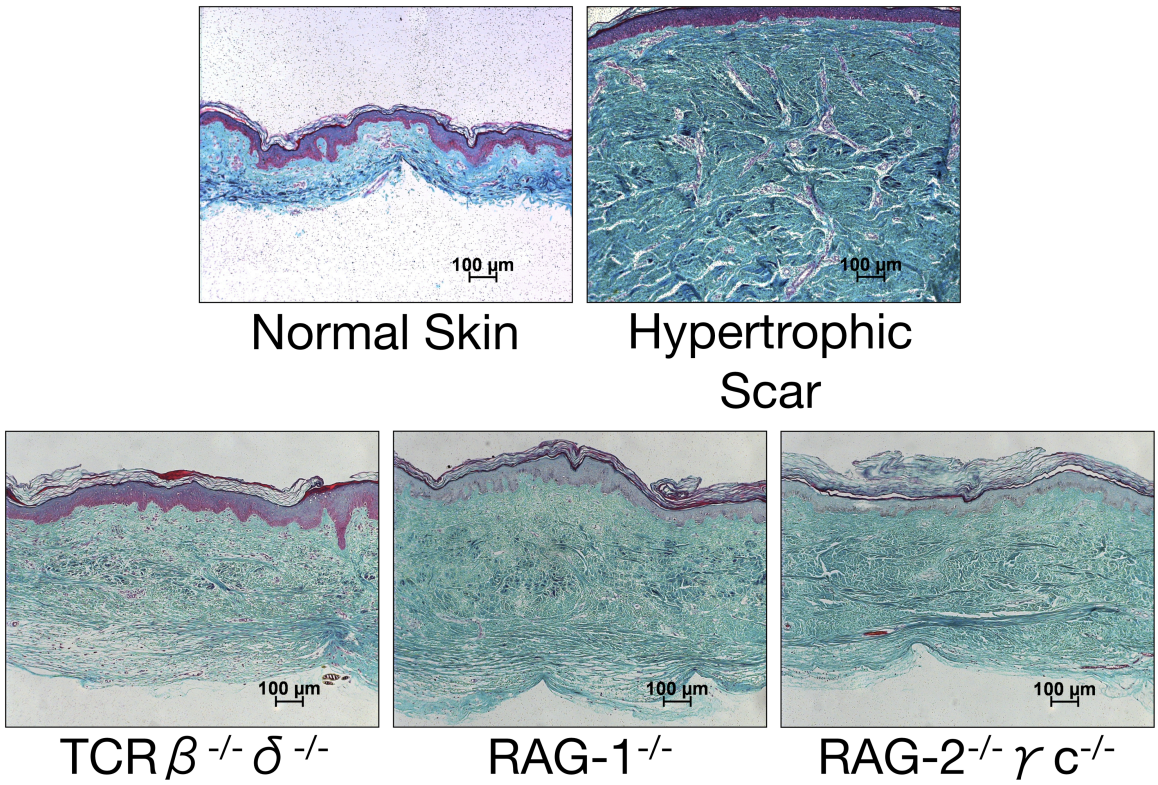

Figure 3-5: Representative images of a Masson's trichrome stained sections of proliferative xenograft scars from *(Second row, left)* TCRβ$^{-/-}$δ$^{-/-}$, *(Second row, center)* RAG-1$^{-/-}$ and *(Second row, right)* RAG-2$^{-/-}$γc$^{-/-}$ mice demonstrate abnormal, whorled collagen bundle morphology consistent with *(First row, right)* human HSc and in contrast to the basket-weave collagen bundle pattern seen in *(First row, left)* normal skin.

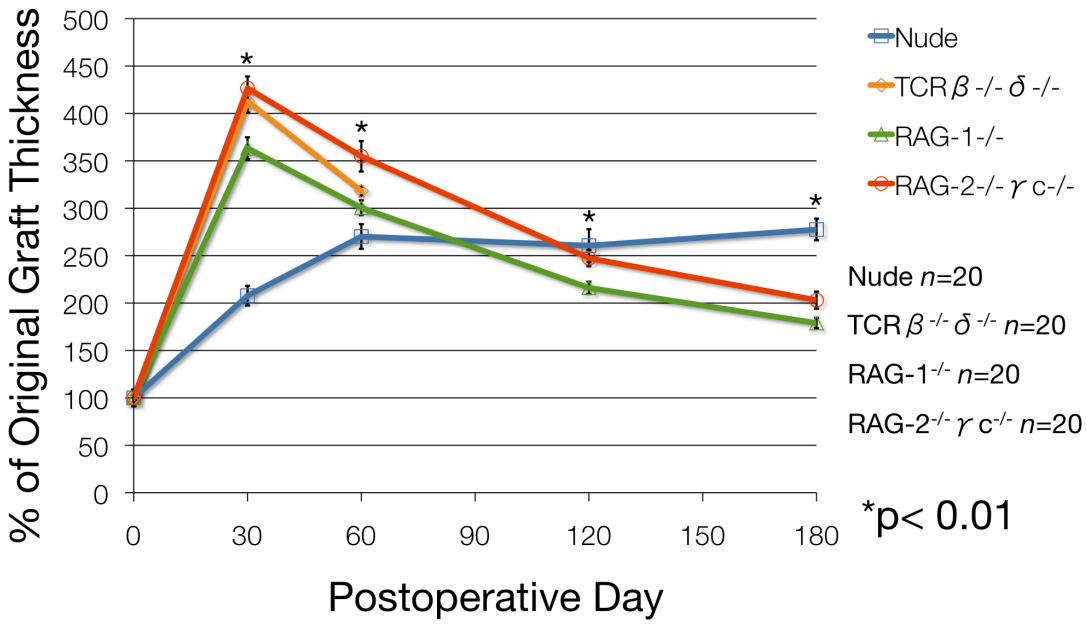

Figure 3-6: Percent increase in the thicknes of nude, TCRβ$^{-/-}$δ$^{-/-}$, RAG-1$^{-/-}$ and RAG-2$^{-/-}$γc$^{-/-}$ proliferative xenograft scars compared to original graft thickness over time. Average nude mouse proliferative xenograft scars increased in thickness by 154.0 ±7.4% compared to 265.3 ±10.8% for TCRβ$^{-/-}$δ$^{-/-}$, 164.7 ±10.2% for RAG-1$^{-/-}$ and 208.0 ±12.8% for RAG-2$^{-/-}$γc$^{-/-}$ mice ($p< 0.01$). Nude mouse proliferative xenograft scars show a persistent increase in thickness, whereas all other strains demonstrate a rapid peak in thickness followed by remodeling over time.

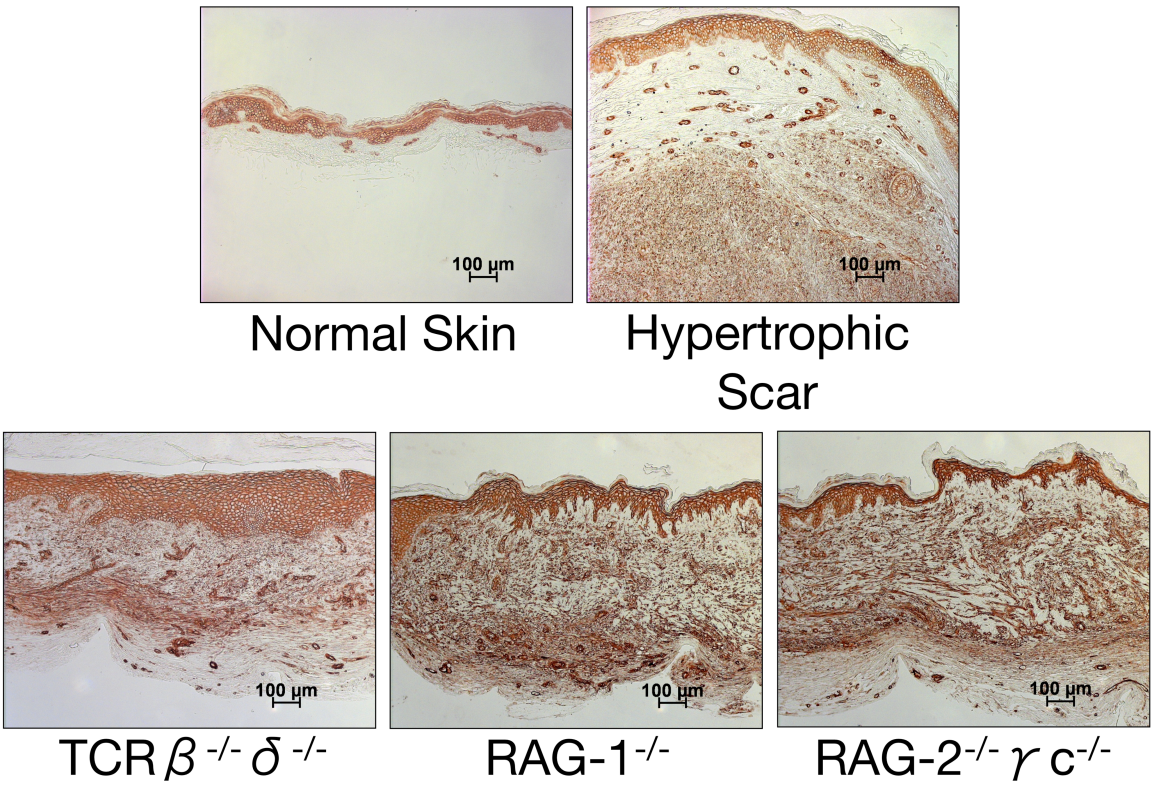

Figure 3-7: Representative images of an α-SMA stained sections of proliferative xenograft scars from *(Second row, left)* TCRβ$^{-/-}$δ$^{-/-}$, *(Second row, center)* RAG-1$^{-/-}$ and *(Second row, right)* RAG-2$^{-/-}$γc$^{-/-}$ mice demonstrate a positive brown staining pattern indicating the presence of myofibroblasts throughout the dermis similar to that seen in *(First row, right)* human hypertrophic scar. In contrast, *(First row, left)* normal human dermis does not stain positive for α-SMA except surrounding blood vessels.

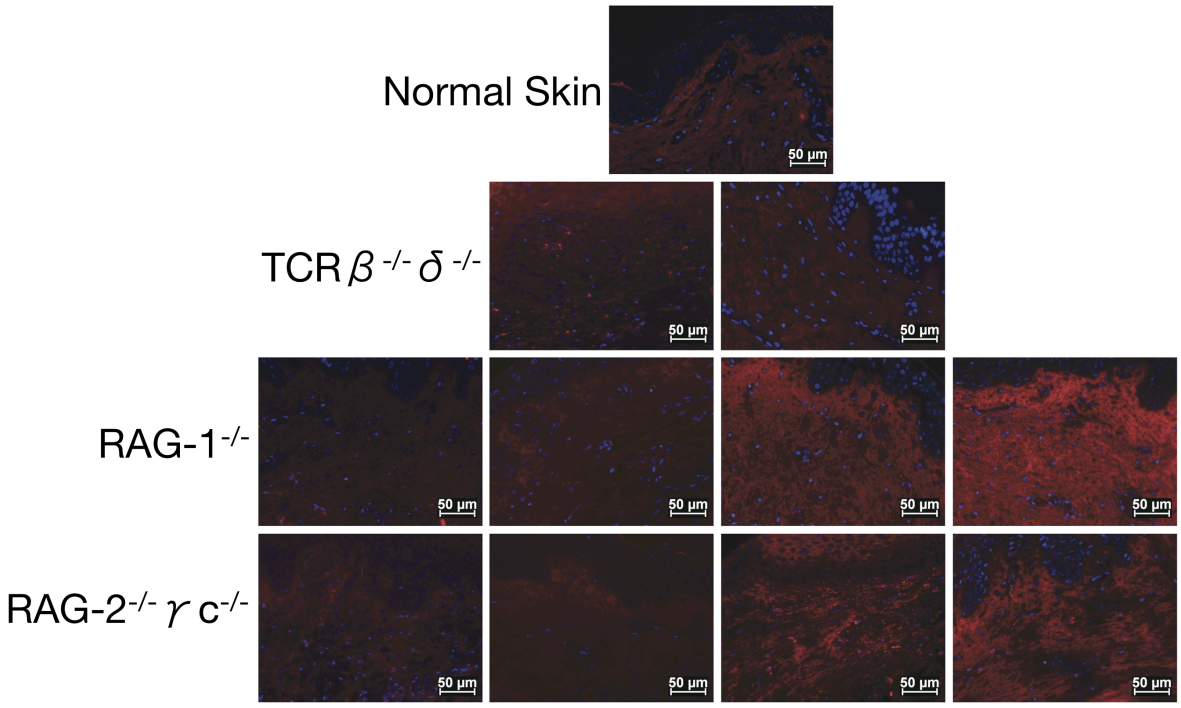

Figure 3-8: Representative immunofluorescent images of decorin stained sections of proliferative xenograft scars from *(Second row, first)* TCRβ$^{-/-}$δ$^{-/-}$, *(Third row, first)* RAG-1$^{-/-}$ and *(Fourth row, first)* RAG-2$^{-/-}$γc$^{-/-}$ mice demonstrate decreased expression at 30 days postoperatively compared to *(First row)* the normal human skin control. Increased decorin expression is observed at 60, 120 and 180 days postoperatively in *(Second row, second)* TCRβ$^{-/-}$δ$^{-/-}$ *(Third row, second, third and fourth)* RAG-1$^{-/-}$ and *(Fourth row, second, third and fourth)* RAG-2$^{-/-}$γc$^{-/-}$ mice.

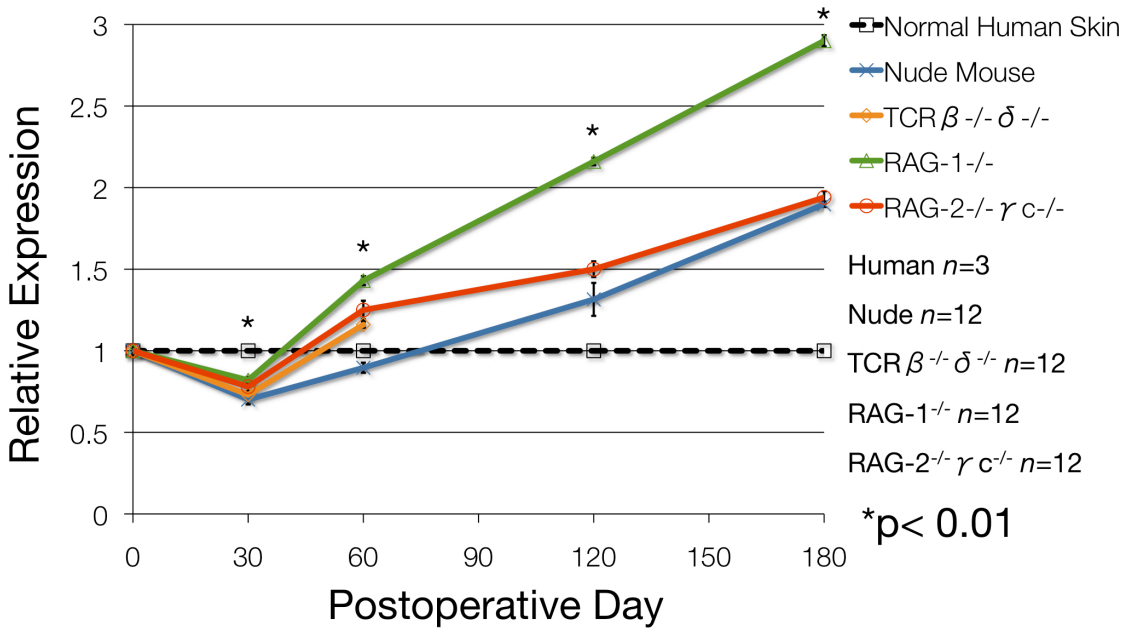

Figure 3-9: Quantification of decorin immunofluorescence in proliferative xenograft scars relative to normal human skin demonstrates less decorin expression at 30 days postoperatively in nude mice and all knockout strains. ($p < 0.01$). This expression pattern changes at 120 and 180 days following transplantation in nude, TCR$\beta^{-/-}\delta^{-/-}$, RAG-$1^{-/-}$ and RAG-$2^{-/-}\gamma c^{-/-}$ mice where there is increased expression of decorin compared to normal human skin.

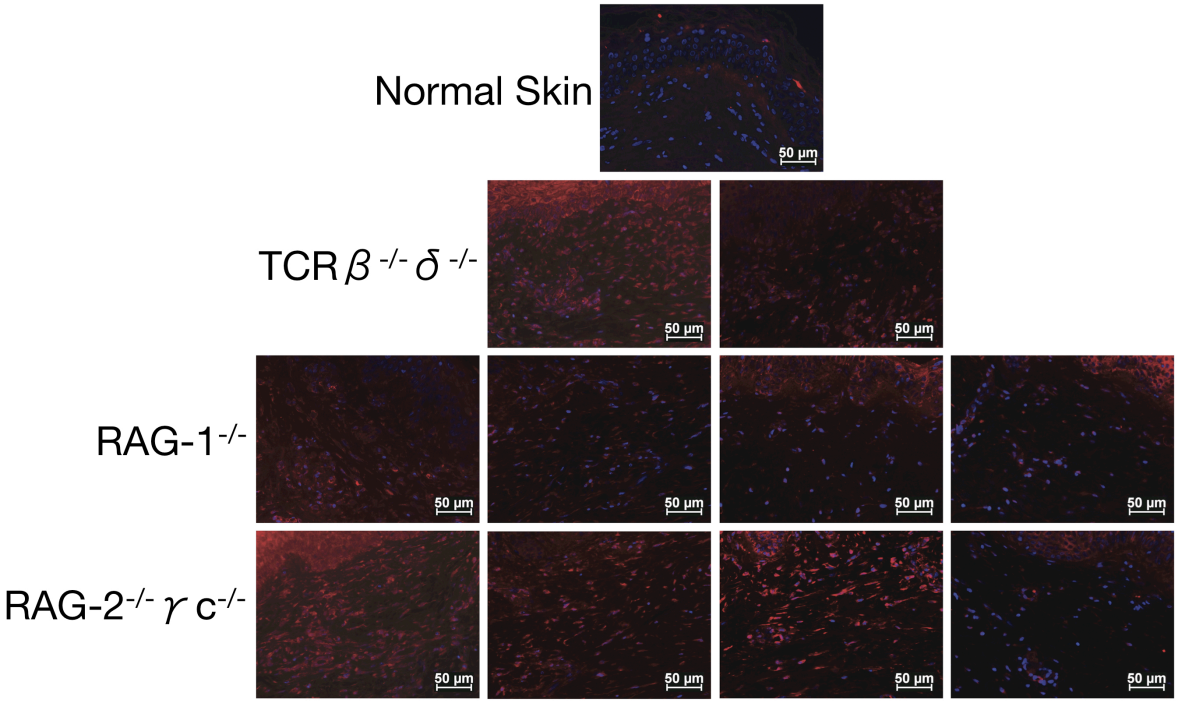

Figure 3-10: Representative immunofluorescent images of biglycan stained sections of proliferative xenograft scars from *(Second row)* TCRβ$^{-/-}$δ$^{-/-}$, *(Third row, first and second)* RAG-1$^{-/-}$ and *(Fourth row, first and second)* RAG-2$^{-/-}$γc$^{-/-}$ mice demonstrate increased expression at 30 and 60 days postoperatively compared to *(First row)* the normal human skin control. Decreased biglycan expression is observed at 120 and 180 days postoperatively in *(Third row, third and fourth)* RAG-1$^{-/-}$ and *(Fourth row, third and fourth)* RAG-2$^{-/-}$γc$^{-/-}$ mice.

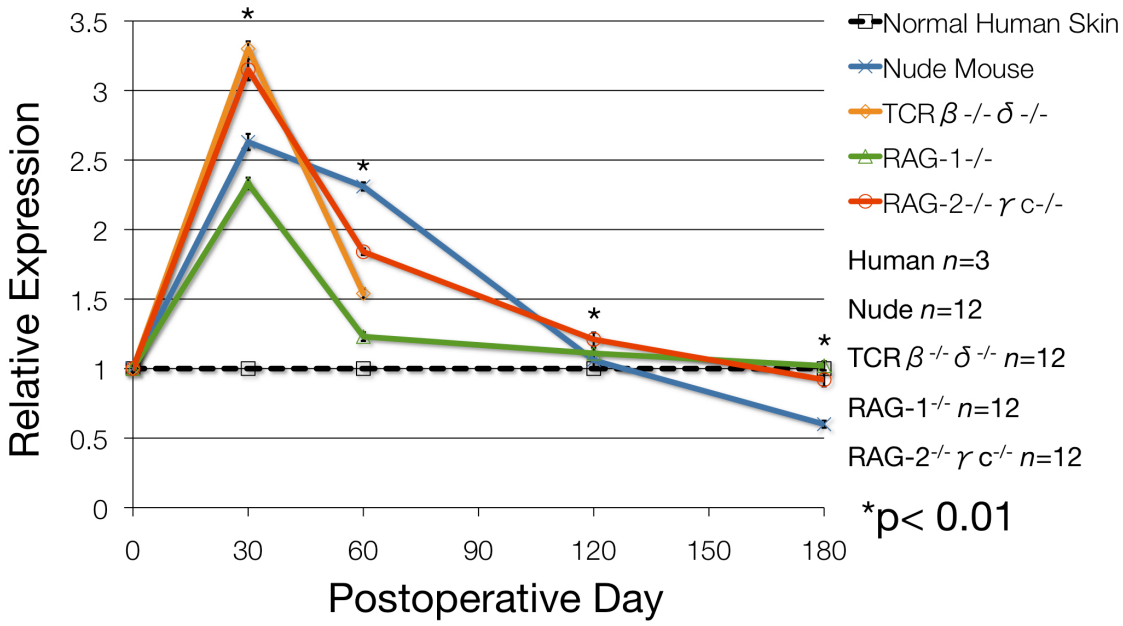

Figure 3-11: Quantification of biglycan immunofluorescence in proliferative xenograft scars relative to normal human demonstrates increased biglycan expression at 30 and 60 days postoperatively in all strains ($p< 0.01$). At 120 days following transplantation there is normalization of biglycan expression in nude, RAG-$1^{-/-}$ and RAG-$2^{-/-}\gamma c^{-/-}$ mice. At 180 days postoperatively only the nude mouse shows decreased biglycan expression compared to normal human skin.

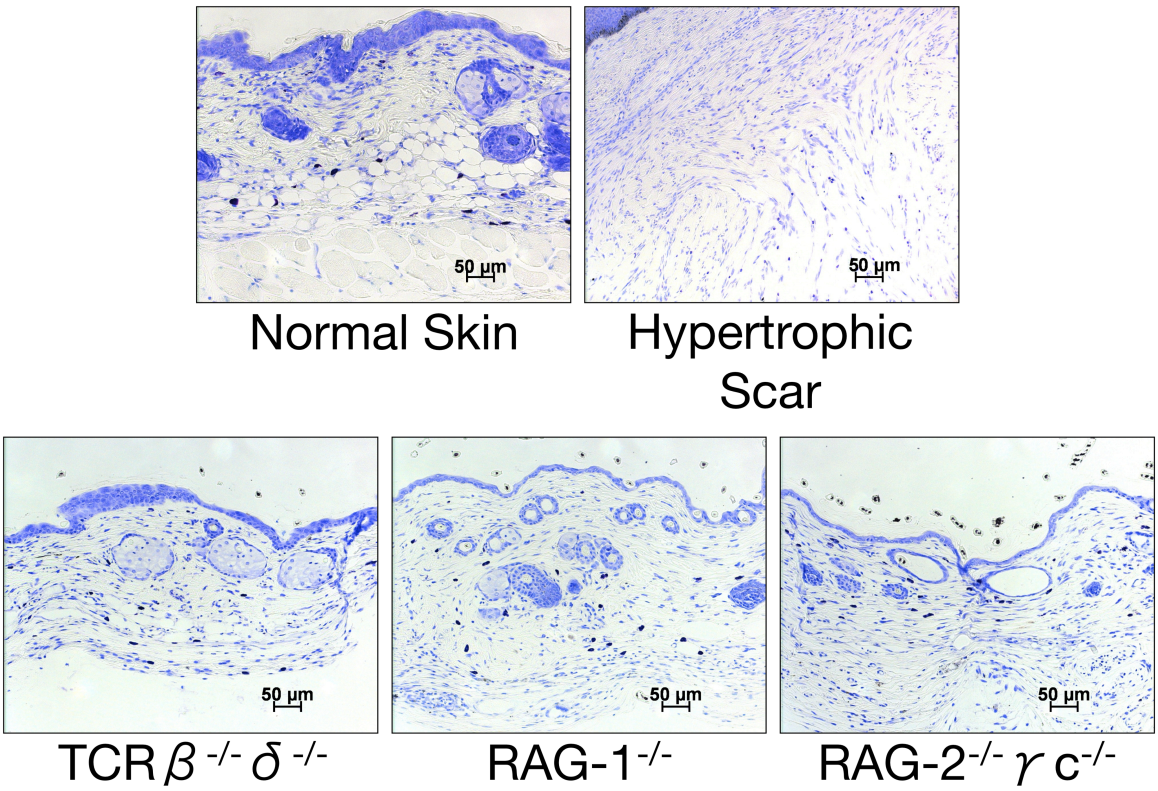

Figure 3-12: Representative images of toluidine blue stained sections of proliferative xenograft scars from *(Second row, left)* TCRβ$^{-/-}$δ$^{-/-}$, *(Second row, center)* RAG-1$^{-/-}$ and *(Second row, right)* RAG-2$^{-/-}$γc$^{-/-}$ mice at 60 days postoperatively demonstrate an increased density of dark, red-purple staining mast cells similar to that seen in *(First row, right)* human hypertrophic scar. In contrast, there are fewer mast cells in *(First row, left)* normal skin.

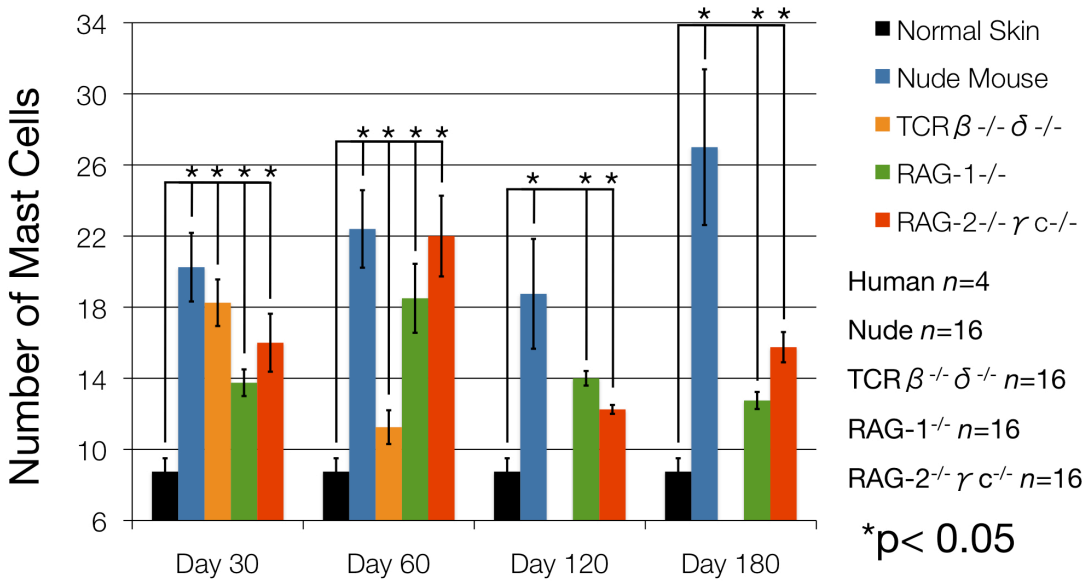

Figure 3-13: Quantification of mast cells in 5 random, high-power fields under 200x magnification demonstrates increased mast cells in all strains of xenografted mice compared to normal mouse skin ($p< 0.05$). Over time, TCR$\beta^{-/-}\delta^{-/-}$, RAG-$1^{-/-}$ and RAG-$2^{-/-}\gamma c^{-/-}$ mice all show an overall reduction in mast cell density, whereas in nude mice a persistent increase in mast cell density is observed.

3.7 Bibliography

1. Murray JC Keloids and hypertrophic scars. *Clin Dermatol* 1994;12:27-37.
2. Dunkin CSJ, Pleat JM, Gillespie PH, et al. *Plast Reconstr Surg* 2007;119:1722-1732.
3. Ryan CM Objective estimates of the probability of death from burn injuries. *N Engl J Med* 1998;338:362-366.
4. Deitch EA, Wheelahan TM, Rose MP, et al. Hypertrophic burn scars: analysis of variables. *J Trauma* 1983;23:895-898.
5. Dedovic Z, Koupilova I, Brychta, P. Time trends in incidence of hypertrophic scarring in children treated for burns. *Acta Chir Plast* 1999;41:87-90.
6. Bombaro KM. What is the prevalence of hypertrophic scarring following burns? *Burns* 2003;29:299-302.
7. Mustoe TA, Cooter RD, Gold MH, et al. International clinical recommendations on scar management. *Plast Reconstr Surg* 2002;110:560-571.
8. Aarabi S, Bhatt KA, Shi Y, et al. Mechanical load initiates hypertrophic scar formation through decreased cellular apoptosis. *FASEB J* 2007;21:3250-3261.
9. Honardoust D, Varkey M, Hori K, et al. Small leucine-rich proteoglycans, decorin and fibromodulin, are reduce in postburn hypertrophic scar. *Wound Repair Regen* 2011;19:368-378.
10. Mustoe TA. Scars and keloids. *Br Med J* 2004;328:1329-1330.

11. Ehrlich HP, Desmoulière A, Diegelmann RF, et al. Morphological and immunochemical differences between keloid and hypertrophic scar. *Am J Pathol* 1994;145:105-113.
12. Wang JF, Ding J, Jiao H, et al. Human hypertrophic scar-like nude mouse model: Characterization of the molecular and cellular biology of the scar process. *Wound Repair Regen* 2011;19:274-285.
13. Brigham, PA, McLoughlin, E. Burn incidence and medical care use in the United States: estimates, trends, and data sources. *J Burn Care Rehabil* 1996;17:95-107.
14. Greenhalgh DG. Models of wound healing. *J Burn Care Rehabil* 2005;26:293-305.
15. Morris DE, Wu L, Zhao LL, et al. Acute and chronic animal models for excessive dermal scarring: quantitative studies. *Plast Reconstr Surg* 1997;100:674-681.
16. Ramos, MLC, Gragnani A, Ferreira LM. Is there an ideal animal model to study hypertrophic scarring? *J Burn Care Res* 2008;29:363-368.
17. Momtazi M, Kwan P, Ding J, et al. A Nude Mouse Model of Hypertrophic Scar Demonstrates Histological and Morphologic Characteristics of Human Hypertrophic Scar. Manuscript submitted for publication.
18. Pantelouris EM. Absence of thymus in a mouse mutant. *Nature* 1968;217:370-371.
19. Mecklenburg L, Tychsen B, Paus R. Learning from nudity: lessons from the nude phenotype. *Exp Dermatol* 2005;14:797-810.

20. Kennedy JD, Pierce CW, Lake JP. Extrathymic T-cell maturation. Phenotypic analysis of T-cell subsets in nude mice as a function of age. *J Immunol* 1992;148:1620-1629.
21. MacDonald HR, Lees RK, Sordat B, Zaech P, Maryanski JL, Bron C. Age-associated increase in expression of the T-cell surface markers Thy-1, Lyt-1 and Lyt-2 in congenitally athymic (nu/nu) mice: analysis by flow microfluorometry. *J Immunol* 1981;126:865-870.
22. Hilbert DM, Holmes KL, Anderson AO, et al. Long-term thymic reconstitution by peripheral CD4 and CD8 single-positive lymphocytes. *Eur J Immunol* 1993;23:241-248.
23. Ferrick DA, Sambhara SR, Chadwick BS, et al. The T-cell receptor repertoire is strikingly similar in older nude mice compared to normal adult mice. *Thymus* 1989;13:103-111.
24. Mombaerts P, Clarke AR, Rudnicki MA, et al. Mutations in T-cell antigen receptor genes alpha and beta block thymocyte development at different stages. *Nature* 1992;360:225-231.
25. Shortman K. Cellular aspects of early T-cell development. *Curr Opin Immunol* 1992;4:140-146.
26. Thompson CB. RAG knockouts deliver a one/two punch. *Curr Biol* 1992;2:180-182.
27. Swanson PC. The bounty of RAGs: recombination signal consequences and reaction outcomes. *Immunol Rev* 2004;200:90-114.

28. Chen J, Shinkal Y, Young F, et al. Probing immune functions in RAG-deficient mice. *Curr Opin Immunol* 1994;6:313-319.

29. Nedelec B, Shankowsky H, Scott PG, Ghahary A, Tredget EE. Myofibroblasts and apoptosis in human hypertrophic scars: The effect of interferon-α2b. *Surgery* 2001;130:798-808.

30. Grundy MA, Sentman CL. Immunodeficient mice have elevated numbers of NK cells in non-lymphoid tissues. *Exp Cell Res* 2006;312:3920-3916.

31. Galy A, Travis M, Cen D, et al. Human T, B, natural killer, and dendritic cells arise from a common bone marrow progenitor cell subset. *Immunity* 1995;3:459-473.

32. Muhanna N, Tiar LA, Doron S et al. Amelioration of hepatic fibrosis by NK cell activation. *Gut* 2011;60:90-98.

33. Esposito I, Perna F, Ponticiello A, Perrella M, Gilli M, Sanduzzi A. Natural killer cells in Bal and peripheral blood of patients with idiopathic pulmonary fibrosis (IPF). *Int J Immunopathol Pharmacol* 2005;18:542-545.

34. Segel MJ, Izbicki G, Cohen PY et al. Role of interferon-gamma in the evolution of murine bleomycin lung fibrosis. *Am J Physiol Lung Cell Mol Physiol* 2003;285:1255-1262.

35. Ghahary A, Shen YJ, Nedelec B, Scott PG, Tredget EE. Interferons gamma and alpha-2b differentially regulate the expression of collagenase and tissue inhibitor of metalloproteinase-1 messenger RNA in human

hypertrophic and normal dermal fibroblasts. *Wound Repair Regen* 1995;3:176-184.

36. Tredget EE, Wang R, Shen Z, Scott PG, Ghahary A. Transforming growth factor-beta mRNA and protein in hypertrophic scar tissues and fibroblasts: Antagonism by IFN-alpha and IFN-gamma *in vitro* and *in vivo*. *J Interferon Cytokine Res* 2000;20:143-151.
37. Park JE, Barbul A. Understanding the role of immune regulation in wound healing. *Am J Surg* 2004;187:11s-16s.
38. Wynn, TA. Fibrotic disease and the Th1/Th2 paradigm. *Nat Rev Immunol* 2004;4:583-594.
39. Zhu Z, Homer RJ, Wang Z, et al. Pulmonary expression of interleukin-13 causes inflammation, mucus hypersecretion, subepithelial fibrosis, physiologic abnormalities, and eotaxin production. *J Clin Invest* 1999;103:779-788.
40. Lee CG, Homer RJ, Zhu Z, et al. Interleukin-13 induces tissue fibrosis by selectively stimulating and activating transforming growth factor β1. *J Exp Med* 2001;194:809-821.
41. Tredget EE, Yang L, Delehanty M, Shankowsky H, Scott PG. Polarized Th2 cytokine production in patients with hypertrophic scar following thermal injury. *J Interferon Cytokine Res* 2006;26:179-189.
42. Ishida Y, Toshikazu K, Takayasu T, Iwakura Y, Mukaida N. The essential involvement of cross-talk between IFN-gamma and TGF-beta in the skin wound-healing process. *J Immunol* 2004;172:1848-1855.

43. Ishikawa H, Saito K. Congenitally athymic nude (nu/nu) mice have Thy-1 bearing immunocompetent helper T-cells in their peritoneal cavity. *J Exp Med* 1980;151:965-968.

44. Wynn TA. Cellular and molecular mechanisms of fibrosis. *J Pathol* 2008;214;199-210.

45. Sandler NF, Mentink-Kane MM, Cheever Aw, Wynn TA. Global gene expression profiles during acute pathogen induced pulmonary inflammation reveal divergent roles for Th1 and Th2 responses in tissue repair. *J Immunol* 2003;171:3655-3667.

4. Summary

4.1 General Discussion

Grafting human skin onto the backs of nude, TCRβ$^{-/-}$δ$^{-/-}$, RAG-1$^{-/-}$ and RAG-2$^{-/-}$γc$^{-/-}$ mice is sufficient to induce proliferative xenograft scars that appear morphologically and histologically consistent with human HSc [1]. Moreover these scars possess immunohistochemical properties associated with HSc. Proliferative xenograft scars in knockout strains in particular behave similar to human HSc in that they demonstrate the ability to remodel over time, becoming flatter, paler and relatively less cellular [1]. Within the knockout strains, scars from RAG-1$^{-/-}$ mice showed a reduction in the overall magnitude of scar thickness compared to TCRβ$^{-/-}$δ$^{-/-}$ and RAG-2$^{-/-}$γc$^{-/-}$ mice [1]. In examining these differences two important questions arose: 1. Given that nude and TCRβ$^{-/-}$δ$^{-/-}$ mice are both T-cell deficient, what accounts for the discrepancy in their scar behavior over time? 2. Can the reduction in overall scar magnitude seen in RAG-1$^{-/-}$ animals compared to RAG-2$^{-/-}$γc$^{-/-}$ mice be attributed to the presence of IFN-γ production by NK cells in the former?

Despite a similar functional T-cell deficiency, proliferative xenograft scars in nude and TCRβ$^{-/-}$δ$^{-/-}$ animals behave differently with regard to the pattern of percent increase in scar thickness over time. One possibility is that these differences occur because of inconsistency in the background strain. In our experiments BALB/c nudes and C57BL/6 TCRβ$^{-/-}$δ$^{-/-}$ mice were used. This issue

could be remedied by repeating our experiments in the nude population on a B6 background. These animals are readily available and would allow us to better understand the contribution of background strain to scarring in our model.

The second source of divergence between these two groups of mice is the mechanism by which they acquire T-cell deficiency. Nude mice fail to receive a maturation stimulus during thymocyte development [2-5], while TCR$\beta^{-/-}\delta^{-/-}$ mice lack β and δ genes necessary for functional TCR rearrangement [6,7]. As a result, reports have demonstrated that in nudes, extrathymic T-cell maturation results in the presence of T-cells in older animals [2-5]. Therefore, the presence of T-cells in nude mice is a potential cause for the divergence in scarring in these animals. The first step in investing this hypothesis is to analyze blood, spleen and lymph node samples from nude and TCR$\beta^{-/-}\delta^{-/-}$ mice at various time points to determine if T-cells are present. If T-cells are detected they can be further characterized based on the surface markers they express. This will be valuable in assessing the potential biological significance of these cells and their effects on scar formation.

The role of IFN-γ as an anti-fibrotic T_H1 cytokine has been previously shown [8-10]. *In vivo*, we observed a reduction in the overall magnitude of scars in RAG-$1^{-/-}$ compared to RAG-$2^{-/-}\gamma c^{-/-}$ mice [1]. NK cells are the only immune cell population present in the RAG-$1^{-/-}$ mouse, whereas these cells are lacking in the RAG-$2^{-/-}\gamma c^{-/-}$. The first step in determining if the differences in RAG-$1^{-/-}$ and RAG-$2^{-/-}\gamma c^{-/-}$ scars are attributable to IFN-γ is to confirm the presence of NK cells

in proliferative xenograft scar sections from RAG-1$^{-/-}$ mice. We have attempted to identify NK cells as per a previously reported method [11] using rat anti-mouse CD49b antibody (Biolegend, San Diego, CA). Unfortunately, we were unable to successfully identify NK cells in these sections. One explanation is the time at which our proliferative xenograft scar sections were harvested. Our earliest scar biopsy is from 30 days after grafting. It is possible that NK cells migrate into human xenografts earlier and exert their effects. As such repeating these experiments and harvesting scar biopsies from earlier time points may confirm the presence of NK cells in proliferative xenograft scars. Errors in staining technique are also a potential source for the lack of NK cells seen. We will continue to refine and seek new methods of identifying these cells in RAG-1$^{-/-}$ sections.

4.2 Conclusions

In conclusion, while our studies on HSc formation in nude, TCR$\beta^{-/-}\delta^{-/-}$, RAG-1$^{-/-}$ and RAG-2$^{-/-}\gamma c^{-/-}$ mouse models have provided us with new and interesting insights and a potential animal model for the study of human HSc they have also left us with several new questions regarding the differences we observed between the various types of scars. Although morphologic and histologic features of human HSc could be demonstrated in all strains, knockout strains in particular offer an advantage over nude mice because they demonstrate remodeling characteristics more in keeping with human HSc. Amongst the knockout strains, use of RAG-1$^{-/-}$ and RAG-2$^{-/-}\gamma c^{-/-}$ mice provides the opportunity to dissect the role of NK cells on HSc formation, and to test the potential for IFN-γ to be used as a

scar modulating treatment option in patients.

4.3 Bibliography

1. Momtazi M, Kwan P, Ding J, et al. Morphologic and histological comparison of hypertrophic scar in nude and knockout mice deficient in T, B and natural killers cells. Manuscript submitted for publication.
2. Kennedy JD, Pierce CW, Lake JP. Extrathymic T-cell maturation. Phenotypic analysis of T-cell subsets in nude mice as a function of age. *J Immunol* 1992;148:1620-1629.
3. MacDonald HR, Lees RK, Sordat B, Zaech P, Maryanski JL, Bron C. Age-associated increase in expression of the T-cell surface markers Thy-1, Lyt-1 and Lyt-2 in congenitally athymic (nu/nu) mice: analysis by flow microfluorometry. *J Immunol* 1981;126:865-870.
4. Hilbert DM, Holmes KL, Anderson AO, et al. Long-term thymic reconstitution by peripheral CD4 and CD8 single-positive lymphocytes. *Eur J Immunol* 1993;23:241-248.
5. Ferrick DA, Sambhara SR, Chadwick BS, et al. The T-cell receptor repertoire is strikingly similar in older nude mice compared to normal adult mice. *Thymus* 1989;13:103-111.
6. Mombaerts P, Clarke AR, Rudnicki MA, et al. Mutations in T-cell antigen receptor genes alpha and beta block thymocyte development at different stages. *Nature* 1992;360:225-231.
7. Shortman K. Cellular aspects of early T-cell development. *Curr Opin Immunol* 1992;4:140-146.

8. Ghahary A, Shen YJ, Nedelec B, Scott PG, Tredget EE. Interferons gamma and alpha-2b differentially regulate the expression of collagenase and tissue inhibitor of metalloproteinase-1 messenger RNA in human hypertrophic and normal dermal fibroblasts. *Wound Repair Regen* 1995;3:176-184.
9. Tredget EE, Wang R, Shen Z, Scott PG, Ghahary A. Transforming growth factor-beta mRNA and protein in hypertrophic scar tissues and fibroblasts: Antagonism by IFN-alpha and IFN-gamma *in vitro* and *in vivo*. *J Interferon Cytokine Res* 2000;20:143-151.
10. Wynn, TA. Fibrotic disease and the Th1/Th2 paradigm. *Nat Rev Immunol* 2004;4:583-594.
11. Oertelt S, Lian Z-X, Cheng C-M, et al. Anti-mitochondrial antibodies and primary biliary cirrhosis in TGF-β receptor II dominant-negative mice. *J Immunol* 2006;177:1655-1660.